DEPARTMENT OF ELECTRICAL AND

COMPUTER ENGINEERING

ENABLING TECHNOLOGIES FOR ASSISTED-BASED COMMUNICATIONS: FUNDAMENTAL LIMITS AND PROTOCOL DESIGN

DOCTOR OF PHILOSOPHY DISSERTATION

ANDREAS NICOLAIDES

2024

University of Cyprus

DEPARTMENT OF ELECTRICAL AND

COMPUTER ENGINEERING

ENABLING TECHNOLOGIES FOR ASSISTED-BASED COMMUNICATIONS: FUNDAMENTAL LIMITS AND PROTOCOL DESIGN

ANDREAS NICOLAIDES

A Dissertation Submitted to the University of Cyprus

in Partial Fulfillment of the Requirements

for the Degree of Doctor of Philosophy

MAY 2024

APPROVAL PAGE

Andreas Nicolaides

Enabling Technologies for Assisted-based Communications:

Fundamental Limits and Protocol Design

The present Doctorate Dissertation was submitted in partial fulfillment of the requirements

for the Degree of Doctor of Philosophy in the Department of Electrical and Computer Engi-

neering, and was approved on April 25, 2024 by the members of the Examination Committee.

Committee Chair
_____
Georgios Ellinas, Professor

Research Supervisor
_____
Ioannis Krikidis, Professor

Committee Member
_____
Themistoklis Charalambous, Assistant Professor

Committee Member
_____
Petros Elia, Professor

Committee Member
_____
Athanasios Kanatas, Professor

DECLARATION OF DOCTORAL CANDIDATE

The present doctoral dissertation was submitted in partial fulfillment of the requirements for the degree of Doctor of Philosophy of the University of Cyprus. It is a product of original work of my own, unless otherwise mentioned through references, notes, or any other statements.

Andreas Nicolaides

....

Περίληψη

Η πρωτοφανής αύξηση των ασύρματων συσκευών επικοινωνίας και η εμφάνιση του δια-δικτύου των πραγμάτων έχουν οδηγήσει σε μια σημαντική κλιμάκωση στον αριθμό των ασύρματων συνδέσεων και στη ζήτηση της κυκλοφορίας δεδομένων. Ως εκ τούτου, η υλο-ποίηση καινοτόμων ιδεών χαμηλής πολυπλοκότητας είναι απαραίτητη προϋπόθεση για τη δημιουργία αποδοτικών ασύρματων δικτύων πέμπτης γενεάς, καθώς και των μελλοντικών επικοινωνιών έκτης γενεάς, και την ικανοποίηση των απαιτήσεων των δικτύων εκτενούς συνδεσιμότητας υψηλής απόδοσης. Για την επίτευξη των πιο πάνω στόχων, η χρήση κόμ-βων μεταγωγής πολλαπλών βημάτων και επαναδιαμορφώσιμων έξυπνων επιφανειών (ΕΕΕ) αναδεικνύονται ως υποσχόμενες τεχνολογίες που μπορούν να ενισχύσουν την επικοινωνία και τη συνδεσιμότητα των ασύρματων δικτύων.

Η παρούσα διδακτορική διατριβή πραγματεύεται τον απαιτητικό σχεδιασμό πρωτοκόλ-λων χαμηλής πολυπλοκότητας, με στόχο τη βελτίωση της απόδοσης των ασύρματων δι-κτύων υποστηριζόμενων από τη χρήση των πιο πάνω τεχνολογιών. Η εφαρμογή των προτεινόμενων πρωτοκόλλων μπορεί να αποφέρει σημαντικά οφέλη στα συμβατικά συ-στήματα επικοινωνίας, όπως μεγαλύτερη δικτυακή κάλυψη, ενισχυμένη αποδοτικότητα και ευελιξία. Συγκεκριμένα, χρησιμοποιούνται αποτελεσματικές τεχνικές στο φυσικό επίπεδο για τη μεταφορά πληροφορίας στους τελικούς χρήστες, οι οποίες παρέχουν υψηλότερα κέρδη απόδοσης με την αξιοποίηση των ασύρματων καναλιών στα πεδία του χώρου και του χρόνου. Αρχικά, μελετάται η απόδοση ενός συνεργατικού πρωτοκόλλου σε δίκτυα πολλαπλών βημάτων, όπου οι κόμβοι μεταγωγής μεταδίδουν δεδομένα βάσει μιας στρα-τηγικής περιορισμένης συνεργασίας μεταξύ των κόμβων του δικτύου, ενώ μπορούν να λειτουργήσουν σε δύο καταστάσεις επικοινωνίας με διαφορετικές δυνατότητες μεταφοράς δεδομένων. Για τη μοντελοποίηση της χρονικής εξέλιξης της κατάστασης του δικτύου, προτείνεται μια ευέλικτη μεθοδολογία με τη χρήση Μαρκοβιανών αλυσίδων.

Έπειτα, εστιάζουμε στο σχεδιασμό απλών λύσεων για συστήματα υποστηριζόμενα α-πό ΕΕΕ με περιορισμένες απαιτήσεις γνώσης των καναλιών. Συγκεκριμένα, ερευνάται η

i

απόδοση συστημάτων πολλαπλής-εισόδου πολλαπλής-εξόδου υποστηριζόμενων από ΕΕΕ με μηδενικές απαιτήσεις γνώσης των καναλιών, όπου τα στοιχεία ανάκλασης διαχωρίζονται σε υπο-επιφάνειες που δύνανται να αναδιαμορφώνονται περιοδικά μέσω τροποποίησης του πλάτους ή της μετατόπισης φάσης. Επιπρόσθετα, για τη μείωση των απαιτήσεων εκμάθησης των καναλιών, προτείνεται η υλοποίηση ενός υβριδικού σχήματος διαμόρφωσης της ΕΕΕ και μελετάται η απόδοσή του όταν η εκμάθηση των καναλιών είναι ανακριβής. Το προτεινόμενο σχήμα προσαρμόζει το συντελεστή ανάκλασης ενός υποσυνόλου των στοιχείων της ΕΕΕ βάσει των εκτιμώμενων καναλιών, ενώ τα υπόλοιπα στοιχεία ανακλούν τα σήματα τυχαία. Τέλος, ερευνώνται τα πιθανά πλεονεκτήματα της χρήσης μιας ΕΕΕ για τη διευκόλυνση της εφαρμογής της τεχνικής χρονικής ανάκλασης (ΧΑ) σε ευρυζωνικά δίκτυα υψηλών συχνοτήτων. Η ΕΕΕ χρησιμοποιείται για να εμπλουτίσει το περιβάλλον σκέδασης παρέχοντας πολλαπλές διαδρομές διάδοσης για την αποδοτική εφαρμογή της ΧΑ, χωρίς να χρειάζεται η γνώση των καναλιών για τη διαμόρφωση της επιφάνειας.

Η απόδοση των προτεινόμενων λύσεων αξιολογείται διεξοδικά με τη χρήση εργαλείων από τη θεωρία πληροφορίας, τη θεωρία πιθανοτήτων και τη θεωρία επεξεργασίας σήματος. Μέσα σε αυτό το αναλυτικό πλαίσιο, παρέχονται θεωρητικά αποτελέσματα για σημαντικές μετρικές απόδοσης, όπως ο λόγος σήματος-προς-θόρυβο στο δέκτη, η πιθανότητα διακοπής της επικοινωνιακής κάλυψης ή η ανταλλαγή διαφορισμού-πολυπλεξίας, τα οποία παρέχουν χρήσιμες πληροφορίες για τα όρια απόδοσης των προτεινόμενων λύσεων. Επιπρόσθετα, μελετάται η επίδραση διάφορων παραμέτρων στην απόδοση κάθε συστήματος, όπως ο αριθμός των κόμβων μεταγωγής ή των στοιχείων ανάκλασης και η ισχύς μετάδοσης.

Abstract

In recent years, the unprecedented increase in wireless devices and the emergence of Internet-of-Things applications have led to a tremendous increase in the number of connections that need to be established, resulting in high data traffic demands. As such, innovative solutions with low implementation complexity need to be conceived for the efficient deployment of fifth generation and beyond communications, in order to satisfy the stringent requirements of ultra-reliable networks with massive connectivity. Towards addressing these challenges, multi-hop relaying and reconfigurable intelligent surfaces (RISs) are regarded as key enabling technologies to assist the communication and provide ubiquitous connectivity.

The present thesis deals with the challenging design of low-complexity protocols, aiming to enhance the performance of wireless networks aided by the employment of the aforementioned candidate technologies. Applying these protocols in conventional communication systems provides significant gains, such as increased coverage range, enhanced reliability and flexibility. Specifically, efficient techniques for conveying information to the end users are applied, which enable higher performance gains by exploiting the wireless channels in both space and time domains. Firstly, we study the performance of a novel cooperative protocol over a multi-hop network, where the relays transmit data based on a myopic strategy, enabling limited cooperation between neighboring nodes, and can operate in two communication modes affecting their transmission capabilities. For modeling the evolution of the network status over time, we propose a flexible methodology by using a Markov chain formulation.

Then, we focus on the design of low-complexity solutions for RIS-aided systems with low-to-zero channel state information (CSI) requirements. Specifically, we investigate the performance of RIS-assisted multiple-input multiple-output systems, by employing partition-based schemes. The elements of the RIS are divided into

sub-surfaces and are sequentially modified through an amplitude-based or a phase-based approach, without requiring any CSI knowledge for their reconfiguration. In addition, we propose a hybrid scheme for an RIS-assisted system under imperfect CSI. The proposed scheme requires channel estimation for only a subset of the elements to adjust their reflection coefficients, thus reducing the channel training overhead, while the remaining elements perform random rotations. Finally, we explore the potential gains of employing an RIS for facilitating the time reversal (TR), which is a suitable signal processing technique for rich scattering environments in high-frequency wideband communications. In this case, an RIS operating in the antenna's near-field region is employed to enrich the poor scattering environment by generating multiple propagation paths, while its configuration does not require any CSI knowledge.

The performance for each of the proposed solutions is investigated through a complete analytical framework, by utilizing tools from the areas of information theory, probability theory and signal processing. Under this framework, tractable theoretical expressions are derived for key performance metrics, such as the achieved signal-to-noise ratio, the outage probability and the diversity-multiplexing tradeoff. The provided expressions provide useful theoretical and practical insights on the fundamental limits of the considered communication schemes. Moreover, several system design parameters affecting the overall performance, such as the number of relays or reflecting elements, the transmit power etc., are discussed.

Acknowledgments

First and foremost, I would like to express my sincere gratitude to my research supervisor Prof. Ioannis Krikidis for giving me the opportunity to join his team and delve into the fascinating area of wireless communications. Throughout the course of my doctoral studies, he was always encouraging me to explore innovative ideas and interesting topics, while his constant support and patience gave me the strength to carry out my research. His profound scientific expertise and invaluable guidance were essential for achieving the goals of this work. It was a great privilege and honor to work and study under his guidance.

I would also like to thank all the members of my examination committee for their time to review and handle this Ph.D. dissertation. Special thanks to Prof. Georgios Ellinas and Assistant Prof. Themistoklis Charalambous for their participation to all of my scientific exams for the Ph.D. program and their valuable comments throughout my research journey. Moreover, I want to thank Prof. Petros Elia from EURECOM and Prof. Athanasios Kanatas from the University of Piraeus for kindly accepting the invitation to be part of my examination committee.

I am also grateful to Dr. Constantinos Psomas for his invaluable guidance and scientific insights. Our fruitful discussions were undoubtedly inspirational for my research and our close collaboration was an important asset in reaching the milestones of my studies. Moreover, I would like to thank Associate Prof. Ghassan Kraidy from the Norwegian University of Science and Technology and Prof. Sheng Yang from the Paris-Saclay University for our productive collaboration. Their contribution in the work performed in this thesis has been significant.

Particular thanks are due to my colleagues and friends from the IRIDA Research Centre for Communication Technologies for all their support and assistance, as well as the wonderful and memorable moments we spent together during these years. Their constructive feedback and forward thinking were really important and helped

me enhance the quality of this work considerably.

Most importantly, I would like to deeply thank and devote this thesis to my parents, Nicos and Eleni, and my siblings, Constantinos and Eliana, for their constant support and unconditional love. The motivation from my family throughout all these years has truly filled me with passion and confidence about my research. The completion of this dissertation would not have been possible without their encouragement.

Publications

Published journal publications

1. A. Nicolaides, C. Psomas, and I. Krikidis, "A Markov chain approach for myopic multi-hop relaying: Outage and diversity analysis," *IEEE Journal of Selected Topics in Signal Processing*, Special Issue on Advanced Signal Processing for Local and Private 5G Networks, vol. 16, pp. 56–69, Jan. 2022.

2. A. Nicolaides, C. Psomas, G. Kraidy, S. Yang, and I. Krikidis, "Outage and DMT analysis of partition-based schemes for RIS-aided MIMO fading channels," *IEEE Journal on Selected Areas in Communications*, Special Issue on Beyond Shannon Communications: A Paradigm Shift to Catalyze 6G, vol. 41, no. 8, pp. 2336–2349, Aug. 2023.

Published conference proceedings

1. A. Nicolaides, C. Psomas, and I. Krikidis, "Outage analysis of myopic multi-hop relaying: A Markov chain approach," in *Proceedings of IEEE Global Communications Conference*, Taipei, Taiwan, Dec. 2020.

2. A. Nicolaides, C. Psomas, G. Kraidy, and I. Krikidis, "A partition-based scheme for IRS-aided MIMO fading channels: Outage and DMT analysis," in *Proceedings of IEEE International Symposium on Information Theory*, Espoo, Finland, Jun. 2022.

3. A. Nicolaides, C. Psomas, S. Yang, and I. Krikidis, "A hybrid scheme for reconfigurable intelligent surfaces: How many elements should be estimated?," in *Proceedings of IEEE Global Communications Conference*, Kuala Lumpur, Malaysia, Dec. 2023.

Unpublished journal publications

1. A. Nicolaides, C. Psomas, and I. Krikidis, "An RIS-enabled time reversal scheme for multipath near-field channels," *IEEE Communications Letters*, under revision.

List of Abbreviations

3D	**T**hree **D**imension
3GPP	**3**rd **G**eneration **P**artnership **P**roject
4G	**F**ourth **G**eneration
5G	**F**ifth **G**eneration
6G	**S**ixth **G**eneration
AF	**A**mplify-and-**F**orward
AI	**A**rtificial **I**ntelligence
AR	**A**ctivate-**R**eflect
AP	**A**ccess **P**oint
AWGN	**A**dditive **W**hite **G**aussian **N**oise
BS	**B**ase **S**tation
CB	**C**oherent **B**eamforming
cdf	**c**umulative **d**istribution **f**untion
CF	**C**ompress-and-**F**orward
CIR	**C**hannel **I**mpulse **R**esponse
CLT	**C**entral **L**imit **T**heorem
CSI	**C**hannel **S**tate **I**nformation
D2D	**D**evice-to-**D**evice
DAM	**D**elay **A**djustable **M**etasurface
DC	**D**irect-**C**urrent
DF	**D**ecode-and-**F**orward
DFT	**D**iscrete **F**ourier **T**ransform
DMT	**D**iversity-**M**ultiplexing **T**radeoff
EH	**E**nergy **H**arvesting
EM	**E**lectro**M**agnetic
eMBB	**e**nhanced **M**obile **B**road-**B**and

ETSI	European Telecommunications Standards Institute
FPGA	Field-Programmable Gate Array
FR	Flip-Reflect
IEEE	Institute of Electrical and Electronics Engineers
IoE	Internet of Everything
IoT	Internet of Things
IRS	Intelligent Reflecting Surface
ISG	Industry Specification Group
ISI	Inter-Symbol Interference
ITU	International Telecommunication Union
KPI	Key Performance Indicator
LoS	Line-of-Sight
LTE-A	Long Term Evolution-Advanced
M2M	Machine-to-Machine
MC	Markov Chain
MIMO	Multiple-Input Multiple-Output
MISO	Multiple-Input Single-Output
mMTC	massive Machine-Type Communications
mmWave	millimeter-Wave
NOMA	Non-Orthogonal Multiple Access
OMA	Orthogonal Multiple Access
OWC	Optical Wireless Communications
pdf	probability density function
PIN	Positive-Intrinsic Negative
PR	Pure Reflection
QoS	Quality of Service
QRM	Quadrature Reflection Modulation
RF	Rotate-and-Forward
RIS	Reconfigurable Intelligent Surface
RPM	Reflection Pattern Modulation
RR	Random Rotations
SAA	Small Argument Approximation
SI	Self-Interference

SINR	**S**ignal-to-**I**nterference-plus-**N**oise **R**atio
SISO	**S**ingle-**I**nput **S**ingle-**O**utput
SNR	**S**ignal-to-**N**oise **R**atio
SRE	**S**mart **R**adio Environment
SWIPT	**S**imultaneous **W**ireless **I**nformation and **P**ower **T**ransfer
THz	**T**era**H**ertz
TR	**T**ime **R**eversal
UAV	**U**nmanned **A**erial **V**ehicle
UE	**U**ser **E**quipment
URLLC	**U**ltra-**R**eliable **L**ow-**L**atency **C**ommunications
USW	**U**niform **S**pherical **W**ave
UWC	**U**nderwater **W**ireless **C**ommunications
VLC	**V**isible **L**ight **C**ommunications
VR	**V**irtual **R**eality
WiMAX	**W**orldwide **I**nteroperability for **M**icrowave **A**ccess
WPT	**W**ireless **P**ower **T**ransfer

Contents

List of Figures

List of Tables

Chapter 1

Introduction

Wireless communications is one of the most vibrant and fastest growing areas in the field of digital communication. Since the first successful radio transmission demonstrated by Guglielmo Marconi in 1895, the ability of communicating and exchanging information without requiring physical connections has evolved tremendously. Especially in the last decades, advances in wireless technology and the advent of digital communications revolutionized the development of wireless networks. Nowadays, wireless communications have become an essential utility of people's everyday lives and a driving force for nearly every sector of society, from entertainment and news reporting to healthcare and emergency services. Due to this inseparable link between the evolution of wireless networks and the economic and social development, several new opportunities are constantly arising, while the ever-growing demands make the design of the forthcoming wireless systems even more challenging. Therefore, researchers in both academia and industry need to conceive innovative solutions to address these challenges and identify potential features and emerging technologies that will shape the future of wireless communications.

1.1 Motivation

Over the past decade, the vast proliferation of Internet-of-Things (IoT) services and the exponential increase of mobile devices have led to a rapid surge in global mobile data traffic. According to the latest reports, in 2023 the total number of connected wireless devices reached around 15 billion, following a ten-times higher rate of growth than the population growth rate, while this trend is expected to keep esca-

lating [1]. Such devices include smartphones, portable computers and connected television sets, while the rise of Machine-to-Machine (M2M) applications, such as smart sensors and healthcare monitors, also burden wireless networks with a considerable number of connections. Furthermore, it is expected that these devices will support a wide range of new applications and data-demanding services, including high-quality video streaming, social networking platforms, home automation, vehicle navigation, etc. [1,2]. Researchers in both academia and industry have therefore the challenging task to address these demands and provide solutions to support massive connectivity networks with high data rates, enhanced reliability and low latency.

Currently, the world witnesses a paradigm shift in the area of wireless communications, as the era of fifth-generation (5G) wireless networks has already begun. Since 2019, several global operators started developing new 5G networks, while the commercial launch of 5G has already been rolled out in several countries. The backbone of 5G can be defined by three key pillars, which were firstly recommended by the International Telecommunications Union (ITU) in 2015 [3,4]:

- Enhanced mobile broad-band (eMBB): This feature is an extension to the fourth generation (4G) broad-band services. It refers to data-driven use cases that require higher data rates, such as multimedia content and cloud-based applications. eMBB covers a wide range of scenarios, including hot-spot connectivity, where the user density is high, and wide area coverage with higher user mobility.

- Ultra-reliable low-latency communications (URLLC): This service area refers to use cases that require high network reliability, more than $99,999\%$, and extremely low latency of approximately 1 millisecond for data transmission. Such stringent requirements are critical for scenarios with high accuracy and mission-critical services, and could set up the conditions for various potential applications, such as autonomous vehicles or emergency systems.

- Massive machine-type communications (mMTC): This use case is closely linked to the IoT concept and focuses on providing connectivity to a massive number of low-cost, low-powered devices and sensors. This service area caters to several application scenarios, including intelligent agricultural systems and smart cities.

2

Based on the aforementioned use cases, 5G networks target to provide a 1000-fold network capacity increase compared to the previous 4G systems [5]. Towards achieving this goal, Shannon's capacity theorem is a crucial indicator for understanding and optimizing the performance of 5G networks. In general, Shannon's capacity theorem defines the maximum amount of information that can be sent over a noisy communications channel with a specified bandwidth. In other words, it sets the theoretical upper limit on the achievable data rate over any communications channel, which is given by the following formula

$$C = m\frac{W}{n}\log(1 + \text{SINR}) \text{ bits/s,} \tag{1.1}$$

where W denotes the available bandwidth, n corresponds to the number of users connected to the same base station (BS), m denotes the number of spatial streams between the BS and the user(s) and SINR is the achieved signal-to-interference-plus-noise ratio [6]. Based on the above expression, it is observed that the network capacity can be increased by improving the *spectral* (SINR, m), *spectrum* (W) or *spatial efficiency* (n). Considering these areas of improvement, several new technologies and protocols have been proposed for the deployment of 5G networks, aiming to increase the capacity and meet the targeted performance requirements. Specifically, for increasing the spectral efficiency the deployment of massive multiple-input multiple-output (MIMO) systems has been proposed, where the transmitter and/or receiver use antenna arrays with hundreds of antennas simultaneously [7–9]. The capacity of wireless networks can be also enhanced by increasing the available bandwidth. In 5G networks, a shift towards the millimeter-Wave (mmWave) spectrum has been considered, ranging from 30 GHz to 300 GHz, offering great opportunities for bandwidth expansion [10, 11]. Finally, significant performance improvement is achieved through network densification, which enables a larger number of small cells to be deployed for cellular networks, increasing the overall space [12, 13].

Although the commercial deployment of 5G networks is still in progress, early discussions on the forthcoming development in the area of wireless technologies and the potential applications that could be integrated imply that 5G networks are very likely to reach their limits by the beginning of the next decade. It is expected that in the following years the concept of IoT will take a further leap towards the Internet of Everything (IoE), which will enable a massive number of intelligent connections between people, processes, data and things [14, 15]. Moreover, numer-

3
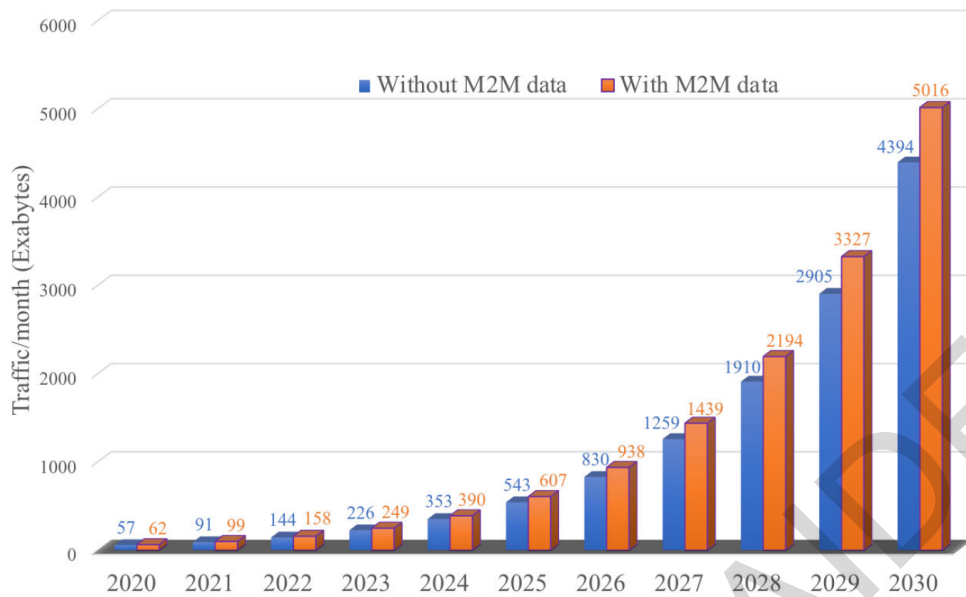
Figure 1.1: Global mobile data traffic forecast by ITU [17].

ous emerging services and applications are envisioned to become available through wireless communications, such as high-quality three-dimensional (3D) video, tactile internet, virtual reality (VR), augmented reality, autonomous systems and remote surgery [4, 15–17]. All the above are only some indicative scenarios highlighting the demanding traffic content that future networks will experience. According to the ITU, the overall mobile data traffic is estimated to reach 5 zettabytes per month in 2030 [18] (see Fig. 1.1). It is therefore apparent that the future requirements in latency, reliability and data rate will be beyond the capabilities of the current 5G systems.

In order to meet these requirements, research in both industry and academia has already shifted its focus towards the next generation of wireless communications, the so-called sixth generation (6G), and several institutions started exploring the key characteristics of the new era in communications [19]. It is envisioned that 6G will realize a paradigm shift in the way wireless networks are designed, transforming from machine and human-centric connectivity to connected intelligence. It will also enable the combination of physical and virtual environments in a unified framework with advanced communication, sensing and computing capabilities. In comparison with the 5G networks, the key performance indicators (KPIs) of the 6G era will be substantially improved to support future demands, as it is also shown in Fig. 1.2. Specifically, 6G wireless communication networks are expected to support data rates up to 1 Tbps, with extremely high reliability and 10 times lower latency, compared

4
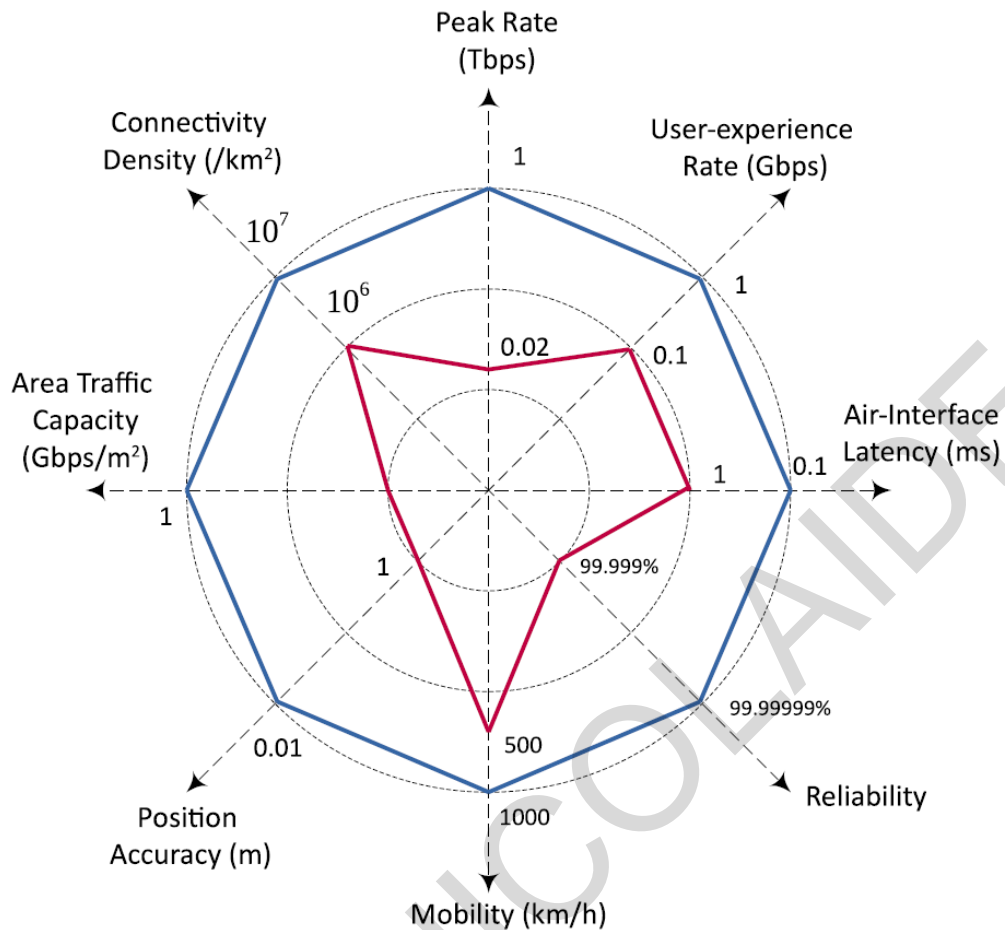
Figure 1.2: A comparison between 5G (inner polygon) and 6G (outer polygon) networks for eight KPIs [4].

to 5G networks. Moreover, given that 6G systems are envisioned to support IoE and smart cities, the connection density could be 10 times higher than the target of 5G, with much better position accuracy. Finally, energy efficiency will be a core component for 6G networks, both in terms of power consumption per device and transmission efficiency [4, 15–17].

The above specifications set the basis for 6G networks that will lead to the vision of intelligent and ubiquitous connectivity. Towards this direction, several emerging technologies are currently being studied as potential enablers of 6G, with most distinctive examples the technological advances in artificial intelligence (AI), as well as the employment of higher-spectrum communications, such as Terahertz (THz) communications and visible light communications (VLC) [15–17]. However, although significant advances in wireless technologies have been made to meet the challenging requirements of future networks, the wireless propagation environment is still a crucial bottleneck for the efficient deployment of 6G communications. Its

unpredictable nature and its sensitivity to blockages, especially at high operating frequencies, can severely affect the availability of wireless connectivity, resulting in high performance degradation. It is therefore essential for the next generation of wireless communications to provide solutions that can jointly tackle the stringent network demands and limit the negative effects of the propagation channel in a holistic fashion.

Towards this direction, multi-hop relaying and reconfigurable intelligent surfaces (RISs), also called intelligent reflecting surfaces (IRSs), are regarded as key enabling technologies that can assist the communication and realize uninterrupted wireless connectivity, by providing alternative propagation paths between the nodes of a communication system [20,21]. These two concepts have been identified as promising low-cost solutions, which can help the connection of a large number of devices and enhance the performance of 6G networks by extending their coverage capabilities and improving their scalability, flexibility and efficiency. However, in order to provide sufficient performance gains, the employment of multiple relays with broadcast capabilities or large surfaces may be required. In such scenarios, the complexity of their employment becomes significantly high, especially in terms of the required training overhead and the number of wireless links that need to be handled, which may constrain the potentials of the aforementioned assisting technologies. As such, we need to develop smart and flexible solutions to reduce the implementation complexity of such networks and maintain a sufficient performance, based on the network requirements.

1.2 Thesis Outline and Contributions

Motivated by the above challenges, this thesis presents low-complexity protocols designed to improve the performance of relay-assisted and RIS-assisted wireless networks. By leveraging tools from information theory and probability theory, we establish analytical frameworks to evaluate the performance of the proposed protocols and we investigate the fundamental limits of the considered communication paradigms in terms of the achieved signal-to-noise ratio (SNR), outage probability or diversity-multiplexing tradeoff (DMT). The outline of the thesis, along with the publications supporting the contributions of each chapter, is as follows.

In Chapter 3, we propose a novel cooperative protocol for a multi-hop network

in which the participating relays have buffers of finite size and may support different communication modes. The protocol is based on the myopic strategy, where each transmitter forwards data to a limited number of subsequent nodes. Each relay stores in its buffer the messages that were successfully decoded, in order to forward them through the appropriate channel links, based on its supported communication modes. With this protocol, we provide a fundamental approach on how the flow of information from source to destination can be conveyed, based on the status of the buffers and the communication capabilities of each relay. For modeling the evolution of the buffers and the transitions at the operations of each relay we provide an elegant and flexible methodology by using a Markov chain (MC) formulation. Based on the state transition matrix and the related steady state of the MC, we investigate the performance limits of the proposed protocol under different design parameters. The material included in this chapter has been presented in:

[P1] A. Nicolaides, C. Psomas, and I. Krikidis, "Outage analysis of myopic multi-hop relaying: A Markov chain approach," in *Proceedings of IEEE Global Communications Conference*, Taipei, Taiwan, Dec. 2020.

[P2] A. Nicolaides, C. Psomas, and I. Krikidis, "A Markov chain approach for myopic multi-hop relaying: Outage and diversity analysis," *IEEE Journal of Selected Topics in Signal Processing*, Special Issue on Advanced Signal Processing for Local and Private 5G Networks, vol. 16, pp. 56–69, Jan. 2022.

In Chapter 4, we shift our focus on RIS-assisted wireless networks and we investigate the performance of a MIMO system assisted by an RIS under the employment of partition-based schemes for the RIS configuration. The proposed schemes have low implementation complexity and do not require any channel state information (CSI) knowledge at the transmitter side or for adjusting the reflection coefficients of the elements, which makes them attractive for practical applications. In particular, the RIS is partitioned into non-overlapping sub-surfaces, which are periodically modified in an efficient way to assist the communication between the transmitter and the receiver. Under this framework, two low-complexity partition-based schemes are proposed, where each sub-surface is adjusted by following an amplitude-based or a phase-based approach. As such, a parallel channel in the time domain is created, which can provide higher diversity gains. Based on the presented framework, we

study the fundamental limits of the proposed schemes from a communication theory standpoint and obtain useful insights on how various parameters affect the performance of the considered system. The content of this chapter has been published in:

[P3] A. Nicolaides, C. Psomas, G. Kraidy, and I. Krikidis, "A partition-based scheme for IRS-aided MIMO fading channels: Outage and DMT analysis," in *Proceedings of IEEE International Symposium on Information Theory*, Espoo, Finland, Jun. 2022.

[P4] A. Nicolaides, C. Psomas, G. Kraidy, S. Yang, and I. Krikidis, "Outage and DMT analysis of partition-based schemes for RIS-aided MIMO fading channels," *IEEE Journal on Selected Areas in Communications*, Special Issue on Beyond Shannon Communications: A Paradigm Shift to Catalyze 6G, vol. 41, no. 8, pp. 2336–2349, Aug. 2023.

In Chapter 5, we extend the approach of the previous chapter and propose a novel hybrid scheme for an RIS-aided wireless network, which requires channel estimation for only a subset of the elements. The proposed scheme partitions the RIS into two sub-surfaces, which are sequentially activated to assist the communication. The elements of the first sub-surface optimize their phase shifts, based on the acquired CSI from a channel training period, while the remaining elements randomly rotate the phase of the incident signals. Through this approach, the proposed scheme can significantly reduce the channel training overhead for the RIS configuration and can be easily adapted to several channel estimation methods. By studying the effect of an imperfect CSI scenario on the performance of the considered system, we provide a tradeoff between the number of elements that we need to consider for channel estimation and the resulting training overhead, in order to optimize the performance of the considered system. The material included in this chapter has been presented in:

[P5] A. Nicolaides, C. Psomas, S. Yang, and I. Krikidis, "A hybrid scheme for reconfigurable intelligent surfaces: How many elements should be estimated?," in *Proceedings of IEEE Global Communications Conference*, Kuala Lumpur, Malaysia, Dec. 2023.

Table 1.1: Assisting technology and performance metrics studied in each chapter

	Ch. 3 [P1, P2]	Ch. 4 [P3, P4]	Ch. 5 [P5]	Ch. 6 [P6]
Multi-hop relaying	✓	-	-	-
RIS	-	✓	✓	✓
CSI knowledge	Yes	No	Limited	No
Outage prob./SNR gain	✓	✓	✓	✓
DMT	✓	✓	-	-

In Chapter 6, we introduce an alternative utilization of the RIS in wireless communications. Specifically, we propose a novel technique where the RIS acts as an enabler for the efficient application of the time reversal (TR) transmission scheme. In general, TR is a signal processing technique that takes into advantage the multipath environment occurring in high-frequency wideband communications, in order to achieve energy focusing on both time and space domains. However, the efficiency of this technique requires a rich scattering environment. In this chapter, we focus on a TR scheme facilitated by an RIS which, due to the higher frequency and large array aperture, operates in the near-field region. The RIS is employed to artificially enrich the propagation environment for the TR. The proposed scheme is mutually beneficial to the RIS since we do not need to provide accurate CSI knowledge for its configuration. By considering near-field channels, we derive a performance bound for the proposed RIS-enabled TR scheme and we examine the effect of various design parameters on the system's performance. The content of this chapter has been included in:

[P6] A. Nicolaides, C. Psomas, and I. Krikidis, "An RIS-enabled time reversal scheme for multipath near-field channels," *IEEE Communications Letters*, under review.

Finally, in Chapter 7 we conclude this thesis and discuss possible directions for future works.

Table 1.1 outlines the considered assisting technology and the most important attributes of the analytical framework that are adopted in each technical chapter of this thesis. The overall contribution of this thesis is the design of novel and flexible schemes with reduced computational complexity, based on sophisticated communication theory and signal processing techniques, that can enhance the performance

of relay-assisted or RIS-aided systems, and the investigation of their fundamental limits. Specifically, the main contributions of the thesis are summarized as follows:

- One of the principal novelties of the thesis is the conceptualization of sophisticated solutions for the efficient integration of multi-hop relaying and the RIS technology in wireless systems, that can be implemented with reduced computational complexity and can still boost the performance. Moreover, in every communication scenario under study, the proposed schemes have been designed to provide high flexibility, adjustability to the available resources and to be easily scalable.

- Since the availability of the CSI knowledge in such networks usually incurs high training overhead, which is considered to be a bottleneck for the overall performance, in most works of the thesis the presented solutions have low-to-zero CSI requirements. Even in Chapter 3, where (global) CSI is assumed to be perfectly known, the proposed myopic-based protocol can adapt, in practice, the degree of cooperation between the participating nodes to the available resources in order to achieve a balance between the channel estimation process and the system performance.

- In all the presented works, we provide a complete analytical methodology for the investigation of the performance gains of the proposed schemes, by deriving useful theoretical expressions in terms of the SNR gain at the receiver, the outage probability or the achieved DMT. Through the presented analysis, we aim to explore the fundamental performance limits of all the proposed schemes based on the specific assumptions and channel models considered in each chapter. In addition, we provide useful insights on how some key design parameters affect the potential performance gains of each scheme.

As such, the contributions of this thesis can be of particular importance, since the proposed solutions can have a significant impact on the deployment of wireless systems assisted by the employment relays and RISs. The presented schemes as well as their associated performance analysis can provide a thorough understanding of the actual behavior of such assisted-based networks, which will enable the potentials of truly intelligent and uninterrupted connectivity, leading to the design and realization of highly efficient wireless networks in the 6G era.

Chapter 2

Background

The concept of relaying and the employment of RISs have been identified as two of the most appealing technologies for assisting the connectivity between several nodes in a wireless system, by generating different communication paths for data transmission. The utilization of these two technologies can therefore improve the efficiency of wireless networks by increasing their coverage and enabling the connection between a large number of devices. However, the integration of relays and RISs in wireless systems entails some technical and design issues that need to be considered. In this chapter, we present an overview of the fundamental features and the potential benefits of relay-aided and RIS-aided communications, along with a detailed literature review. We also refer to the main challenges that need to be resolved for the efficient deployment of each technology.

2.1 Relay networks

Up until recently, wireless systems have mainly followed a centralized scheme of connectivity through the deployment of cellular networks, where users connect exclusively through their nearest BSs. However, the rapid increase in data-traffic consumption by cellular users caused this connectivity approach to reach its fundamental limits. Moreover, the emergence of IoT applications and its envisioned transition towards the concept of IoE, is expected to further stress current connectivity solutions. In order to provide seamless connectivity to support a large number of devices, fading is an important factor that needs to be addressed, as it shortens the delivery distance in wireless systems. As such, future generations of wireless

communications need to adopt new connectivity schemes to meet the challenging network demands. Towards this direction, relay networks are regarded as an appealing solution which can provide uninterrupted connectivity for a massive number of devices and extend the coverage area of wireless networks.

2.1.1 The classical relay channel and multiple-relays extensions

As a concept, the idea of relaying in wireless communications has been known for a long time. The traditional two-hop relaying scheme was initially introduced and investigated in the seminal work of Van der Meulen in 1971 [22]. In general, the classical relay channel considers a set of three nodes, the source-destination pair and an intermediate node called "relay", which is used to assist the communication between the source and the destination. The distinctive property of the relay channel is that this additional node receives the transmitted signal from the source node, processes the received signal and re-transmits the processed signal to the destination. Although relaying technologies have been actively studied in the past, due to the recent technological advances and the need for low-cost and flexible solutions for addressing the challenges of 5G and 6G networks, relay-assisted communications have re-gained considerable attention by the researchers in the last few years [23,24].

To fully exploit the potential benefits of relay-based networks in wireless communications, advanced cases of the classical relay channel can also be considered through the employment of multiple relaying nodes. An advanced relaying technique that has received considerable attention is *multi-hop relaying*. In this case, multiple relays cooperate through a single transmission path to forward the information to the final destination node [20,25]. By breaking a long-distance low-quality link into more high quality segments, multi-hop relaying can be used to enable the communication between nodes in much greater distances. This approach has therefore numerous benefits, which favor its implementation in future wireless networks. First of all, multi-hop relaying can increase the network's coverage and capacity, since it enables connectivity for users with limited or no access to a BS [26]. Moreover, this approach provides higher reliability, due to the reduced path loss between the nodes, and benefits from better fairness in resource allocation and enhanced energy efficiency. Due to the easily distributed deployment of relaying nodes, multi-hop relaying is also advantageous in terms of scalability and flexibility. Finally, a multi-

hop topology can efficiently support tremendous access, which is appealing for IoT applications [26].

Although the idea of multi-hop relaying has several benefits, enabling the connectivity between the participating nodes over only a single transmission path does not exploit the broadcast nature of wireless communications and remains sensitive to random obstructions that can interrupt the connectivity towards the end user. For this, *cooperative diversity* is another relaying technique that has been considered as an appealing solution to significantly improve the networks' reliability. In this case, a wireless system employs multiple relays in dual-hop or multi-hop scenarios to enable broadcast transmission of the signals [27]. With this approach, the system becomes more robust to obstacles, since a larger number of propagation paths is generated. Moreover, the system's spectral efficiency is significantly improved by the exploitation of spatial diversity among the participating nodes [28].

2.1.2 Relaying schemes

A relaying scheme refers to the method of processing that is performed at the received signal by the relay node before the re-transmission. The main objective of this operation is to improve the quality of the received signal at the destination. Below, we provide the main relaying schemes that have been proposed in the literature.

Amplify-and-Forward (AF)

In this scheme, the received signal at the relay is simply amplified and re-transmitted to the destination (see Fig. 2.1a) [27]. The main advantage of the AF strategy arises from the fact that, apart from the amplification process in the analog domain, no further signal processing is required at the relay. As a result, this scheme benefits from its low implementation complexity and low energy consumption. However, with this approach the received noise, as well as any potential interference, is also amplified and forwarded to the destination. Therefore, the AF scheme can be considered in scenarios where the received signal power at the relay node is significantly stronger than the received noise.

13
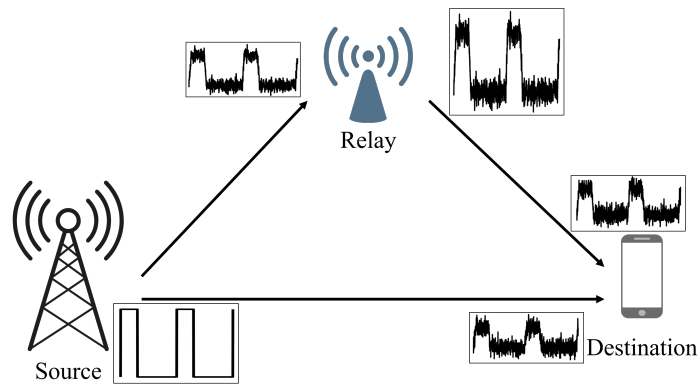
(a) Amplify-and-Forward
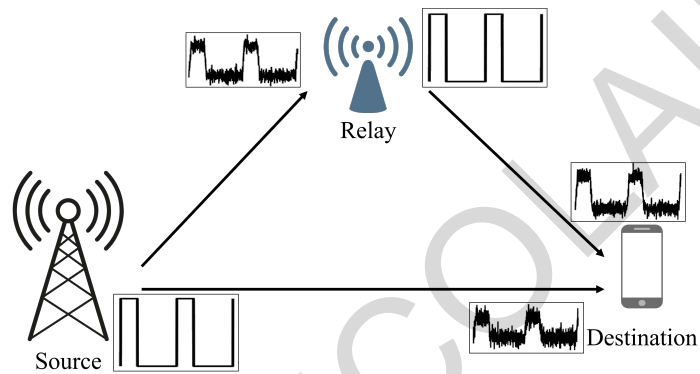
(b) Decode-and-Forward

Figure 2.1: The two most widely used relaying schemes, AF and DF.

Decode-and-Forward (DF)

In the DF scheme, the relay performs a two-task operation: it first decodes the received signal and then re-encodes the acquired data to forward it to the destination (see Fig. 2.1b) [27, 29, 30]. Compared to the AF scheme, DF can provide higher throughput, since the received noise and the impairments of the source-relay channel can be eliminated at the decoding phase of the relay [31]. On the other hand, due to the more advanced signal processing that is required to successfully estimate the message, the DF scheme has a significantly higher implementation complexity, while the power consumption at the relay is also increased.

Compress-and-Forward (CF)

The main idea of the CF scheme is that, the relay creates a quantized and compressed version of its own received signal via the use of an independent codebook, which then forwards to the destination [29, 30]. The compression performed at the relay

is usually achieved through the Wyner-Ziv coding, i.e., lossy source coding [32]. The destination then tries to decode the signal that was directly received through the source-destination link, by using the compressed signal forwarded by the relay as side information. Even though the CF scheme can reduce the bit error rate, depending on the number of quantization levels, its implementation complexity is significantly higher and its extension to multiple relays is a non-trivial task [30].

Rotate-and-Forward (RF)

The RF scheme can be performed in cooperative diversity networks where the intermediate layer has at least two relays. For this scheme, no within-layer cooperation is considered and the relays can simultaneously re-transmit their signals to the destination. The main idea of the RF is that each relay forwards to the destination a rotated version of its own received signal, according to a preassigned distributed rotation sequence [33]. This time-varying rotation can recover spatial diversity, which provides significant performance gains compared to other relaying schemes in similar scenarios.

2.1.3 Duplex modes in relay networks

When we refer to the duplex mode of a relay node, we indicate the way the relay is able to receive and transmit information. In general, a relay can operate in either *half-duplex* or *full-duplex* mode. Each mode of operation has different hardware requirements and affects the overall performance of the network. Below, we provide a more detailed description of the two duplex modes.

Half-duplex

If a relay operates in half-duplex mode, the reception and the transmission of the signals at the relay occur at different (orthogonal) channels. In other words, the source-to-relay and the relay-to-destination channels are kept orthogonal, through either frequency or time division multiplexing, so that the relay can separately receive data from the source and re-transmit it to the destination [20, 34]. This approach is widely used in relay-aided communication systems due to its low complexity in terms of hardware implementation. However, the use of orthogonal channels for relaying the signals results in reduced spectral efficiency.

Full-duplex

When a full-duplex relay is employed, only one channel is utilized for the end-to-end transmission. Specifically, in this case both the source and the relay share a common time-frequency space, so that the relay can simultaneously receive data from the source and re-transmit information towards the destination [20, 34]. The main advantage of this mode is the improvement of the spectral efficiency compared to the half-duplex mode due to the single channel use. On the other hand, in practice the employment of full-duplex relays is difficult to be achieved. This is due to the self-interference (SI) observed at the receiving antenna of the relay caused by the transmitting antenna of the same node, which significantly affects the reliability of the system and cannot be eliminated completely. In the last decade, there has been a lot of research interest on the SI mitigation by proposing various analog and digital cancellation techniques [35, 36]. Recent advancements in this area reveal that up to 120 dB of SI cancellation can be achieved, making the full-duplex mode an appealing solution for future 6G networks [35, 36]. Still, full-duplex relays lead to increased hardware complexity, compared to half-duplex relays, and require advanced signal processing techniques for their realization.

2.1.4 Related works

Motivated by the numerous benefits of relay-aided networks, several studies have investigated the performance of wireless systems assisted by a single relay (dual-hop relaying). More specifically, the single-relay channel was firstly introduced by Van der Meulen [22], while Cover and El Gamal significantly contributed to the performance evaluation of such channels, by studying the capacity of degraded, reversely degraded and feedback relay channels [29]. The end-to-end performance of a dual-hop network with fixed gain relays was also analyzed in [37], by providing closed-form expressions for the outage probability and the average probability of error. In addition, [38] extended the classical dual-hop relaying to a generalized model with hardware impairments.

Other studies extended this approach to multi-hop schemes. In [39], the outage probability performance of a multi-hop system over Nakagami fading channels was studied. In addition, the authors in [40] presented a new protocol for half-duplex multi-hop relaying networks based on the concept of buffer-aided relaying and

investigated the corresponding achievable rates. Multi-hop relaying has been also proposed to assist connectivity for mmWave communications [41, 42], a technology that is considered as one of the main components of 5G networks, but is highly susceptible to path blockage. In particular, [41] investigated a joint scheduling and congestion control policy in multi-hop mmWave networks, in order to maximize the throughput under fairness requirements. On the other hand, the connectivity of mmWave networks with multi-hop relaying was analyzed in [42] by considering a stochastic geometry approach, where the obstacles are modeled as a Boolean model.

Cooperative diversity has also attracted the interest of the research community and several solutions have been proposed and analyzed in the literature. In the seminal work in [27], Laneman *et al.* proposed several techniques of cooperative communication, such as selection relaying and incremental relaying, and investigated their outage performance. Moreover, the authors in [28] studied general cooperating setups, consisting of multiple transmission paths that include an arbitrary number of cooperating hops, and derived asymptotic expressions for the average symbol error probability. These setups consisted of either a single relay or multiple relays in parallel transmission paths.

Cooperative diversity schemes have also been studied in multi-hop relaying systems. Specifically, a cooperation scenario for multi-hop networks was introduced in [43], where it has been shown that the spatial diversity gain could be achieved by combining at each node the signals that have been concurrently sent by all the preceding terminals along a single transmission path. Based on this idea, in [44], a class of cooperative diversity protocols was proposed, where each relay combines the signals received from an arbitrary number of previous nodes. The authors proved that this class of cooperative protocols can achieve the same diversity gain as [43]. Significant diversity gain can be also achieved, according to [45], if we consider a multi-hop buffer-aided system, where every relay has a buffer of sufficient size and at each time-slot a stored packet is transmitted over the best hop, based on the received SNR. Furthermore, in [46], the maximum diversity and multiplexing gain, as well as the achieved DMT of various multi-hop cooperative network topologies are characterized. The DMT was also investigated in [47] for MIMO multi-hop relay channels, and various space-time relay processing schemes were proposed to increase the diversity gain by creating a parallel channel in the time domain.

2.1.5 Potential applications in 5G/6G networks

Due to the aforementioned benefits, relay-assisted communications and multi-hop connectivity networks can be utilized in several application scenarios, towards the deployment of 5G networks and future 6G communications. In what follows, we briefly present some potential use cases which can benefit from the integration of a multi-hop relaying topology.

- **Device-to-device (D2D) communications:** In future 6G, D2D communications will be a key element for increasing spectral efficiency and providing traffic offloading. With D2D communications, the information is transmitted through a direct link between the users, without the involvement of a BS. Integrating the idea of multi-hop relaying in D2D communications could provide several new opportunities for next generation wireless networks. Specifically, several devices could act as relays creating a D2D path for transmitting information among the users in a decentralized fashion [26,48]. Such approach can enhance the connectivity among the users with higher quality of service (QoS) and better energy efficiency.

- **mmWave and THz communications:** One of the main challenges that future wireless systems need to resolve is the scarcity of the available spectrum in the conventional sub-6 GHz frequency band used for the operation of wireless networks. To satisfy the bandwidth requirements of the 6G application scenarios, a shift to higher frequency bands has been recently proposed, such as the mmWave band, ranging from 30 to 300 GHz, and the THz band, with frequencies from 0.1 to 10 THz, in order to surpass the spectrum shortage of the current systems [11, 49]. Due to the more abundant spectrum resources and the ability to provide much higher transmission rates, mmWave and THz communications have attracted significant attention by the researchers [50,51]. However, this type of technologies suffers from serious path attenuation and is highly susceptible to path blockage, which makes their efficient implementation a challenging task. Multi-hop relaying can assist connectivity in higher spectrum networks, as it can provide alternative Line-of-Sight (LoS) paths between the transmitter and the receiver [41, 52].

- 4-**Tier coverage:** Future generations of wireless communications will have to

provide ubiquitous connectivity not just to terrestrial networks. It is envisioned that 6G networks will integrate all network tiers: space, air, terrestrial, and under-sea. In order to extend the coverage and provide reliable connectivity in every tier, relay-assisted networks can be a promising approach. For example, multi-hop networks could assist the connectivity in underwater communications for various applications, such as search and rescue missions, as underwater optical wireless networks have limited range [53], [54]. Air-to-ground networks could be also deployed via multiple devices that act as relays, e.g., unmanned aerial vehicles (UAVs), especially in cases where the available infrastructure is insufficient [55]. Finally, terrestrial networks can be assisted by the employment of satellites for relaying information in scenarios where terrestrial relays cannot be deployed [56].

2.1.6 Standardization of relay networks

The idea of relaying has widely been considered as a concept that has the potential to increase the coverage and capacity of cellular communications, such as during the development of Worldwide Interoperability for Microwave Access (WiMAX) by the Institute of Electrical and Electronics Engineers (IEEE), and has been standardized by the 3rd Generation Partnership Project (3GPP) for the Long Term Evolution-Advanced (LTE-A) towards 4G mobile networks. Specifically, the IEEE 802.16j-2009 standard incorporated the use of two types of relays for multi-hop relaying in WiMAX-based networks, namely the transparent and non-transparent relays, with different characteristics in terms of scheduling capabilities and implementation complexity [57]. Based on the relay functionalities specified in this standard, in the IEEE 802.16m standard the considered advanced relay stations use a DF relaying scheme and support time-division and frequency-division duplex modes [58].

The 3GPP has introduced the concept of relay nodes for cellular communications in Release 10 of LTE standards and classified the relays as layer 1, layer 2 and layer 3 relays [59]. A layer 1 relay works only at the physical layer acting as a repeater with AF capabilities. On the other hand, layer 2 relays employ the DF relaying scheme, while the layer 3 relay is similar to the layer 2 case but it acts like an LTE BS. The concept of relaying has been also considered by the 3GPP for D2D communications. In particular, following the standardization of D2D communication in the 3GPP

Release 12 [60], the 3GPP Release 13 enhanced the D2D communication with the user equipment (UE)-to-Network relaying scenario [61]. Further enhancements of the UE-to-Network relaying included initial scenarios and requirements for IoT devices and wearables in the 3GPP Release 14 [62], while several key issues regarding the architecture of the UE-to-Network relaying were addressed in the 3GPP Release 15, like security and service continuity [63]. Finally, the 3GPP Release 17 defined an architecture and a protocol stack for the UE-to-UE relaying use-case of the D2D communications [64].

2.1.7 Challenges for relay networks

Based on the aforementioned use cases, it is envisioned that relay networks, and especially multi-hop relaying systems, will be a core technology in the deployment of wireless networks in the near future. However, important challenges regarding the deployment of relay-assisted networks are still to be addressed. In what follows, we mention two major challenges related to the implementation performance of wireless networks assisted by multi-hop relaying and their efficient design from a communication theory standpoint.

Performance limits of multi-hop relaying

Although multi-hop relaying has been a popular area of investigation for wireless communications and several studies consider this approach, the fundamental performance limits of multi-hop networks are yet to be found. In particular, the exact capacity of a general multi-hop relay network has not been provided yet. Even for the single relay network, the derivation of the exact system's capacity still remains an open problem, while to this day the proposed solutions can only provide theoretical upper bounds for this problem [65, 66]. Therefore, further research efforts are required in order to provide better knowledge on the true capabilities of multi-hop relaying systems.

Multinode coordination

Another challenging task is the efficient design of relaying protocols to ensure that the final destination is able to receive information with high QoS. In general, although multi-hop relaying over a single transmission path can enhance the reliability and

20
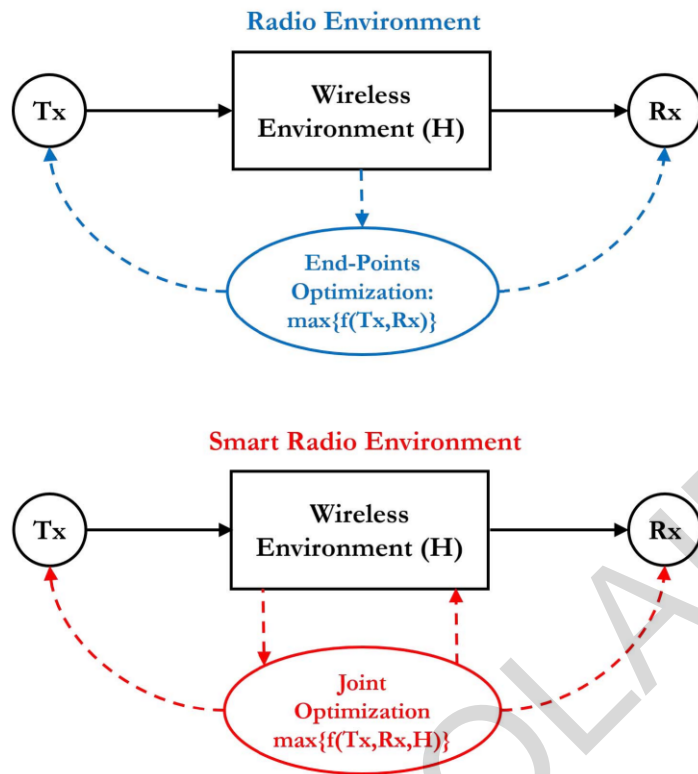
Figure 2.2: The concept of smart radio environments [68].

coverage of wireless networks, it ignores the broadcast nature of wireless communications, while connectivity interruptions are still possible. By enabling the participating nodes to cooperate with more than one relay, significant performance gains can be achieved through spatial diversity [43]. However, with this approach the overall data traffic in the network is increased, which results in higher implementation complexity due to multinode coordination, power control and interference management.

2.2 Reconfigurable intelligent surfaces

In current wireless communication systems, the capacity of the networks is still limited by the uncontrollable nature of the channel environment. Moreover, multipath propagation resulting in fading phenomena and reflections or refractions from several objects causing unpredictable interference has usually a negative effect on the communication efficiency and the QoS. Most of the available solutions that are currently being used, such as MIMO techniques, consider the channel environment as an inevitable limitation, and either counteract or exploit its effects without changing its behavior [67]. As such, one of the principal visions towards the realization of

21

future communication networks is to incorporate the wireless environment, along with the transmitters and receivers, as part of the optimization process that can be programmed and controlled (see Fig. 2.2). By customizing the channel environment and turning it into a smart radio environment (SRE), through the control of the propagation of radio waves, the environment can become an active component for transferring and processing information in wireless systems [68]. During the past few years, the concept of RIS has been proposed as an appealing solution to realize the vision of SREs, as it can be used to reconfigure the wireless propagation environment in an intelligent and low-cost fashion, by controlling the radio waves striking its surface [69]. Due to its capability to modify the wireless channel, the RIS can enable ubiquitous connectivity and significantly improve the performance of wireless systems.

2.2.1 Fundamentals of RISs

In view of the aforementioned requirements and challenges derived from the current and future wireless systems, RIS has emerged as a promising new paradigm for the deployment of intelligent information networks, aiming to assist the connectivity between a large number of devices. In general, an RIS is an inexpensive thin planar surface that can be controlled with integrated electronics to modify the incident signals in a favorable way to improve the QoS of the system [21, 68, 70]. In the most commonly considered case, the RIS is equipped with a large number of (nearly) passive tunable elements that can be actively controlled through external stimuli to individually alter the reflection/refraction amplitude and/or phase of the incident signals [71, 72]. Therefore, the most prominent property of the RIS is its capability of being reconfigurable after its deployment in a wireless network, based on the dynamic nature of the wireless environment. Through this approach, the RIS can support several functions to improve the performance of wireless networks, such as creating multiple virtual LoS paths that can be smartly controlled to bypass obstacles between transceivers, focusing incident signals towards a desired direction to improve signal strength, as well as mitigating co-channel or inter-cell interference [71].

The core notion behind this technology is the concept of metasurfaces. A metasurface is a man-made surface made of electromagnetic (EM) material which is

specifically designed to exhibit properties that cannot be found in naturally occurring materials [68,69,73]. It consists of a large array of passive elements (also called meta-atoms), with electrical thickness in the order of the sub-wavelength of the operating frequency of interest, which can be digitally controlled. Through this control, the physical properties of the elements can be altered, resulting in the incident signals to be adjusted [73,74]. Depending on the properties of the elements, the metasurfaces can achieve various tunable functions in order to control the EM waves [68,75]. Some of the most widely considered tunable functions are the following:

- *Anomalous reflection* [76,77]: the elements act as reflectors to enable the communication between devices on the same side of the surface by controlling the impinging signals towards a desired direction.

- *Anomalous refraction* [78,79]: the communication occurs at the two sides of the surface, and the elements refract the incident waves in the desired direction by adjusting their phase as they pass through the surface.

- *Absorption* [80,81]: the elements are intelligently designed to null, for a given incident radio wave, the radio waves that are reflected or refracted. This function can be applied in scenarios where interference suppression is required.

Through this adaptive reconfiguration of metasurfaces, the RIS provides a new perspective to further enhance the wireless communication performance. Among the possible tunable functions, the utilization of the RIS to perform anomalous reflection in wireless communications has mostly attracted researchers' interest. Henceforth, this thesis will focus on RIS-assisted networks where the elements of the RIS are controlled to reflect the radio waves.

Due to its simple operation, an RIS possesses several practical advantages which advocate its integration in future implementations of wireless networks [21,71,72]. One of its main benefits arises from the passive nature of the reflecting elements. Since the elements only passively reflect the signals, the RIS does not require any dedicated energy source for data transmission, promoting its deployment as an energy efficient solution. Moreover, the RIS operates in ideal full-duplex mode, without introducing nor amplifying any additional noise to the reflected signal, which enables higher spectral efficiency. RIS is also a cost-effective alternative, since it benefits from the use of inexpensive passive scattering elements embedded in the
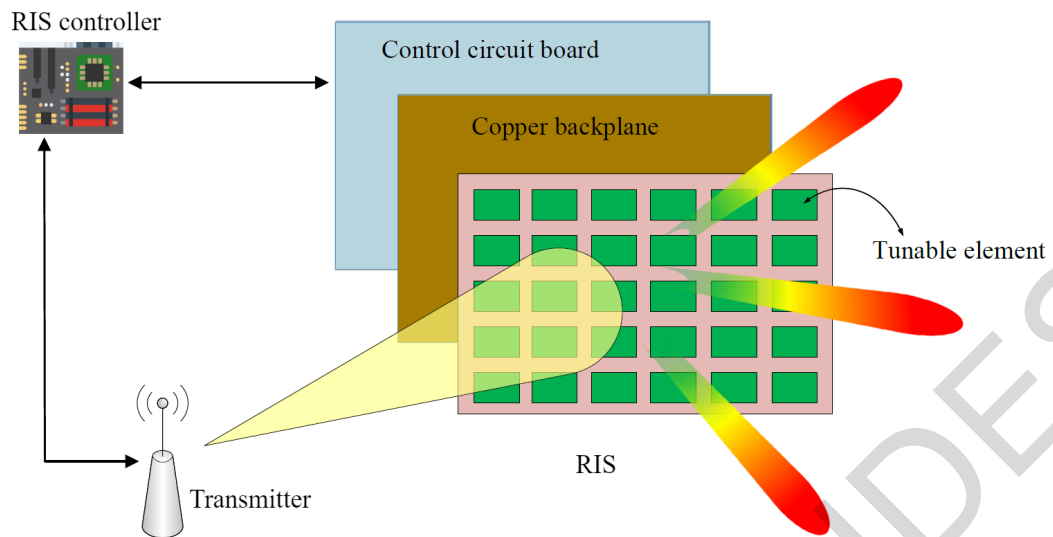
Figure 2.3: Structure layers of a typical RIS architecture [71].

metasurface. Finally, the RIS can be easily deployed on several environment objects (e.g. building walls or billboards) and provides great flexibility and compatibility with existing wireless systems. All of the above features showcase RIS as a key candidate technology for assisting the communication and improving the performance of wireless networks.

2.2.2 RIS Architecture

A typical architecture of an RIS consists of three layers and a smart controller, as it is illustrated in Fig. 2.3 [71, 72]. The outer layer is equipped with a large number of metallic tunable elements, which are printed on a dielectric substrate in order to have a direct interaction with the incident signals. The second layer is a copper plate and is utilized to stop the incident radio wave from penetrating the panel, i.e., for the minimization of the signal energy leakage during the RIS reflection. The last (inner) layer consists of a control circuit board that is used to adjust the reflection coefficient of each element. The control circuits are triggered by the smart controller attached to the RIS. Specifically, based on the input that each circuit takes from the controller, the response of the circuit is accordingly formed so that the corresponding elements on the outer layer will induce a specific change on the incident radio wave.

In practice, the smart controller that is connected to the RIS is typically implemented using field-programmable gate array (FPGA) boards. The controller is also usually used as a gateway to communicate and coordinate with other network de-

vices, such as BSs and user terminals [72]. Moreover, each RIS element should be able to modify its reflection amplitude and/or phase shift in real time. Several approaches have been proposed towards this direction, with the use of electronic devices being the most widely adopted solution, due its fast response time, low reflection loss and relatively low energy consumption. For example, an RIS element can be tuned with the help of an embedded positive-intrinsic negative (PIN) diode, that can be switched between the ON and OFF states by applying different direct-current (DC) voltage to generate a phase shift difference of π [82]. Other example designs for the elements' structure include the use of field-effect transistors or micro-electromechanical system switches.

2.2.3 Related works

Motivated by the aforementioned promising advantages, the use of RISs has been considered in several applications, and the performance of RIS-aided wireless networks has been investigated for various communication scenarios. Specifically, the authors in [83] studied the performance of a single-input single-output (SISO) system and provided tight closed-form approximations for fundamental metrics such as the ergodic capacity and the outage probability. In [84], the system performance of RIS-aided orthogonal multiple access (OMA) and non-orthogonal multiple access (NOMA) SISO networks was studied in terms of outage probability and ergodic rate. It was shown that such networks obtain significant performance gains with the employment of an RIS, which is superior to the use of full-duplex DF relays. Furthermore, the work in [85] proposed RIS-enabled random-rotation schemes for SISO networks, which can be implemented with limited or without CSI knowledge. It was demonstrated that the presented schemes improve the performance in terms of energy efficiency, outage probability and diversity gain. The diversity order achieved by an RIS-aided SISO system was also studied in [86], where the authors derived the minimum number of required quantization levels for the RIS discrete phase shifts to achieve full diversity. In [87], the authors introduced an RIS-assisted system for two-way communications and proposed two transmission schemes, for which they investigated the performance limits in terms of outage probability and spectral efficiency.

The employment of RISs has also been considered to assist the communication in

wireless networks with multiple antennas at the transmitter and/or the receiver. In particular, a single-cell wireless network, where an RIS is deployed to assist the communication between a multi-antenna access point (AP) and multiple single-antenna users, was investigated in [88]. It was demonstrated that the system's performance can be enhanced in terms of both spectral and energy efficiency, by jointly optimizing the active and passive beamforming vectors at the AP and the RIS, respectively. Furthermore, in [89] the RIS was considered for assisting NOMA communications, and it was demonstrated that RIS-assisted NOMA improves spectral efficiency and can be used to serve additional users. The implementation of RISs has been also considered under index modulation schemes, enabling simultaneous passive beamforming and information transfer of the RIS in multiple-input single-output (MISO) systems [90, 91]. Specifically, in [90], the authors introduced an amplitude-based scheme, called the reflection pattern modulation (RPM) scheme, where the joint passive beamforming and information transfer occurred by activating different subsets of elements at the RIS. It was shown that the presented approach achieves great improvement of the achievable rate performance. In [91], an RIS reflection modulation scheme was proposed, referred to as the quadrature reflection modulation (QRM) scheme, which was proven to outperform the RPM scheme. Moreover, a multi-hop RIS-enabled scenario was considered in [92], where multiple RISs were deployed to assist the communication between a multi-antenna AP and multiple users with single antennas, in order to improve network coverage of THz communications.

The fundamental capacity limit for an RIS-aided MIMO network was provided in [93], by developing algorithms for jointly optimizing the RIS reflection coefficients and the transmit covariance matrix. The same optimization parameters were also considered for multi-cell communications in [94], where the weighted sum-rate of a multi-cell multi-user MIMO system was enhanced by employing an RIS at the cell boundary. Furthermore, the asymptotic performance of an RIS-aided MIMO channel was investigated in [95], where it was demonstrated that the achieved multiplexing gain can be enhanced if the information data stream is available both at the transmitter and the RIS. In [96], the authors provided a closed-form approximation for the outage probability of an RIS-aided MIMO system and proposed a gradient descent algorithm to minimize the outage probability with statistical CSI. In addition, they characterized the achieved DMT for a finite SNR regime. Furthermore, an opportunistic rate splitting scheme was proposed in [97] for an RIS-aided two-user

MISO system. In particular, by utilizing the RIS to modify the channel characteristics through an alternating CSI formulation, which was inspired by the information theoretic framework presented in [98], it was shown that the achievable rate of such systems can be improved.

2.2.4 Potential Applications in 5G/6G networks

Due to the numerous benefits associated with RIS-assisted intelligent connectivity, the concept of RIS is envisioned to be a core technology for various future applications of wireless networks. RIS-assisted communications can be used to significantly improve the performance and tackle the potential design challenges of other emerging technologies. As such, the employment of RISs in wireless networks is advocated as a promising solution for high-rate applications, such as high-quality video streaming, VR and augmented reality, while its potential gains can be also foreseen in the connectivity support of low-rate applications, such as massive IoT networks. In what follows, some example use cases are mentioned in which the RIS could play a fundamental role for providing extended coverage, enhancing the spectral and energy efficiency, or for reducing the implementation complexity and power consumption of wireless networks.

- **Massive connectivity:** The emergence of IoE will promote a rapid growth in IoT communication demand, and ubiquitous connectivity will be required for billions of physical devices in the near future. To address the enormous data rate demands, RISs can be used to assist the communication in massive IoT networks. Due to their large aperture and easy deployment on several environment surfaces (e.g. walls, ceilings etc.) such solution can increase the capacity and extend the coverage of IoT networks [99]. Moreover, RIS-assisted IoT networks can be used to create high-capacity hotspots for several scenarios, such as stadiums and shopping centers.

- **mmWave and THz communications:** As previously mentioned, mmWave and THz communications are considered as promising technologies to potentially increase spectrum efficiency in wireless networks. However, a critical challenge for their implementation is their high vulnerability to blockages. To address this issue, the communication with such technologies can be assisted

by the employment of an RIS [100–102]. Specifically, the RIS can provide an alternative virtual LoS path between the transmitter and a receiver possibly located in a dead zone, thus avoiding the obstacles between the two entities and extending the coverage of mmWave and THz communications.

- **Wireless power transfer:** Energy efficiency is expected to be one of the core requirements for the realization of future wireless systems. An emerging technology for addressing this challenging demand is far-field wireless power transfer (WPT), i.e., the transmission of energy through EM radiation. In particular, simultaneous wireless information and power transfer (SWIPT), where the transmitted signal is used to convey both information and energy, will be of critical importance in 6G networks, as it is envisioned to enable the massive deployment of IoT sensors and devices with a battery-less structure [17]. Due to the easily adjustable properties of its reflecting elements, the RIS can achieve high beamforming gain, which is a promising approach to drastically enhance the efficiency of SWIPT systems. As a result, some initial studies regarding RIS-assisted SWIPT networks have recently been made, focusing on the optimization of both the spectral and energy efficiency of such systems [103, 104].

2.2.5 Standardization of RIS

In recent years, the idea of employing an RIS for assisting the communication in wireless systems has significantly attracted the interest of both academia and industry. This has led to extensive research efforts globally, aiming to propose new applications enabled by RIS for future communications and study their performance, while numerous research projects have been supported through funding agencies worldwide to evolve this technology [105]. The recent advances made towards the efficient integration of RIS in wireless networks, along with the potential gains obtained from using this technology, impelled several standards developing organizations to start working on the standardization of RIS, both regionally and globally [105, 106]. However, standardization of this technology is still at a very early stage. In China, two different organizations started working RIS standardization, namely the FuTURE Mobile Communication Forum and the China Communications Standards Association [106]. Recently, some standardization activities on RIS were also initiated by the European Telecommunications Standards Institute (ETSI). In particular, the ETSI

approved an Industry Specification Group (ISG) on RIS in September 2021, aiming to define the requirements to establish global standardization. The ISG has already released three work items focusing on RIS related use cases and deployment scenarios, communication and channel models, as well as the technological challenges and associated impact on standardization [107–109]. Besides, the ZTE Corporation was the first company submitting a proposal to 3GPP during the March 2021 meeting for the inclusion of the RIS in Release 18 as a key component in 5G-Advanced networks [110]. However, since this technology is not mature enough, standardization on RIS has not yet been considered in 3GPP. Nevertheless, active discussions on RIS standardization plans are still underway in 3GPP, as it is expected to be a study item in future Releases (possibly Release 19) as one of the key enabling technologies in 5G-Advanced networks or 6G communications.

2.2.6 Challenges in RIS application

It is apparent from the previous examples that the integration of RIS in wireless networks will provide several new opportunities for 5G networks and beyond. However, several critical challenges still exist regarding the efficient development of RIS-based solutions in wireless communications. Below, we discuss two basic challenges that need to be addressed in designing and implementing RIS-assisted wireless networks from the signal processing and communication perspective, namely the passive beamforming design and the channel acquisition.

Passive beamforming design

One important challenge relies on the design of the reflecting elements of the RIS. In order to provide high beamforming gains, which in return will improve the performance of RIS-aided systems, the configuration of each reflecting element should be appropriately adjusted. Several works focus on optimizing passive beamforming at the RIS, and thus deriving the optimal values for the reflection coefficient of each element [88, 91, 92]. However, in most cases the proposed solutions to this optimization problem are derived for continuous amplitude and phase-shift values, which results in a costly RIS design requiring expensive high-precision elements. Moreover, continuously adjusting the reflection coefficients of each element may be beneficial for the network performance, but increases the implementation complex-

ity. On the other hand, adopting a more cost-effective solution by using tunable elements with discrete amplitude/phase shift levels can reduce the computational complexity of RIS-assisted networks [111]. Nevertheless, such approach may suffer from significant performance loss, due to the quantization errors.

Channel acquisition

In order to obtain the high performance gains associated with passive beamforming at the RIS, the accurate knowledge of the channels between the BS and the RIS or between the users and the RIS are required. In the existing literature, most of the works focusing on passive beamforming optimization assume that perfect knowledge of the CSI is already available, thus simplifying the implementation of the proposed schemes [88, 91]. However, acquiring this knowledge is a very challenging and resource-consuming procedure, especially for a large number of reflecting elements. First of all, due to the passive operation of the RIS elements the channels between the BSs/users and the RIS cannot be separately estimated through traditional training-based methods. Recently, several channel training methods have been proposed for estimating the cascaded BS-RIS-user channel [112–114]. However, estimating the channels for all the elements of the RIS may lead to increased computational complexity and a large training overhead, which will negatively affect the performance of the RIS-aided systems.

2.3 Comparison between relays and RISs

Based on the general idea of how a relay and an RIS operate, it can be seen that the two technologies are conceptually similar in the sense that they can assist the communication in wireless systems. As pointed out, when two devices are unable to connect directly, or their communication link is of insufficient quality, then relays and RISs can interchangeably be used to establish alternative paths between the devices [115, 116]. Through this approach, both technologies can enable the connectivity between devices that normally would not be able to communicate, or enhance the QoS of systems with poor communication links. Apart from the conceptual similarities, relay-aided and RIS-assisted networks share several common benefits that favor their employment [20, 72]. An important advantage of both technologies is

Table 2.1: Comparison between relays and RIS from different aspects

Enabling Technology	**Relay**	**RIS**
Operation	Active	Passive
Duplex	Half/Full-duplex	Full-duplex
Hardware complexity	Medium to High	Low
Energy consumption	High	Low
Additive noise	Yes	No
Signal range	High	Relatively Low

that they can be easily deployed with little or no dependency on the existing infrastructure. In particular, relays can be placed on various fixed or mobile objects, while an RIS can be easily mounted on several surfaces (e.g. facade of buildings). Another appealing benefit is the simple scalability of the deployed networks. In other words, the number of relays in multi-hop and/or cooperative systems and the number of elements in RIS-based solutions can be easily adapted to satisfy the demands and constraints of the networks.

Although these two technologies have conceptual similarities regarding their application, relays and RISs exhibit some fundamental differences concerning various aspects of operation [71, 115]. First of all, relays are typically viewed as active components that require a dedicated source power in order to be able to retransmit their received signals towards the final destination. In contrast, the RIS is equipped with nearly passive elements that adjust and reflect the signals without requiring any transmit radio-frequency chains [71]. The signal processing capabilities of each technology also vary, resulting in different hardware complexity for their deployment. In general, relays are more complex to be employed, since several electronic components are required for implementing the presented relaying schemes, such as the AF and DF schemes. On the other hand, the configuration of the RIS is based on low-complexity electronic circuits, such as switches and varactors [115]. As such,

the total energy consumption required for the RIS operation is lower than what a relay needs for its efficient use. The active electronic components of the relays are also responsible for the additive noise that appears in the relays, while the passive nature of the elements at the RIS does not incur any additional noise [115]. Moreover, unlike the relay that can operate in half-duplex or in full-duplex mode, with the latter requiring sophisticated techniques for SI cancellation, the RIS operates in an ideal full-duplex fashion and is free of SI [71]. However, due to the fact the RIS passively reflects the signals towards the destination, a large number of elements is required in order to achieve a potentially higher coverage range extension compared to the relay [116]. A summary of the above differences can be found in Table 2.1.

It is therefore deduced that, taking into consideration the distinctive characteristics of each technology, the employment of relays and RISs can be considered for different applications in both indoor and outdoor communication scenarios, according to the performance requirements and objectives. Specifically, in cases where successful connectivity needs to be achieved over large distances from the transmitter or the employment of large surfaces may not be feasible (e.g. underground wireless networks) the utilization of relays and multi-hop relaying solutions may be the optimal option. In such scenarios the active operation of relays can significantly compensate for the path loss effects and achieve sufficient performance gains at the end users, with appealing applications in D2D communications and wireless sensor networks [48]. On the other hand, the RIS employment can be considered in cases where the network resources are limited and the end users have high performance requirements, e.g., in high-demand scenarios such as stadiums or special events areas. Under such scenarios, the RIS can be used to passively control the propagation environment and improve the performance [99].

Recently, some initial works considering active RISs have been proposed, i.e., RISs with elements that are able to amplify the incident signals before reflecting them to the intended receiver [117,118]. Such approach can provide additional performance gains but at the expense of significantly higher implementation complexity, active components for the elements and additional noise introduced and amplified by the active RIS [119]. Another approach that has attracted researchers' interest is the joint deployment of relays and RISs in a single wireless system. Specifically, the proposed solutions combine the two technologies in a synergistic manner to benefit from both active processing and passive reflection and reap the key advantages of both RISs and

32
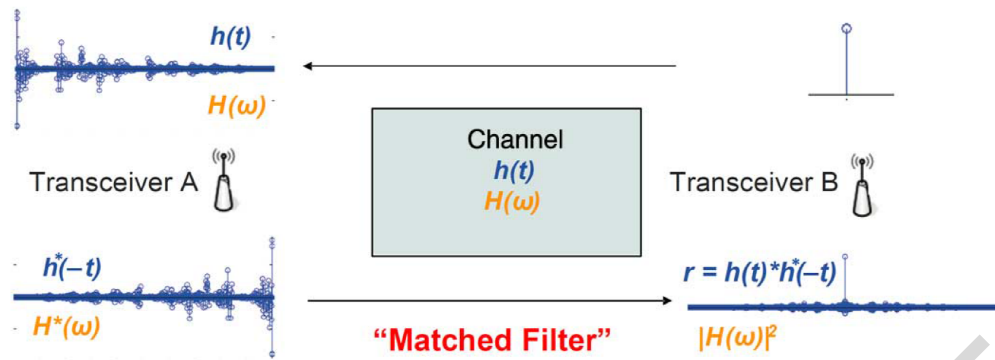
Figure 2.4: Principle of TR technique [126].

relays [120–123]. Such solutions can address some of the challenges associated with the separate deployment of each technology and provide some notable benefits, such as achieving higher spectral efficiency and extending the coverage with a reduced number of elements at the RIS.

2.4 Basic Principle of TR for 6G communications

According to the latest visions and trends for the deployment of 6G communications, it is expected that the future wireless networks will consist of RISs with extreme numbers of elements to obtain sufficient performance gains and will operate at very high frequencies. However, in wideband communications this paradigm shift results in the realization of multiple propagation paths, which may cause destructive interference at the receiver [124]. In contrast to most technologies trying to alleviate the negative effects of multipath propagation, TR is an appealing solution that exploits the multipath propagation environment by treating each path as a virtual antenna [125].

In principle, TR is a signal processing technique that uses the time reversed impulse response of the multipath channel as a prefilter at the transmitter, as shown in Fig. 2.4. Specifically, TR consists of two phases: the *channel probing phase*, where the receiver sends an impulse-like pilot signal towards the transmitter through the available scattering environment, and the *data transmission phase*, where the transmitter time-reverses the received waveform and transmits it back to the receiver [126]. Assuming channel reciprocity and channel stationarity, with this technique the energy is focused at the intended receiver in both space and time domains, referred as the *focusing effect* [127].

Although the TR technique was initially introduced for acoustic communications [128], its potential performance benefits in wireless communications have attracted significant academic and industrial interest [127, 129, 130]. Specifically, in [129] the applicability of the TR was experimentally tested for ultra-wideband communications, where it was indicated that the TR results in reduced complexity and increased system's capacity. The authors in [127] demonstrated that the TR-based transmission scheme reduces the power consumption significantly and achieves better interference alleviation compared to direct transmission using a conventional Rake receiver. Moreover, in [130] it was shown that the TR system, under a sufficiently large bandwidth, can obtain similar performance gains as massive MIMO systems with only a single antenna at the transmitter.

2.5 Mathematical Modeling and Performance Metrics

In this section, we introduce some mathematical preliminaries from probability theory and information theory that are required for the performance analysis of the proposed schemes in the considered systems and the investigation of their fundamental limits. Specifically, we provide the definitions of the main performance metrics and useful analytical tools used in this thesis and present the basic system models for the relay-assisted and RIS-assisted system, which can be used as baselines for the models considered in the following chapters.

2.5.1 Summary of the main notation

First, we provide here a summary of the main notation used throughout the remaining of this thesis. In particular,

- Lower and upper case boldface letters denote vectors and matrices, respectively; $\mathbf{I}_L$ denotes the $L \times L$ identity matrix, $[\cdot]^\dagger$ is the conjugate transpose operator and $\|\cdot\|_F$ is the Frobenius matrix norm.

- $\mathbb{P}\{X\}$ denotes the probability of the event X and $\mathbb{E}\{X\}$ represents the expected value of X; $\mathbb{1}_X$ is the indicator function, where $\mathbb{1}_X = 1$ if X is true, otherwise $\mathbb{1}_X = 0$.

- $\Phi(\cdot)$ is the cumulative distribution function (cdf) of the standard normal distribution; $\Gamma(\cdot)$ denotes the complete gamma function and $\gamma(\cdot, \cdot)$ is the lower incomplete gamma function [131]; $I_0(\cdot)$ is the modified Bessel function of the first kind of order zero and $Q_1(\cdot, \cdot)$ denotes the first-order Marcum Q-function; $G_{p,q}^{m,n}\left(\begin{smallmatrix} a_1,\dots,a_p \\ b_1,\dots,b_q \end{smallmatrix} \middle| x\right)$ is the Meijer-G function [131] and $H_{p,q}^{m,n}\left[\begin{smallmatrix} (a_i,\alpha_i,A_i)_{1,p} \\ (b_i,\beta_i,B_i)_{1,q} \end{smallmatrix} \middle| x\right]$ is the generalized upper incomplete Fox's H function [132].

- $\mathfrak{R}(x)$ and $\mathfrak{I}(x)$ return the real and imaginary part of x, respectively, and $\jmath = \sqrt{-1}$ denotes the imaginary unit; $O(\cdot)$ denotes the big O notation; $[x]^+ = \max(0, x)$, $\lceil x \rceil = \min\{z \in \mathbb{Z} | z \geq x\}$ and $\lfloor x \rfloor = \max\{z \in \mathbb{Z} | z \leq x\}$; $\binom{n}{k} = \frac{n!}{k!(n-k)!}$ and $(2n-1)!! = (2n-1)(2n-3)\dots 3 \cdot 1$.

2.5.2 Outage Probability

A performance metric from information theory that is usually considered to evaluate the quality of a communication scheme is the outage probability. In general, an outage event occurs if the achievable rate at the desired receiver is less than a predefined threshold ρ_{th}. The achieved outage probability is therefore given by

$$P_{out} = \mathbb{P}\left\{\log_2\left(1 + \gamma_c\right) < \rho_{th}\right\} = \mathbb{P}\left\{\gamma_c < \gamma_{th}\right\}, \tag{2.1}$$

where γ_c is the achieved SINR and $\gamma_{th} = 2^{\rho_{th}} - 1$. Below, we present the outage probability expressions for the typical system models of a relay-aided system employing a full-duplex DF relay and an RIS-assisted SISO system shown in Fig. 2.5. These models will be used as a reference for the extended versions considered in the following chapters.

Relay-aided system with full-duplex DF relay

For the reference system model of the relay-aided system, we consider a dual-hop network where the source (S) transmits data to the destination (D) with the assistance of a DF relay (R) that operates in full-duplex mode, as illustrated in Fig. 2.5a. We assume that the direct communication between the S and the D is blocked. Moreover, let h_{SR} and h_{RD} denote the $S-R$ and $R-D$ channel links, respectively, and h_{RR} denotes the SI at the R resulting from the full-duplex mode. Thus, assuming that the signals are transmitted from each node with power P, the achieved SINR at the R and D are
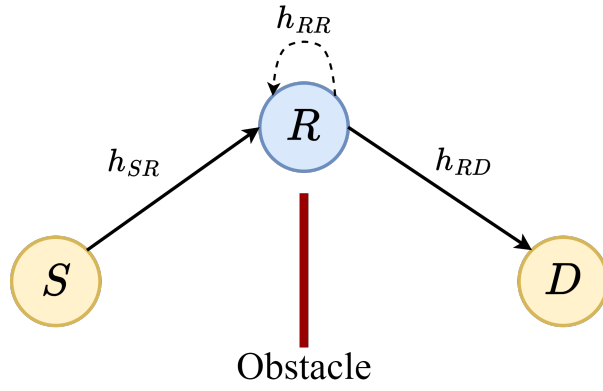
(a) Relay-aided system
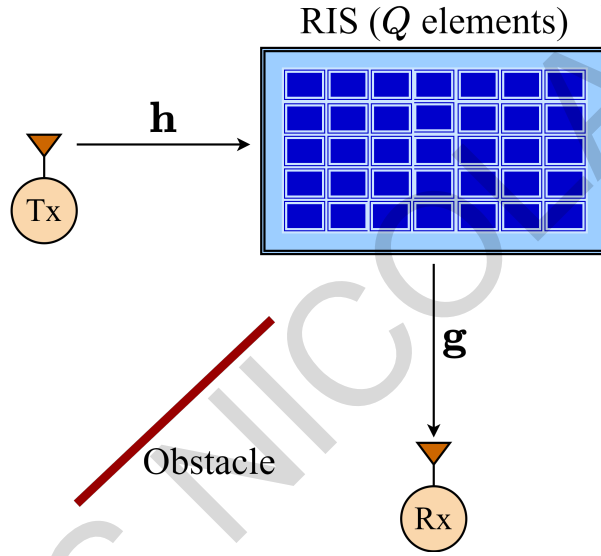
(b) RIS-aided system

Figure 2.5: Reference system models for the two considered technologies.

equal to

$$\gamma_R = \frac{P\,|h_{SR}|^2}{P\,|h_{RR}|^2 + \sigma_R^2} < \frac{P\,|h_{SR}|^2}{\sigma_R^2}, \tag{2.2}$$

and

$$\gamma_D = \frac{P\,|h_{RD}|^2}{\sigma_D^2}, \tag{2.3}$$

where σ_R^2 and σ_D^2 denote the variance of the additive white Gaussian noise (AWGN) at the R and D, respectively. Note that the upper-bound SNR expression at the R is obtained by assuming the ideal scenario where SI can be fully suppressed. The D can successfully decode the transmitted signal if both the R and the D are able to decode their received signals, otherwise an outage event occurs. The outage probability of

the considered relay-supported system is therefore expressed as

$$P_{out,\text{DF}} = \mathbb{P}\{\gamma_R < \gamma_{th}\} + \mathbb{P}\{\gamma_D < \gamma_{th}\}\,\mathbb{P}\{\gamma_R \geq \gamma_{th}\}. \tag{2.4}$$

RIS-aided system

For the typical system model of the RIS-aided network, we consider the basic point-to-point communication system where an RIS equipped with Q reflecting elements is employed to assist the communication between a single-antenna transmitter (Tx) and a single-antenna receiver (Rx) (see Fig. 2.5b). Similar to the previous case, we assume that the direct link between the Tx and the Rx is not available. Let $\mathbf{h} = \left[h_1\, h_2 \cdots h_Q\right]^\top$ and $\mathbf{g} = \left[g_1\, g_2 \cdots g_Q\right]^\top$ denote the channel vectors from the Tx to the RIS and from the RIS to the Rx, respectively. Moreover, we denote by

$$\mathbf{\Phi} = \text{diag}[a_1 e^{\jmath\phi_1}\ a_2 e^{\jmath\phi_2}\ \dots\ a_Q e^{\jmath\phi_Q}], \tag{2.5}$$

the diagonal reflection matrix of the RIS, where $a_i \in [0,1]$ and $\phi_i \in [0, 2\pi)$ are the reflection amplitude and the phase shift induced by the i-th element of the RIS, respectively. The SNR at the Rx is expressed as

$$\gamma_{\text{RIS}} = \frac{P\left|\sum\limits_{i=1}^{Q} h_i g_i a_i e^{\jmath\phi_i}\right|^2}{\sigma^2}, \tag{2.6}$$

where σ^2 is the variance of the AWGN at the Rx. The outage probability of the considered RIS-assisted system is given by

$$P_{out,\text{RIS}} = \mathbb{P}\left\{ \frac{P\left|\sum\limits_{i=1}^{Q} h_i g_i a_i e^{\jmath\phi_i}\right|^2}{\sigma^2} < \gamma_{th} \right\}. \tag{2.7}$$

2.5.3 Diversity-Multiplexing Tradeoff

We now move on to the DMT that can be achieved by a communication scheme. The DMT is a powerful metric that can be used to evaluate the fundamental performance limits of the considered scheme in the asymptotic SNR regime ($P \to \infty$). It was firstly introduced by Zhang and Tse in [133], and its formal definition is stated as follows.

Definition 2.1 (Diversity-multiplexing tradeoff)**.** *A communication scheme achieves multiplexing gain r and diversity gain d(r) if the target data rate R(P) ∼ r log P and the outage probability of the scheme $P_{out}(P)$ satisfy the conditions*

$$\lim_{P\to\infty} \frac{R(P)}{\log P} = r,$$

and

$$\lim_{P\to\infty} -\frac{\log P_{out}(P)}{\log P} = d(r). \tag{2.8}$$

Essentially, the DMT can provide a tradeoff between the reliability and the degrees of freedom of the system. Note that the *diversity order* of the considered scheme denotes the maximum diversity gain that can be achieved by the scheme when $r = 0$ and is given by $d(0)$.

2.5.4 Useful Theorems and Methods

In what follows, we refer to the basic theorems and methods from probability theory, that are used in this thesis. Specifically, the definitions of the *Gil-Pelaez inversion theorem*, the *central limit theorem (CLT)* and the *moment matching method* are provided below.

Gil-Pelaez Inversion Theorem

A theorem that is considered useful for the analysis of the wireless networks is the Gil-Pelaez inversion theorem [134]. In general, the characteristic function of a scalar random variable X is defined as the expected value of the transformed random variable $\exp(\jmath tX)$, i.e. [135],

$$\phi_X(t) = \mathbb{E}\left\{\exp\left(\jmath tX\right)\right\}.$$

Through this theorem, the inversion formulas of the characteristic function over $(-\infty, \infty)$ are derived for the numerical evaluation of the probability density function (pdf) and the cdf of X.

Definition 2.2 (Gil-Pelaez inversion theorem)**.** *The pdf of a scalar random variable X with characteristic function $\phi_X(t)$ is given by*

$$f_X(x) = \frac{1}{\pi} \int_0^\infty \Re\left[\exp\left(-\jmath tx\right)\phi_X(t)\right] dt. \tag{2.9}$$

Moreover, if x is a continuity point of the cdf of X, then the cdf is given by

$$F_X(x) = \frac{1}{2} - \frac{1}{\pi} \int_0^\infty \frac{1}{t} \Im \left[\exp\left(-\jmath t x\right) \phi_X(t) \right] dt. \tag{2.10}$$

As such, this theorem is a convenient tool to numerically calculate the outage probability of the proposed schemes.

Central Limit Theorem (CLT)

Another theorem that is mainly used in this thesis is the well-known CLT. This theorem provides a simple method for deriving approximate probabilities for sums of independent random variables [135]. Therefore, through this approach we can simplify the analysis of the proposed schemes and provide tight approximations of the actual performance that can be achieved.

Definition 2.3 (Central limit theorem). *Let $\{X_1, X_2, \ldots, X_n\}$ be a set of independent random variables with mean μ_i and variance σ_i respectively, $i = 1, \ldots, n$. By setting $\mu = \mu_1 + \mu_2 + \ldots + \mu_n$ and $\sigma = \sigma_1 + \sigma_2 + \ldots + \sigma_n$, the distribution of*

$$X = \frac{X_1 + X_2 + \ldots + X_n - n\mu}{\sigma \sqrt{n}},$$

tends to the standard normal distribution as $n \to \infty$. Moreover,

$$F_X(z) = \mathbb{P}\left\{X \leq z\right\} \xrightarrow{n \to \infty} \Phi(z). \tag{2.11}$$

Moment Matching Method

The moment matching method is also used in the thesis to provide approximated expressions for the channel distributions. The main idea behind this approach is to match the moments of a random variable to the parameters of a known distribution. In the available literature, the Gamma distribution is widely used to approximate a random variable with a complicated distribution [87]. As such, this technique is a useful tool that can provide elegant and tractable expressions for approximating the performance of the considered schemes.

Definition 2.4 (Moment matching method). *Consider a scalar random variable X with the first and second moment denoted as*

$$\mu_1 = \mathbb{E}\left\{X\right\} \quad and \quad \mu_2 = \mathbb{E}\left\{X^2\right\},$$

respectively, and the variance given by

$$\sigma^2 = \mu_2 - \mu_1^2.$$

The distribution of X can be approximated by the Gamma distribution where the shape parameter κ and scale parameter ξ are calculated as

$$\kappa = \frac{\mu_1^2}{\sigma^2} \quad and \quad \xi = \frac{\sigma^2}{\mu_1}. \tag{2.12}$$

Chapter 3

A Markov Chain Approach for Myopic Multi-hop Relaying: Outage and Diversity Analysis

Multi-hop relaying is a promising low-cost solution with high flexibility, which can help the connection of trillions of devices, while the concept of cooperative diversity in multi-hop networks can enhance the reliability of such systems. However, full cooperation of the nodes in such networks can result in significantly higher implementation complexity. In this chapter, a cooperative protocol is investigated for a multi-hop network consisting of relays with buffers of finite size, which may operate in different communication modes. The protocol is based on the myopic DF strategy, where each node of the network cooperates with a limited number of neighboring nodes for the transmission of the signals. Each relay stores in its buffer the messages that were successfully decoded, in order to forward them through the appropriate channel links, based on its supported communication modes. A complete theoretical framework is investigated that models the evolution of the buffers and the transitions at the operations of each relay as a state MC. We analyze the performance of the proposed protocol in terms of outage probability and derive an expression for the achieved DMT, by using the state transition matrix and the related steady state of the MC.

3.1 Introduction

As we previously mentioned, nowadays there is a continuous need for an increasing number of applications and devices to be connected, leading to an ever-growing network of nodes that have to communicate. Especially in 6G networks, research needs to conceive innovative ideas to satisfy the challenging demands of URLLC for massive connectivity networks [136]. Cooperative relay communications is an appealing and cost-effective solution with high flexibility, which can assist the connectivity between a massive number of devices with enhanced reliability. Due to the implementation simplicity and easy scalability of this technology, relay communications can be considered for the implementation of 5G and future 6G networks, as they provide an adaptive physical layer and flexible transmission protocol and can enable D2D communications [137]. Due to their potential advantages towards future generations of wireless communications, cooperative relay networks have attracted considerable research interest and have been considered for several practical applications, such as in wireless ad-hoc networks [25], mmWave communications [41], underwater and air-to-ground networks [53, 55], and secrecy communications [138].

Motivated by the numerous benefits, the performance of cooperative networks with multiple relays over a single transmission path (multi-hop relaying) has been investigated in several studies and over various fading channel models [37–40]. Multi-hop relaying has also been recently considered in several application scenarios towards the realization of 5G and beyond networks, such as to support the connectivity in mmWave communications [41, 42]. In order to improve the performance of relay-assisted networks through spatial diversity, several works proposed cooperative communication schemes that enable broadcast transmission from the network nodes, considering multiple parallel propagation paths assisted by single relays or cooperative diversity protocols for multi-hop networks [27, 43]. However, full cooperation of the nodes in such networks exhibits a number of practical difficulties in its implementation, especially in terms of multi-node coordination and power management. To overcome these issues, the authors in [139] proposed the *myopic* DF strategy as an information theory concept. In this strategy, each node of the network cooperates with a limited number of subsequent neighboring nodes. They showed that the achievable rate increases considerably, while the complexity of its implementation remains low.

In several cases, the devices that need to be connected in wireless networks may support different transmission policies affecting their communication capabilities, e.g., for energy conservation. Such devices could be utilized to provide further optimized services in order to improve the networks' performance, based on the available resources. The authors in [140] presented a queuing model for the performance analysis of several sleep and wakeup strategies in a network with solar-powered wireless sensors. In [141], a relay selection scheme was considered for a cooperative network with energy harvesting (EH) relays that can assist the communication from source to destination only if they have sufficient energy. It was observed that, the overall performance of such networks depends on the EH parameters of the relays. A similar scenario was considered in [142], where a new relay selection method was proposed, based on the throughput gain of the EH relays with enough stored energy, which improved the overall performance of the cooperative network. Moreover, in [143], the on-off transmission policy for a buffer aided EH node was studied in terms of outage probability and average throughput, where the EH node transmits information only if the stored energy exceeds a certain value, otherwise it remains silent.

It is, therefore, an important and challenging problem to understand how the utilization of relaying nodes with different communication capabilities affects the performance of a multi-hop network with limited cooperation. Motivated by this, in this chapter, we propose a general cooperative protocol over a multi-hop network, where the relays have buffers of finite size and may operate in different communication modes affecting their signal forwarding capabilities. The protocol is inspired by the myopic DF strategy [139], and can be applied to networks with an arbitrary number of relays with different modes of operation. For example, such scenario could be considered for wireless networks, where some intermediate nodes are crucial for the sustainability of the communication and so they are connected to the power grid and are always able to transmit information. The remaining nodes could be self-powered through EH and could transmit data only if the harvested energy is above a required level [141, 142]. The main contributions of the chapter are summarized as follows:

- A novel myopic-based cooperative protocol over a multi-hop network is proposed. Through this chapter, we extend the idea presented in [139] by studying the performance of the myopic strategy in terms of outage probability and di-

versity gain. To our knowledge, no previous work in the literature analyzes myopic strategy from a communication theory perspective. A system model is presented, where the flow of information is assisted by using buffers of finite size at each relay of the network. Finally, the myopic-based protocol is extended to the case where relays may operate in different communication modes regarding their transmission capabilities. Therefore, a fundamental approach of how the flow of information from source to destination can be conveyed is presented, based on the status of the buffers and the communication capabilities of each relay.

- For the analysis of the system in terms of outage probability, we model the evolution of the considered network as a state MC, by taking into account the transitions that take place at the buffers and the communication modes of the relays. This approach provides a flexible and elegant modeling of the different instances that the network can be found. By using the state transition matrix and the related steady state of the MC, we investigate a complete theoretical framework for the performance analysis of such cooperative networks in terms of the outage probability and the DMT. The presented framework is general and can be adapted to an arbitrary number of relays, any myopic strategy and several communication strategies supported by the participating relays.

- Our results demonstrate that as the number of cooperating nodes increases, the performance of the system is enhanced both in terms of outage probability and diversity gain. Furthermore, it is shown that the diversity order that can be achieved by the proposed protocol depends significantly on the communication strategy that is supported by every relay of the network. Finally, by extending the proposed protocol for multi-branch networks, the outage probability of the system is improved, while the overall diversity gain depends on the diversity gain that each branch can separately achieve.

As such, the proposed myopic protocol can provide useful insights for the design and realization of 5G networks and future 6G communications with reduced computational complexity and memory requirements and increased energy efficiency.

3.2 System Model

3.2.1 Network topology

A wireless network topology is considered, which consists of a single source S, N intermediate relays $R_1, R_2, \ldots, R_N$, and a single destination D. For ease of notation, we let node i correspond to the relay R_i, $1 \leq i \leq N$, and nodes 0 and $N+1$ correspond to the source S and destination D, respectively. At the relays, the DF scheme is employed for forwarding the signals. Moreover, time is assumed to be slotted and $x(t)$ is used to denote the signal that S sends to R_1 at time-slot t with normalized energy, i.e., $\mathbb{E}\{|x(t)|^2\} = 1$. Each transmitter (the source S or a relay R_i) transmits with the same fixed power P. The destination D receives data based on a k-hop myopic DF strategy [139], $1 \leq k \leq N+1$, where k represents the maximum number of nodes that a transmitter can forward data to. More specifically, node i ($0 \leq i \leq N$) can send data to $L_i = \min(k, N - i + 1)$ subsequent nodes. As such, at each time-slot, the i-th transmitter splits its power to L_i partitions. Therefore, a signal is sent through the link $i \rightarrow j$ with transmit power $a_{i,j}P$, where $a_{i,j}$ denotes the power splitting parameter, such that $\sum_{j=i+1}^{L_i+i} a_{i,j} = 1$. However, at a given time-slot t, only the successfully decoded signals can be forwarded to the appropriate nodes. For that reason, each relay R_i has a data buffer (data queue) b_i of finite size L_i, where it can store the decoded signals for forwarding[1], based on the proposed protocol described in Section 3.3. An example of this topology is presented in Fig. 3.1, for $k = 2$ hops and $N = 3$ relays.

3.2.2 Channel model

For the analysis, we consider independent and identically distributed channel links that experience propagation path loss, which is assumed to follow the power law $d_{i,j}^{-\eta}$, where $d_{i,j}$ is the distance between the nodes i and j and η denotes the path loss exponent. Without loss of generality, we assume the ordering $d_{i,j} < d_{i,j+1}$, $\forall\ i, j,\ i < j \leq N+1$. Note that this assumption corresponds to distance-based routing protocols in multi-hop networks that take into consideration the Euclidean distance among the nodes, e.g. the shortest-path-routing [144]. Furthermore, all wireless links exhibit fading which is modeled as frequency-flat Rayleigh block

---

[1]Note that each node sends data to the subsequent L_i nodes *concurrently*. Therefore, a storage space of the same size is required in order to hold the data that will be forwarded.
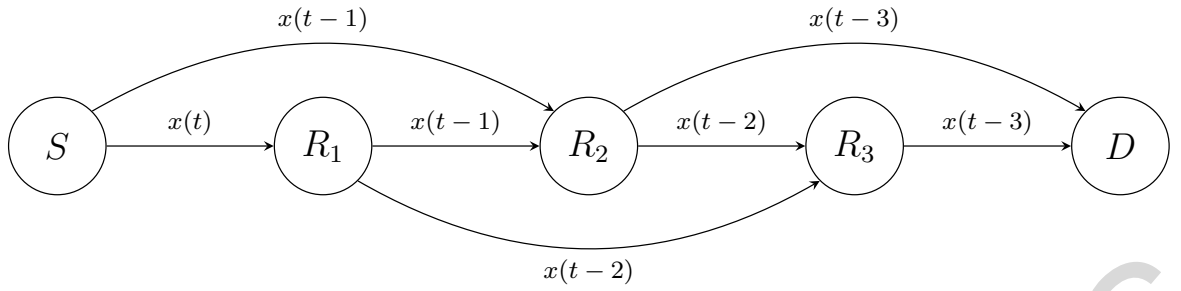
Figure 3.1: Topology for 2-hop myopic DF strategy in a wireless network with three relays. The arrows indicate all the available links in the system and for each link the corresponding signal that will be transmitted is shown.

fading[2]. This signifies that the fading coefficients $h_{i,j}$ remain constant during one time-slot, but change independently for different time-slots, by following a circularly symmetric complex Gaussian distribution with zero mean and unit variance, i.e., $h_{i,j} \sim \mathcal{CN}(0,1)$. We assume that during one time-slot, the relays of the system can receive and transmit data simultaneously, i.e., they operate in full-duplex mode. Since we focus on the performance of the myopic DF scheme, we consider an ideal scenario where we ignore the SI and interference from other relays. Although in practice inter-relay interference and SI cannot be fully eliminated, considerable interference mitigation can be achieved through sophisticated signal processing and equalization techniques [35, 43, 145]. In other words, the presented analysis serves as a performance bound from a communication theory standpoint.

3.2.3 Relay communication model

The relays of the network operate based on two different communication modes, namely the *active* and *silent* modes. If a relay is active during one time-slot, then it is able to simultaneously transmit and receive the decoded signals. In the silent mode, the relay can still receive data but is unable to forward its decoded signals to the following nodes [140]. We consider a scenario where a subset of the participating relays are always active. The remaining relays are able to switch their operations between the two communication modes, and therefore can be either active or silent. Such relays could correspond to devices that are always connected to the power

---

[2]Even though we consider Rayleigh fading, the proposed analytical framework is general and the extension to other fading models is straightforward as we only need to consider their probability distributions.

grid and switch off their transmitters occasionally by design, in order to conserve energy. Alternatively, the switching between the two communication modes could occur probabilistically, based on the EH profile of the devices [143].

We assume that during a time-slot, a relay's communication mode remains constant, but can change independently between the two modes for different time-slots. In the considered scenario, the relay's decision for the communication mode at each time-slot is modeled as a Bernoulli distribution with parameter q, which indicates the probability that a relay operates in silent mode. For the relays that are able to transmit and receive data at every time-slot, or equivalently are always in the active mode, the probability of operating in silent mode is equal to $q = 0$. By using the Bernoulli distribution, we provide a unified analysis for various decision-based scenarios at the relays affecting their communication mode. For example, a simplified EH scenario could be considered, where the decision of a relay being in active or silent mode is related to the status of the energy buffers [146]. However, it is important to note that the proposed analytical framework is general and any other distribution can be applied.

3.3   A k-hop Myopic-based Protocol

We now present our proposed protocol based on the k-hop myopic DF strategy [139]. The protocol describes the procedure over which the flow of information from S to D is conveyed within the considered network. Based on the presented system model, at time-slot t the received signal at the j-th receiver is given by

$$y_j(t) = \sum_{i=[j-k]^+}^{j-1} \mathbb{1}_{i \to j} \sqrt{d_{i,j}^{-\eta} \alpha_{i,j} P} h_{i,j} x(t - j + 1) + w_j(t), \qquad (3.1)$$

where $w_j(t) \sim \mathcal{CN}(0, \sigma^2)$ is the AWGN with variance σ^2 and $\mathbb{1}_{i \to j}$ equals to one if node i transmits a signal to node j at the current time-slot, otherwise it is equal to zero. Recall that, based on the k-hop myopic DF strategy, node j can receive data from at most k previous nodes. In this chapter, we focus on the fundamental analysis of the myopic scheme, so a perfect (global) CSI is assumed and each receiver is able to combine the received signals coherently through co-phasing[3]. Therefore, the

---

[3]In practice, a channel estimation process is required and the associated overhead increases as k increase; note that k can be adapted to the available resources to achieve a balance between estimation and system performance.

corresponding instantaneous SNR at the j-th receiver during one time-slot is given by

$$\mathrm{SNR}_j = \frac{P}{\sigma^2} \left(\sum_{i=[j-k]^+}^{j-1} \mathbb{1}_{i \to j} |h_{i,j}| \sqrt{d_{i,j}^{-\eta} a_{i,j}} \right)^2, \tag{3.2}$$

where $|h_{i,j}|$ is a random variable that follows a Rayleigh distribution with unit scale parameter. We assume that v relays of the network, $0 \le v \le N$, have dual-mode communication capabilities, while the remaining $N - v$ relays are always active. Moreover, S is able to transmit all its available data at every time-slot. A signal at the j-th receiver is successfully decoded if the instantaneous SNR_j is not less than a predefined threshold γ, i.e., $\mathrm{SNR}_j \ge \gamma$, otherwise an outage occurs. Each relay keeps in its buffer the signals that were successfully decoded, in order to forward them through the appropriate channel links. For this, the buffer of each relay is used as an one-dimensional array with indexed elements, where the element $b_i[n]$, $1 \le n \le L_i$, corresponds to the n-th most recent signal that the i-th relay receives.

At each time-slot, the network performs three specific tasks: (*i*) transmission of information, (*ii*) buffer shifting, and (*iii*) information decoding. More specifically, at an arbitrary time-slot t, the network follows the procedure described below:

- *Transmission of information:* At first, the node S sends the signals $x(t - j + 1)$ to the nodes $j = 1, \ldots, k$, respectively. Then, every dual-mode relay determines whether it will operate in active or silent mode. Recall that the relays with a single-mode operation are considered to be always active. The i-th relay of the network, $i = 1, \ldots, N$, forwards the signal $x(t - j + 1)$ to the corresponding node $j = i + 1, \ldots, \min(i + k, N + 1)$, if and only if, it is in active mode and its buffer element $b_i[j - i]$ is not empty, i.e., a signal is stored in this element. Thus, at the specific time-slot, the j-th node of the network can receive the signal $x(t - j + 1)$ simultaneously from at most k previous nodes. The example in Fig. 3.1 shows an instance of the network, where at time-slot t all the relays are active and every buffer's element has a previously decoded signal. As a result, at the transmission phase, all the available links of the system, for the considered 2-hop myopic DF strategy, are used.

- *Shifting operation:* After the transmission phase, each relay prepares its buffer for the next time-slot. In particular, it shifts the elements one position to the right. In other words, $b_i[2]$ will get the data of $b_i[1]$, $b_i[3]$ the data of $b_i[2]$, etc.

48

Therefore, the first element of each buffer becomes unassigned for the decoding of $x(t - j + 1)$ (see decoding process below). The shifting operation is required for the proper transmission of the appropriate signals to the corresponding nodes at each time-slot.

- *Decoding process:* Every relay combines all the received signals $x(t - j + 1)$, acquired at the transmission phase, and attempts to decode the message. The first element of its buffer $b_i[1]$ is used for the outcome of the decoding process: it stores the signal if it is successfully decoded, otherwise it becomes an empty element. It is important to note that, an empty element indicates that the decoding of the signal failed (i.e. similarly to a pointer indicating a null value) and thus is not able to be forwarded. Finally, the destination D combines the received signals $x(t - N)$ and if the message is not successfully decoded, i.e., $\text{SNR}_{N+1} < \gamma$, then the system is in outage and the message is lost.

According to the above procedure, it is clear that some of the elements at the buffers might be empty due to the shifting operation. Consequently, the proper transmission of the successfully decoded signals to the appropriate nodes relies on the communication mode of each relay and the content of its buffer that evolves with time. Based on these features, in the following section, we introduce a theoretical framework that is exploited for the system's outage probability analysis.

3.4   A State Markovian Model Approach

For the analysis of the considered system, we provide a theoretical framework that models the evolution of the relays' buffers and the communication mode of the dual-mode relays as a MC. In this section, the state transition matrix construction and the derivation of the stationary distribution of the MC are presented, which will be used for the computation of the system's outage probability in Section 3.5.

3.4.1   Definition of MC states

Firstly, the MC states are defined in order to represent the different instances that characterize the status of the network. The distinction between these instances depends on the buffers' evolution with time and the transitions at the dual-mode

communication strategy. A state of the MC, or equivalently a *network state*, needs to capture the transitions that take place at the relays' buffers and the dual-mode relays' operations. Thus, it is necessary to represent the evolution of the buffers and the relays' status by dividing the network states into two separate sub-states, namely the *buffer states* and the *relay states*.

Recall from Section 3.3 that, as a result of the decoding process and the shifting operation, each buffer's elements can be found in two possible conditions: either to have the n-th most recently received signal or to be empty. We denote the m-th buffer state by

$$u_m \triangleq (\beta_{1,m}\ \beta_{2,m}\ \dots\ \beta_{N,m}), \tag{3.3}$$

where $\beta_{i,m}$ is a one-dimensional binary array associated with the i-th relay, for which each element $\beta_i[n]$ equals 0 if the corresponding buffer element $b_i[n]$ is empty, otherwise is equal to 1. Therefore, each array $\beta_{i,m}$ indicates the non-empty elements of the corresponding buffer b_i at the buffer state u_m, while from the definition it is apparent that its size equals L_i. The number of the buffer states is given by all the possible combinations that can be derived by each β_i's element. Thus, each buffer state is a vector of finite size $L_\beta = \sum_{i=1}^{N} L_i = (2N - k + 1)\frac{k}{2}$, that represents which elements in each buffer have decoded signals, and the total number of buffer states is equal to $M_B = 2^{L_\beta}$.

However, the buffers' evolution and equivalently the transition between different instances of the network depends also on the communication mode of each dual-mode relay that varies for each time-slot. In the considered scenario, the dual-mode relays are predetermined and are given by the ordered set $H = \{i | R_i \text{ is dual-mode}\}$. The m-th relay state is denoted as

$$v_m \triangleq (\lambda_{H(1),m}\ \lambda_{H(2),m}\ \dots\ \lambda_{H(v),m}), \tag{3.4}$$

where $\lambda_{H(i),m}$ indicates the communication mode of the i-th dual-mode relay at the m-th state and is equal to 0 if the relay operates in silent mode, otherwise equals 1. Note that this parameter is defined only for the dual-mode relays of the network, since the other relays are always active and the operations related to their communication capabilities do not vary with time. Thus, each relay state is a $1 \times v$ vector that captures all the possible transitions at the dual-mode relays' communication modes and depicts which relays are active at each instance of the network. The total number of relay states is then derived as $M_R = 2^v$.

The network states are constructed by the concatenation of the buffer and relay states that were previously defined. Therefore, the m-th network state, $1 \leq m \leq M$, is denoted as

$$s_m \triangleq (v_m \, u_m) = (\lambda_{H(1),m} \ldots \lambda_{H(v),m} \, \beta_{1,m} \ldots \beta_{N,m}),$$

which represents the joint status of the relays' buffers and the dual-mode relays' communication activity. The total number of network states that are considered for the MC is given by all the possible pairs of buffer and relay states that can be derived and is equal to $M = M_B M_R = 2^{L_\beta + v}$. Since this concatenation results in a binary representation of a decimal number, the MC states are predefined and arranged in a numerical ascending order, such that the states s_1 and s_M are denoted by the $1 \times (L_\beta + v)$ binary vectors $(00 \ldots 0)$ and $(11 \ldots 1)$, respectively.

3.4.2 State transition matrix and stationary distribution

The state transition matrix is a square matrix containing information on the transition probabilities between the states of the MC. Specifically, it defines how the system evolves with time and indicates which of the available links will be used at each time-slot. Let $\mathbf{A}$ denote the $M \times M$ state transition matrix of the MC, where the entry $p_{l,m} = \mathbb{P}\{s_m \rightarrow s_l\} = \mathbb{P}\{X_{t+1} = s_l | X_t = s_m\}$ is the probability of the transition from network state s_m at time t to state s_l at time $(t+1)$. The calculation of these probabilities relies on the communication mode of each dual-mode relay and the status of each relay's buffer, and consequently from the corresponding parameters λ_i and β_i.

Algorithm 2.1 shows the proposed procedure for the construction of the state transition matrix $\mathbf{A}$, given the number of relays N, the ordered set of dual-mode relays H and the number of hops k. First of all, we derive the size of each array β_i and the size of the buffer states. Moreover, we compute the number of buffer and relay states and consequently the number of states of the MC, i.e., (lines $1-3$). Then, we need to detect all the possible transitions between the states. Since the decision of the communication mode at each dual-mode relay at time-slot t is independent from what was decided at previous time-slots, the only parameters that affect the validity of a state transition are the arrays β_i, $1 \leq i \leq N$, due to their shifting operation. Thus, for each pair of states (s_m, s_l), we examine if the variations at the elements of each array β_i are consistent with the evolution of the buffers as in the proposed protocol. Each array $\beta_{i,m}$ can be extracted by isolating the buffer state u_m from the network state

<div style="text-align:right">

</div>

Algorithm 3.1: Generation of the state transition matrix.

   Input:

   $N \leftarrow$ Number of relays

   $H \leftarrow$ Set of dual-mode relays

   $k \leftarrow$ Number of hops

   Output:

   $\mathbf{A} \leftarrow$ Transition Matrix

 1 Compute $L_i = \min(k, N + 1 - i), i = 1, \ldots, N$

 2 Compute $L_\beta = (2N - k + 1)\dfrac{k}{2}$

 3 Compute $M_B = 2^{L_\beta}, M_R = 2^v, M = M_B M_R$

 4 **for** $m = 1$ *to* M **do**

 5   **for** $l = 1$ *to* M **do**

 6   Assume $s_m \rightarrow s_l$ exists

 7   **for** $i = 1$ *to* N **do**

 8   Get $\beta_{i,m}, \beta_{i,l}$

 9   **for** $n = 1$ *to* $L_i - 1$ **do**

 10   **if** $\beta_{i,m}[n] \neq \beta_{i,l}[n + 1]$ **then**

 11 $s_m \rightarrow s_l$ does not exist

 12   **end**

 13   **end**

 14   **end**

 15   Compute $p_{l,m}$ using (3.5)

 16   **end**

 17 **end**

---

s_m and taking all the elements of the resulting array from the index $u_m[\sum_{j=1}^{i-1} L_j + 1]$ to the index $u_m[\sum_{j=1}^{i} L_j]$. A transition from s_m to s_l exists, if the contents of all the arrays shift one position to the right. This is equivalent to the equality $\beta_{i,m}[n] = \beta_{i,l}[n + 1]$, $1 \leq n \leq L_i - 1$, for all the arrays β_i, $i = 1, \ldots, N$. If at least one of these equalities does not hold, then the transition is not possible. The first element of each array at the new buffer state $\beta_{i,l}[1]$ indicates if an outage occurred at the corresponding relay, while the elements of the new relay state indicate which dual-mode relays are active. As the decoding is handled separately by each relay, these probabilities are independent and therefore the transition probability is given as their product. The

entries of the state transition matrix are then given by

$$p_{l,m} = \begin{cases} \prod_{i=1}^{v} \prod_{j=1}^{N} \Big[\lambda_{H(i),l}(1-q) + (1-\lambda_{H(i),l})q\Big] \\ \times\Big[\beta_{j,l}[1](1-P_o(j,m)) + \big(1-\beta_{j,l}[1]\big)P_o(j,m)\Big], \\ \qquad\qquad\qquad\qquad \text{if } s_m \to s_l \text{ exists;} \\ 0, \text{otherwise,} \end{cases} \qquad (3.5)$$

where $P_o(j,m)$ is the probability that the j-th node has an outage event, given that the network instance is derived by the state s_m. Note that, due to the two possible values that the elements $\lambda_{H(i),l}$ and $\beta_{j,l}[1]$ can take, the aggregate number of all possible transitions from every state are 2^{v+N}. The analytical expressions for the outage probability are given in Section 3.5.

We are now able to derive the stationary distribution of the MC, which is denoted as π. In this case, the interpretation of the stationary distribution gives an insight to the long-term use of the available channel links in the system, as it indicates how the signals are being transmitted across the relays until they reach the final destination. The calculation of the steady states is given in Lemma 3.1.

Lemma 3.1. *The state transition matrix* **A** *of the defined MC has a unique stationary distribution, which is given by*

$$\pi = (\mathbf{A} - \mathbf{I} + \mathbf{B})^{-1}\mathbf{b}, \qquad (3.6)$$

where π *is the stationary distribution,* $\mathbf{b} = (1\ 1\ \ldots\ 1)^T$ *and* $\mathbf{B}_{l,m} = 1, \forall\, l, m$.

Proof. We first need to verify that some properties of the state transition matrix **A** hold, in order to ensure that it has a unique stationary distribution. Specifically, **A** must be a column stochastic matrix, which is irreducible and aperiodic. A column stochastic matrix is a square matrix of non-negative terms in which the elements in each column sum up to one, while a non-negative matrix is called irreducible if every pair of states can communicate. Finally, the period of a state s_m is the greatest common divisor of the set $\{t \in \mathbb{N} : p_{m,m}^{(t)} > 0\}$ and if the period is 1, the state is aperiodic. The transition matrix is aperiodic if all the states are aperiodic [147].

For any MC under the proposed framework, the transitions from state s_m to all the possible states s_l have probabilities that sum up to one, i.e., $\sum_{l=1}^{M} p_{l,m} = 1$. Therefore, the transition matrix is column stochastic. Moreover, from the structure

of the problem, it is observed that there is a path from any state to any other state of the MC. Consequently, all the states belong to a single communication class and the transition matrix is irreducible. An irreducible MC needs only one aperiodic state to imply that all states are aperiodic. In the defined MC the transition probability from state s_1 to the same state is always non-zero, i.e., $p_{1,1} = \mathbb{P}\{s_1 \rightarrow s_1\} > 0$; hence the state s_1 is aperiodic. Since there is only one communication class, all states are aperiodic and therefore, the transition matrix is aperiodic. As the required properties of the transition matrix hold, we conclude that it has a unique stationary distribution which is given as in [148]. □

In the next section, we provide our main results for the performance analysis of our proposed protocol.

3.5 Outage Probability and Diversity Analysis

Based on the obtained stationary distribution of the MC, we can now analyze the performance of the proposed protocol, in terms of outage probability and diversity gain. Firstly, we provide an expression of the outage probability at each receiver and then the system's outage probability is derived. To conform with the above notation, we assume that S has an array β_0 of finite size k, in which all the elements are equal to one, since S always sends a signal to the k subsequent nodes.

In general, the i-th transmitter sends a signal to the j-th receiver of the network, if the corresponding indicator function $\mathbb{1}_{(i \rightarrow j),m}$ is equal to one and it is calculated as

$$\mathbb{1}_{(i \rightarrow j),m} = \begin{cases} \beta_{i,m}[j-i]\lambda_{i,m}, & i \in H; \\ \beta_{i,m}[j-i], & \text{otherwise.} \end{cases} \tag{3.7}$$

Thus, the number of nodes that transmit a signal to the j-th receiver at state s_m is equal to

$$C_{j,m} = \sum_{i=[j-k]^+}^{j-1} \mathbb{1}_{(i \rightarrow j),m}, \tag{3.8}$$

which can be at most k, based on the presented protocol. Since the signals are transmitted coherently, the outage probability achieved at the j-th node is given as follows.

Theorem 3.1. *The probability of having an outage event at the j-th node is*

$$P_o(j, m) = \frac{1}{2} - \frac{1}{\pi} \int_0^\infty \frac{1}{t} \Im \left[\exp\left(-jt \sqrt{\frac{\gamma \sigma^2}{P}} \right) \prod_{i=[j-k]^+}^{j-1} \phi_{i,j}(t)^{\mathbb{1}_{(i \to j),m}} \right] dt, \tag{3.9}$$

where $\phi_{i,j}(t)$ is the characteristic function of $|h_{i,j}|$ and is equal to

$$\phi_{i,j}(t) = 1 + jt \sqrt{\frac{2\pi a_{i,j}}{d_{i,j}^\eta}} \exp\left(-\frac{a_{i,j} t^2}{2 d_{i,j}^\eta} \right) \Phi\left(jt \sqrt{\frac{a_{i,j}}{d_{i,j}^\eta}} \right). \tag{3.10}$$

Proof. In the proposed protocol, at each time-slot, the SNR at the j-th receiver is calculated based on which nodes transmit a signal to the receiver, given the network state s_m. According to the presented theoretical framework, the i-th node transmit a signal to the j-th receiver, if (3.7) is equal to one, i.e., the node is active and its specific buffer's element is not empty. Thus, the SNR of the j-th node for the transition $s_m \to s_l$ equals

$$\text{SNR}_{j,m} = \frac{P}{\sigma^2} \left(\sum_{i=[j-k]^+}^{j-1} |h_{i,j}| \sqrt{\frac{a_{i,j}}{d_{i,j}^\eta}} \mathbb{1}_{(i \to j),m} \right)^2. \tag{3.11}$$

The probability of having an outage event at the j-th node can be expressed as

$$P_o(j, m) = \mathbb{P} \left\{ \sum_{i=[j-k]^+}^{j-1} |h_{i,j}| \sqrt{\frac{a_{i,j}}{d_{i,j}^\eta}} \mathbb{1}_{(i \to j),m} < \sqrt{\frac{\gamma \sigma^2}{P}} \right\}. \tag{3.12}$$

To simplify the analysis, the characteristic function approach is used for the derivation of the outage probability. Each term of the above sum follows a Rayleigh distribution, hence its characteristic function is [135]

$$\phi_{i,j}(t) = 1 + jt \sqrt{\frac{2\pi a_{i,j}}{d_{i,j}^\eta}} \exp\left(-\frac{a_{i,j} t^2}{2 d_{i,j}^\eta} \right) \Phi\left(jt \sqrt{\frac{a_{i,j}}{d_{i,j}^\eta}} \right). \tag{3.13}$$

Since the sum is a linear combination of independent random variables, its characteristic function is the product of each individual's characteristic function. Using the Gil-Pelaez inversion theorem [134], we can obtain $P_o(j, m)$ as (3.9). □

It is clear that for the case where the j-th node receives a signal from only one transmitter i, the outage probability can be given as the cdf of an exponential distribution, i.e.,

$$P_o(j, m) = 1 - \exp\left(-\frac{\gamma \sigma^2 d_{i,j}^\eta}{a_{i,j} P} \right). \tag{3.14}$$

In the following proposition, we provide a closed form approximation of the derived outage probability expression, based on the small argument approximation (SAA) [149].

55

Proposition 3.1. *Under the SAA, the outage probability at the j-th receiver is approximated by*

$$P_o(j, m) \approx 1 - \exp\left(-\frac{\gamma\sigma^2}{2P\theta_{j,m}}\right) \sum_{c=0}^{C_{j,m}-1} \frac{1}{c!}\left(\frac{\gamma\sigma^2}{2P\theta_{j,m}}\right)^c, \quad (3.15)$$

where

$$\theta_{j,m} = \frac{1}{C_{j,m}}[(2C_{j,m}-1)!!]^{1/C_{j,m}} \sum_{i=[j-k]^+}^{j-1} \frac{a_{i,j}}{d_{i,j}^\eta}\mathbb{1}_{(i\to j),m}. \quad (3.16)$$

Proof. From (3.2) it is observed that the channel gain at each receiver consists of a weighted sum of i.i.d. Rayleigh random variables. For the distribution of the weighted Rayleigh sum, the following inequality holds [150]

$$
\begin{aligned}
P_o(j, m) &= \mathbb{P}\left\{\sum_{i=[j-k]^+}^{j-1} |h_{i,j}| \sqrt{\frac{a_{i,j}}{d_{i,j}^\eta}}\mathbb{1}_{(i\to j),m} < \sqrt{\frac{\gamma\sigma^2}{P}}\right\} \\
&\geq \mathbb{P}\left\{\sum_{i=[j-k]^+}^{j-1} |h_{i,j}|\mathbb{1}_{(i\to j),m} < \sqrt{\frac{C_{j,m}\gamma\sigma^2}{g_{j,m}P}}\right\},
\end{aligned}
\quad (3.17)
$$

where $g_{j,m} = \sum_{i=[j-k]^+}^{j-1} a_{i,j}d_{i,j}^{-\eta}\mathbb{1}_{(i\to j),m}$. Note that the right-hand side of (3.17) follows the distribution of a normalized Rayleigh sum. The approximated expression follows by taking the right-hand side of the inequality and then by using the SAA to the cdf of the normalized sum as in [149]. $\square$

The outage probability of the system $P_{out}(\gamma)$ can be calculated by using the steady state of the MC along with the probability of an outage event at the destination. Thus, $P_{out}(\gamma)$ can be expressed as

$$P_{out}(\gamma) = \sum_{m=1}^{M} \pi_m P_o(N+1, m). \quad (3.18)$$

From the derived expressions for the achieved outage probability, it can be seen that the system's performance depends on the number of relays (N), the number of hops (k) and the set of relays that have dual-mode operations (H). In order to provide more insights on the performance of such networks, we need to explore in greater detail how these parameters affect the overall outage probability. In particular, in the next section the performance of our protocol is investigated in the high SNR regime and the DMT is derived.

3.5.1 Diversity-multiplexing tradeoff

In this section, we use the presented outage expressions to derive a tradeoff between the diversity and multiplexing gains for the proposed protocol. Recall that, a channel achieves multiplexing gain ρ and a corresponding diversity gain $\delta^*(\rho)$, if the target data rate $R(P) \sim \rho \log P$ and the outage probability $P_{out}(P)$ satisfy the conditions [133]

$$\lim_{P \to \infty} \frac{R(P)}{\log P} = \rho \quad \text{and} \quad \lim_{P \to \infty} -\frac{\log P_{out}(P)}{\log P} = \delta^*(\rho). \tag{3.19}$$

Below, we provide the proposition which characterizes the DMT that the proposed protocol can achieve.

Theorem 3.2. *The DMT achieved by the proposed protocol for the considered multi-hop network is given by*

$$\delta^*(\rho) = (1 - \rho) \min_{\substack{1 \leq m \leq M \\ \pi_m \not\to 0}} \mathcal{L}_m, \ \rho \in [0, 1], \tag{3.20}$$

where $\mathcal{L}_m$ denotes the minimum number of disjoint paths from S to D that can be obtained for the network instance derived by the state s_m.

Proof. By considering $P \to \infty$, we notice that the outage probability at the j-th relay converges to zero if it receives a signal from at least one transmitter, i.e., $C_{j,m} > 0$, otherwise it is equal to one. Thus, the relays that receive a signal are almost surely able to decode the message. Moreover, if a transmitter has a full buffer at every time-slot and is always active, then its corresponding receivers will also have constantly a full buffer. For example, a relay that receives information from S will always have a full buffer, and if this relay is not in dual-mode operation, then its corresponding receivers will also have full buffers at every time-slot. This implies that the steady states of the transition matrix that do not conform with the above observations will converge to zero.

According to (3.18), the system's outage probability is a sum of M terms that depends on the stationary distribution of the MC and the outage probability at the destination for each steady state. At the high SNR regime, the terms of the sum in (3.18) that correspond to steady states converging to zero are omitted. For each of the remaining terms, we obtain the network instance associated with the corresponding MC state s_m and derive the flow graph G_m from S to D for the paths that will surely forward the signals to D, i.e., by omitting the dual-mode relays. Let $\mathcal{T}_m = \{T_{1,m}, T_{2,m}, \ldots\}$ denote the complete set of cuts separating S and D at G_m, and

$\mathcal{L}_{i,m}$ denote the number of links crossing the cut $T_{i,m}$. According to the information theoretic max-flow min-cut theorem [151], the DMT that can be achieved by G_m is upper bounded by

$$\delta_m(\rho) \leq \mathcal{L}_m = \min_i(\mathcal{L}_{i,m}). \tag{3.21}$$

Note that $\mathcal{L}_m$ is equal to the minimum number of edge-disjoint paths that forward information from S to D. The system's outage probability is dominated by the terms that have the lowest order, or equivalently by the minimum number of links crossing a cut $T_{i,m}$ from all the derived flow graphs G_m, $1 \leq m \leq M$, $\pi_m \not\to 0$. Thus, by defining the target data rate as $R = \log(1 + \gamma) = \rho \log P$ and based on the results of [46] about the DMT of networks that can organize their relays into parallel paths, the DMT is given by (3.20). $\qquad\square$

Corollary 3.1. *The maximum diversity order of the proposed protocol for a given network topology is achieved when $\rho = 0$ and is equal to $\delta^*(0) = \min\limits_{\substack{1 \leq m \leq M \\ \pi_m \not\to 0}} \mathcal{L}_m$.*

We can observe from Corollary 3.1 that the maximum diversity order can vary between zero and k, i.e., $0 \leq \delta^*(0) \leq k$. The exact behavior of the network in the high SNR regime depends significantly on which relays within the network are dual-mode. Below, we examine how the diversity order of the protocol is affected in different topology scenarios.

Only dual-mode relays ($\nu = N$)

In this scenario, all the relays of the network are dual-mode and so they can transmit information only when they are active. Even though at high SNR each node is able to decode all of its received signals, when all the transmitters of a node are concurrently silent during one time-slot, the node does not receive any signal and so the relays' buffers may still have empty elements. The outage performance of the network is then dominated by the terms for which the destination does not receive information from any relay. Therefore, the system's performance converges to an outage floor value, unless there is a direct link from S to D, i.e., $k = N+1$, which results in diversity order equal to one. For $k \leq N \leq 2k$, we state the following proposition.

Proposition 3.2. *The outage floor value of the considered network for $k < N \leq 2k$ is given by*

$$e(N, k) = q^k e(N - 2, k - 1) + (1 - q^k)e(N - 1, k), \tag{3.22}$$

and for N = k is equal to

$$e(N,k) = q^k. \tag{3.23}$$

Proof. Recall that, by considering $P \to \infty$, the outage probability of a node converges to zero if it receives at least one signal during one time-slot. Thus, a receiver is in outage only if all its corresponding transmitters remain silent. For an arbitrary signal $x(t)$ the system is in outage if the signal cannot reach D, so the outage floor value is given by the aggregate probability of the instances that fail to transfer the signal to D. According to the proposed protocol, until time-slot $(t + k - 1)$ the first k relays will definitely receive and decode the signal $x(t)$ from S, which is always active. If $N = k$, then the next node is D and an outage occurs if all the relays remain silent, for which the probability is calculated as (3.23).

For $N > k$, relay $k + 1$ cannot receive $x(t)$ if the previous k relays remain silent during time-slot $(t + k)$, which occurs with probability q^k. For the remaining time-slots, we can calculate the probability of the system being in outage by equivalently considering the outage probability of another network topology with $N - 2$ relays and $k - 1$ hops, since the first relay cannot contribute anymore to the transmission of $x(t)$ and relay $k + 1$ has not decoded the signal, and so they can be omitted. On the contrary, relay $k + 1$ receives $x(t)$ at time-slot $(t + k)$ if at least one of its transmitters is active, and this occurs with probability $(1 - q^k)$. In this case, the outage probability for the remaining time-slots is matched to the outage probability of an equivalent topology with $N - 1$ relays and k hops, by considering the first relay as the new source node. This recursive behavior leads to the calculation of the outage floor by (3.22). □

For $N > 2k$ the outage floor value can be also extracted by following a similar approach. However, the expressions of these cases are more complex and their exact derivation is out of the scope of this chapter.

Only active relays ($v = 0$)

In contrast to the previous scenario, in this case, all the relays are always active and so they are able to transmit their decoded signals at every time-slot. By considering $P \to \infty$, we notice that the outage probability at each relay and for every received signal converges to zero. This implies that the stationary distribution of the transition matrix is given by $\pi_m \to 0$, $m = 1, \ldots, M - 1$, and $\pi_M \to 1$, as all the buffers are full.

If we follow the same procedure as in the proof of Theorem 3.2 we conclude that for the specific scenario the DMT of the investigated model is equal to

$$\delta^*(\rho) = k(1 - \rho), \ \rho \in [0, 1]. \tag{3.24}$$

and for $\rho = 0$ it can achieve a maximum diversity order equal to the number of hops, i.e., $\delta^*(0) = k$.

Deployment strategy for $0 < \nu < N$

In the previous two scenarios we presented the two extreme cases that a network topology can be found, regarding the number of dual-mode relays. Any intermediate scenario, where only part of the relays are dual-mode, i.e., $0 < \nu < N$, is expected to have a performance that lies between these limits. As previously stated, the selection of which relays will have dual-mode operations can significantly affect the network's performance. The proposed protocol can achieve diversity gain, if a signal can be received from D through transmission paths which consist only of active relays, since the outage probability in these instances will not depend on q and it will converge to zero. Specifically, a network can achieve diversity order $\delta^*(0) = \epsilon$, $1 \leq \epsilon \leq k - 1$, if the number of dual-mode relays satisfies the condition

$$k - \epsilon \leq \nu \leq \left\lceil \frac{N}{k} \right\rceil (k - \epsilon), \tag{3.25}$$

and each subset of k consecutive relays contains a maximum number of $k - \epsilon$ dual mode relays.

3.5.2 Multi-branch multi-hop network

In general, the adaptation of the network deployment, according to the previous cases, is not always achievable or the dual-mode operation may refer to conditions for which our intervention is not feasible. To overcome this issue, the aforementioned framework can be also generalized to multi-branch networks [28]. Specifically, we consider a cooperative system of Z orthogonal branches with common source and destination nodes, where each branch consists of N intermediate relays R_i^z, $1 \leq i \leq N$, $1 \leq z \leq Z$. For each branch a k_z-myopic DF strategy is employed independently, where $1 \leq k_z \leq N + 1$. Moreover, each branch may choose its ν_z dual-mode relays differently. An example of this topology is shown in Fig. 3.2.
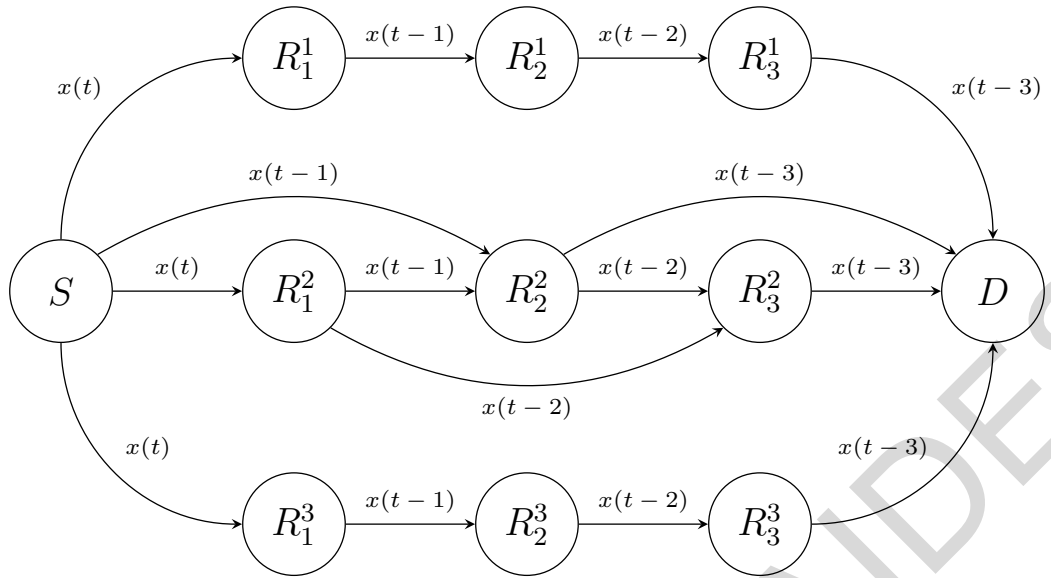
Figure 3.2: Topology of a wireless network with three branches and three relays at each branch. The branches employ the k_z-hop myopic DF strategy independently, where $k_1 = k_3 = 1$ and $k_2 = 2$.

We assume that the destination D receives the transmitted signals by performing the selection combining technique [152]. In this case the combiner chooses the signal of the branch with the highest SNR. Since the branches in this case are orthogonal, the previous outage probability analysis can be performed at each branch separately. Therefore, the system's outage probability for the multi-branch scenario is given by

$$P_{out}(Z, \gamma) = \prod_{z=1}^{Z} P_{out}^z(\gamma) = \prod_{z=1}^{Z} \sum_{m_z=1}^{M_z} \pi_{m_z} P_o(N+1, m_z), \tag{3.26}$$

where $P_o(\cdot)$ is given by (3.9). Note that if the number of hops is the same for all the participating branches, i.e., $k_z = k$, $1 \le z \le Z$, and each branch has equal number of dual-mode relays at the same position, then the outage probability of the system can be rewritten as

$$P_{out}(Z, \gamma) = \left[\sum_{m=1}^{M} \pi_m P_o(N+1, m) \right]^Z. \tag{3.27}$$

Regarding the high SNR regime, the following proposition provides the DMT for the case of multi-branch networks.

Proposition 3.3. *The DMT of the proposed protocol for the considered multi-branch multi-hop network is given by*

$$\delta^*(\rho) = (1 - \rho) \sum_{z=1}^{Z} \min_{\substack{1 \le m_z \le M_z \\ \pi_{m_z} \not\to 0}} \mathcal{L}_{m_z}, \ \rho \in [0, 1]. \tag{3.28}$$

61

By considering $P \to \infty$ and since we assume that the branches are orthogonal, the DMT is derived from (3.19) as

$$\delta^*(\rho) = -\lim_{P \to \infty} \frac{\log \prod_{z=1}^{Z} P_{out}^z(\gamma)}{\log P} = -\sum_{z=1}^{Z} \lim_{P \to \infty} \frac{\log P_{out}^z(\gamma)}{\log P}, \qquad (3.29)$$

which follows by the logarithmic identity $\log(xy) = \log(x) + \log(y)$. The final expression in (3.28) is derived by calculating the DMT of each branch separately, following the result of Theorem 3.2. Based on the above results, the maximum diversity order that can be achieved by a multi-branch network is the sum of the number of hops at each branch, i.e.,

$$\delta^*(0) = \sum_{z=1}^{Z} k_z, \qquad (3.30)$$

which is achieved if each branch topology has only active relays, i.e., $v_z = 0 \; \forall$ $z = 1, \ldots, Z$. Furthermore, by considering the case with an equal number of hops at all branches, the maximum diversity order can be calculated by $\delta^*(0) = Zk$. It is therefore easily observed that the protocol can achieve a performance enhancement of order equal to the number of branches. Even for the case where each branch's performance reaches an outage floor, the utilization of a multi-branch scenario can significantly decrease the overall outage floor value for the considered network.

3.5.3 Illustrative example ($N = 2$ relays, $k = 2$ hops)

We provide an example of the proposed framework that refers to a network topology with $N = 2$ relays and $k = 2$ hops. In this case, the size of the buffers b_1 and b_2 (and therefore of the arrays β_1 and β_2) is $L_1 = 2$ and $L_2 = 1$, respectively. The concatenation of the arrays β_1 and β_2 results in a binary vector of finite size $L_\beta = 3$, which represents a buffer state of the MC. In this example, there are $M_B = 2^3 = 8$ different buffer states. The set of dual-mode relays for the considered network can be any subset of the ordered set $H = \{1, 2\}$. For this example, the system's outage probability is calculated for the case where all the relays are always active, i.e., $H = \emptyset$. Therefore, the resulting MC states are defined only by the buffer states of the network, and are presented in Fig. 3.3. By following the procedure in Algorithm 2.1, the state transition matrix $\mathbf{A}$ is derived as
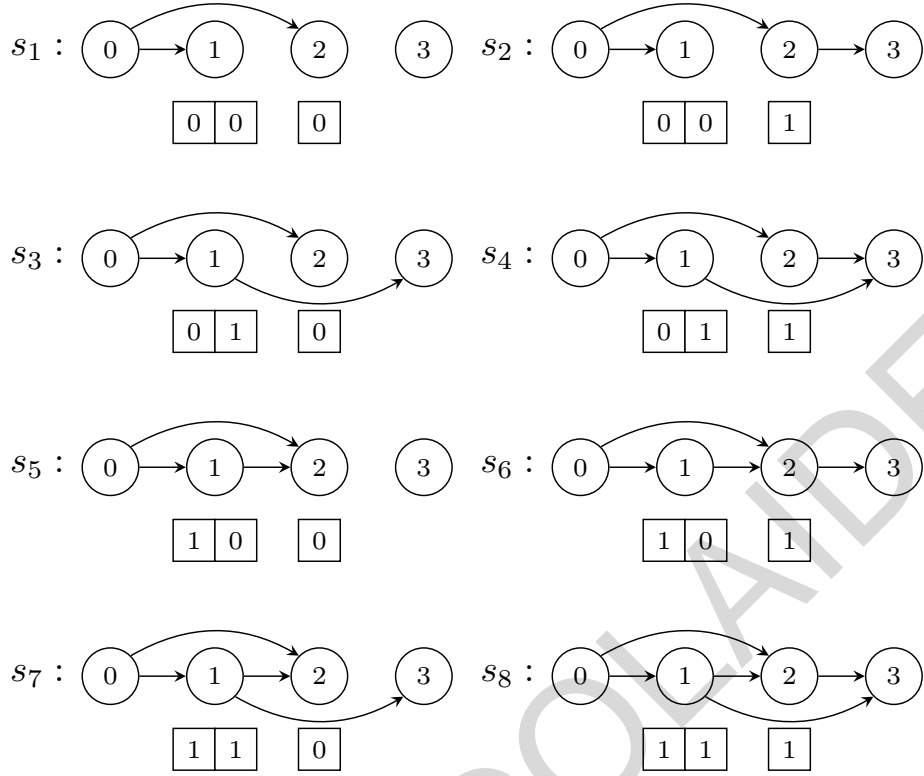
Figure 3.3: The possible states of the MC for a network topology with $N = 2$ relays, $k = 2$ hops and $H = \emptyset$. For each state, the contents of the arrays β_1 and β_2 are presented below the corresponding relay, as well as which of the available links are used.

$$
\mathbf{A} = \begin{pmatrix}
p_{1,1} & p_{1,2} & p_{1,3} & p_{1,4} & 0 & 0 & 0 & 0 \\
p_{2,1} & p_{2,2} & p_{2,3} & p_{2,4} & 0 & 0 & 0 & 0 \\
0 & 0 & 0 & 0 & p_{3,5} & p_{3,6} & p_{3,7} & p_{3,8} \\
0 & 0 & 0 & 0 & p_{4,5} & p_{4,6} & p_{4,7} & p_{4,8} \\
p_{5,1} & p_{5,2} & p_{5,3} & p_{5,4} & 0 & 0 & 0 & 0 \\
p_{6,1} & p_{6,2} & p_{6,3} & p_{6,4} & 0 & 0 & 0 & 0 \\
0 & 0 & 0 & 0 & p_{7,5} & p_{7,6} & p_{7,7} & p_{7,8} \\
0 & 0 & 0 & 0 & p_{8,5} & p_{8,6} & p_{8,7} & p_{8,8}
\end{pmatrix}, \tag{3.31}
$$

where the entries $p_{l,m}$ denote the probabilities of the existent transitions and are given by

$$
p_{l,m} = \Big[\beta_{1,l}[1](1 - P_o(1,m)) + (1 - \beta_{1,l}[1])P_o(1,m)\Big]
$$
$$
\times \Big[\beta_{2,l}[1](1 - P_o(2,m)) + (1 - \beta_{2,l}[1]) P_o(2,m)\Big]. \tag{3.32}
$$

63

By using (3.7) and from the network instances in Fig. 3.3, we observe that S always transmits a signal to R_1, while R_2 always receives from S and at states s_5, s_6, s_7 and s_8 it also receives from R_1. Finally, the transmitters of D are R_1 and R_2 at states s_4 and s_8, only R_1 at states s_3 and s_7 and only R_2 at states s_2 and s_6. At states s_1 and s_5 the destination does not receive any data, so it is on outage with probability one. From the derived results the following relations are obtained

$$
\begin{aligned}
P_o(1,1) &= P_o(1,2) = \ldots = P_o(1,8), \\
P_o(2,1) &= P_o(2,2) = P_o(2,3) = P_o(2,4), \\
P_o(2,5) &= P_o(2,6) = P_o(2,7) = P_o(2,8), \\
P_o(3,m) &= P_o(3,m+4), \ m = 1,\ldots,4.
\end{aligned}
\tag{3.33}
$$

The system's outage probability is given by calculating the stationary distribution of the MC and, based on the aforementioned relations, is equal to

$$
\begin{aligned}
P_{out}(\gamma) &= \sum_{m=1}^{8} \pi_m P_o(3,m) \\
&= P_o(1,1)P_o(2,1) + P_o(1,1)\left[1 - P_o(2,1)\right]P_o(3,2) \\
&\quad + \left[1 - P_o(1,1)\right]P_o(2,5)P_o(3,3) \\
&\quad + \left[1 - P_o(1,1)\right]\left[1 - P_o(2,5)\right]P_o(3,4),
\end{aligned}
\tag{3.34}
$$

where the probabilities $P_o(i,m)$ can be calculated by using the aforementioned outage expressions in (3.9), (3.14) or (3.15).

Regarding the diversity gain of the network, we need to examine which are the dual-mode relays within the network. Thus, if all the relays are active, i.e., $H = \emptyset$, then the proposed protocol can achieve diversity order equal to the number of hops, while for $H = \{1\}$ or $H = \{2\}$, from Corollary 3.1 the maximum diversity order is equal to one. Finally, if all the relays are dual-mode, i.e., $H = \{1,2\}$, then at high SNR the outage probability converges to a floor value which is calculated from (3.23) as $e(2,2) = q^2$.

3.6   Numerical Results

In this section, we validate our theoretical analysis and main analytical results with computer simulations to demonstrate the effect of various network parameters on the performance of our proposed myopic protocol. For the simulations, the following

parameters are considered. The distance between S and D is set to a fixed value of $d_{0,N+1} = 3$ m and the distance between two consecutive nodes is the same for all nodes, i.e., $d_{i,i+1} = d = d_{0,N+1}/(N+1) \; \forall \; i = 0, \ldots, N$. In addition, the path loss exponent is equal to $\eta = 2$, the variance of the AWGN is normalized to $\sigma^2 = 1$ and the energy of the channel coefficients is normalized to $\mathbb{E}\left\{|h_{i,j}|^2\right\} = 1$. Finally, the SNR threshold is set to $\gamma = 0$ dB. Note that, in all the presented figures, the analytical results are illustrated with lines (solid, dashed or dotted) and the simulation results with markers.

It can be easily observed that the system's outage probability depends on how the transmit power of each node is divided. Therefore, our results are numerically optimized with respect to the power splitting parameters $a_{i,j}$. We formulate the system's outage probability minimization problem as follows

$$
\begin{aligned}
\min_{\{a_{i,j}\}} \quad & P_{out}(\gamma) \\
\text{s.t.} \quad & \sum_{j=i+1}^{L_i+i} a_{i,j} = 1, \quad i = 0, \ldots, N, \\
& 0 < a_{i,j} < 1, \quad i = 0, \ldots, N, \\
& q = 0.
\end{aligned}
\tag{3.35}
$$

Note that the second constraint ensures that a portion of the power P will be allocated to all the available channel links. Moreover, the optimization is formulated for the case where all the relays of the network are always active, i.e., $q = 0$, which leads to a simpler implementation of the protocol, since the power management at each relay will not depend on the general knowledge of the communication modes of all the relays at each time-slot. Due to the complexity of the derived expressions, the aforementioned minimization problem can be solved using numerical tools, such as the *NMinimize* function of Mathematica [153].

Figs. 3.4 and 3.5 illustrate the system's outage probability against the transmit power P in a network setting with $N = 2$ and 3 relays, respectively, considering the case where the relays are always active. The outage performance is investigated for all possible k-hop myopic scenarios, i.e., for $k = 1, \ldots, N + 1$. For these scenarios, the conventional multi-hop DF scheme used in [39], where each node sends a signal only to its subsequent node through orthogonal channels, is used as a performance
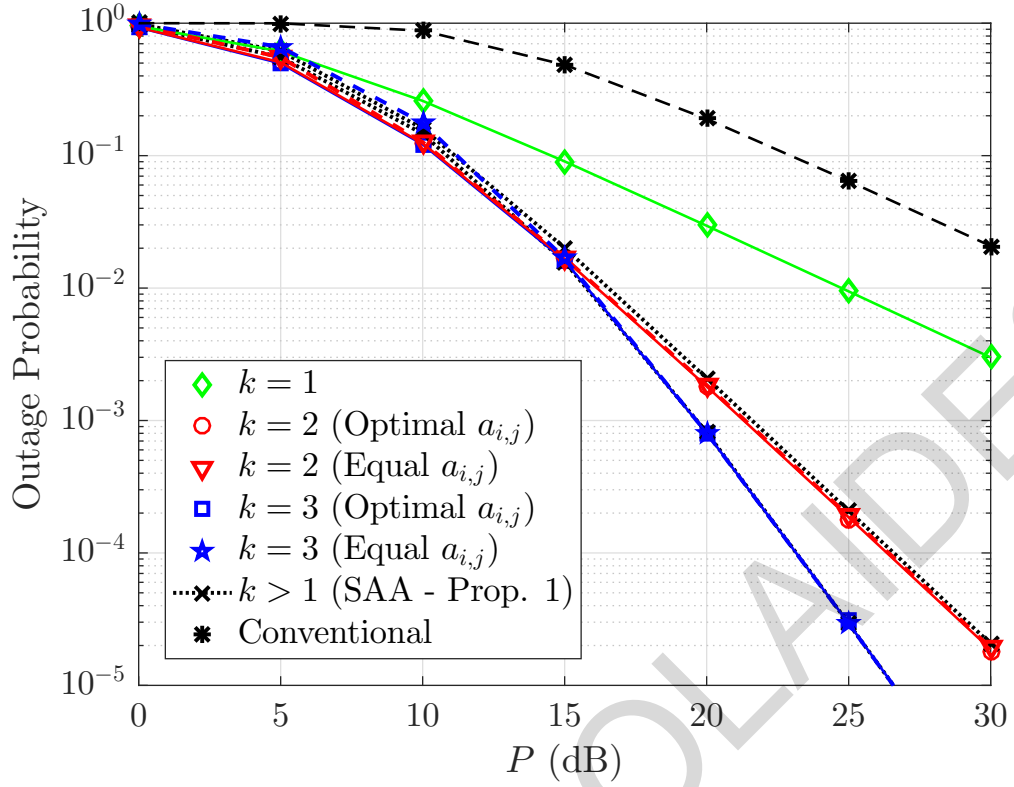
Figure 3.4: Outage probability versus P for a network topology with $N = 2$ relays, $k = 1, 2, 3$ hops, $H = \emptyset$, $\gamma = 0$ dB and $d = 1$ m; the theoretical results are depicted with lines and the simulation results with markers.

benchmark. The outage probability in this case is given by

$$P_{out,c} = 1 - \prod_{j=1}^{N+1} \mathbb{P}\left\{\text{SNR}_j \geq \gamma_c\right\}$$
$$= 1 - \exp\left[-\frac{(N+1)\,\gamma_c d^\eta \sigma^2}{P}\right], \tag{3.36}$$

where $\gamma_c = (\gamma + 1)^{N+1} - 1$. We observe that, in both figures, our proposed protocol is superior to the conventional multi-hop scheme. In particular, it can be seen that the k-hop myopic strategy outperforms the typical multi-hop DF scheme in terms of outage performance and coding gain. Moreover, for $k > 1$ the myopic scheme also achieves a higher diversity gain. Furthermore, in Fig. 3.4, the optimized outage performance of the network, according to (3.35), is also compared to the case where the power at each transmitter is equally divided to each channel link, i.e., $a_{i,j} = 1/\min(k, N - i + 1)$, $0 \leq i \leq N$. It is observed that, while at high SNRs the performance is almost the same for both cases, in the low SNR regime the outage probability is slightly improved for the numerically optimized values of $a_{i,j}$. It is also worth noting that, when P is equally divided, the system cannot fully benefit from
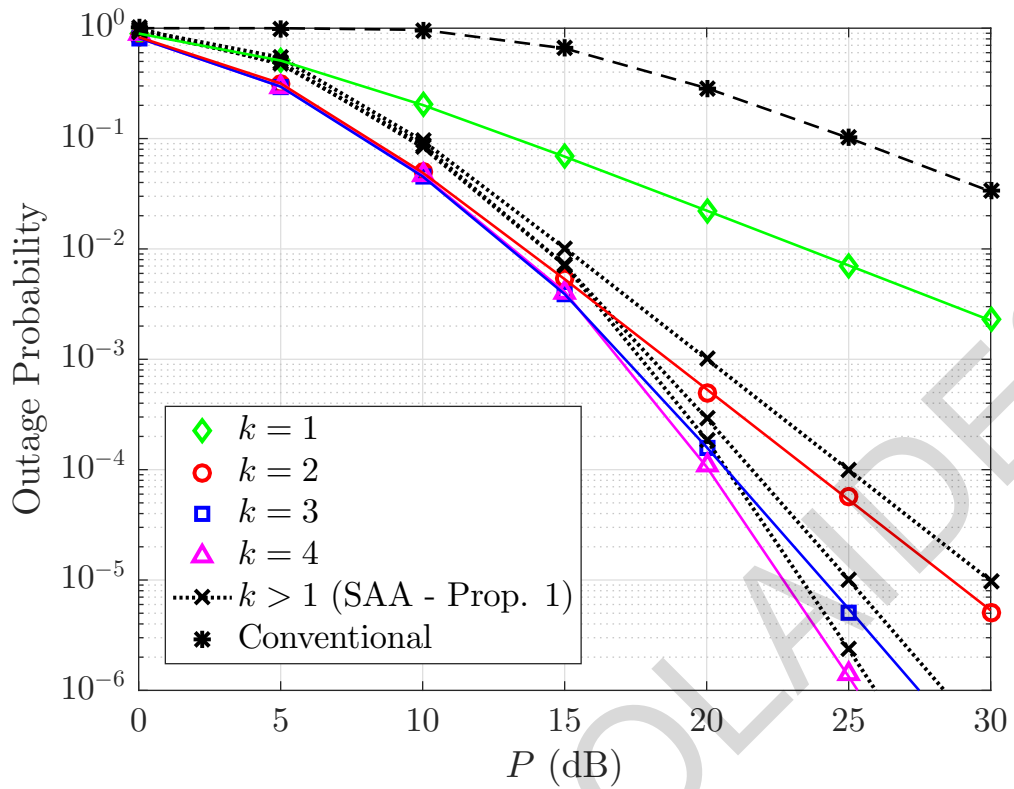
Figure 3.5: Outage probability versus P for a network topology with $N = 3$ relays, $k = 1, 2, 3, 4$ hops, $H = \emptyset$, $\gamma = 0$ dB and $d = 0.75$ m.

the increase on the number of hops, since the outage performance for $k = 3$ is worse than the 2-hop scenario at low transmit power values.

Fig. 3.4 shows that an increase in the number of hops results in an improvement of the outage probability performance, with the cases of $k = 1$ and $k = 2$ revealing the most significant difference (i.e., about 8 dB gain for an outage probability equal to 10^{-2}). However, for a transmit power value up to 15 dB the 2-hop scenario has similar performance with the 3-hop case. Therefore, for lower values of P a topology with $k < N + 1$ can have a performance close to the case of full cooperation; this observation corresponds to the results of [139]. In addition, it can be seen that as the number of hops increases the diversity gain is also improved, which complies with our analysis indicating a maximum diversity order equal to k when the relays of the network are always active. Similar results are derived in Fig. 3.5 for $N = 3$ relays. It is worth noting that in this case the outage probability for our protocol is slightly improved, compared to the results in Fig. 3.4, due to the reduced path loss. On the other hand, the diversity gain remains the same, as it depends only on the number of hops. Finally, we observe that in both figures the theoretical values (lines)

Figure 3.6: Outage probability versus P for different sets of dual-mode relays; $N = 2$ relays, $k = 2$ hops, $q = 0.1$, $\gamma = 0$ dB and $d = 1$ m.

perfectly match to the simulation results (markers), which validates the accuracy of our analysis, while for $k > 1$ the obtained SAA expression in Proposition 3.1 provides a tight approximation of the actual performance of the network.

In Figs. 3.6 and 3.7 the achieved outage probability is presented for various sets of dual-mode relays, under the 2-hop myopic protocol and for a network topology with $N = 2$ and 3 relays, respectively. As expected, the case where all the relays are active is superior to any other scenario and is the only case that can achieve the maximum possible diversity gain $k = 2$. On the other hand, if the network consists of only dual-mode relays, the outage performance is significantly deteriorated and as P increases, the outage probability converges to the floor value calculated in Proposition 2. The performance of any other deployment scenario lies between the limits set by the previous two extreme cases.

Specifically, in Fig. 3.6 it is observed that both intermediate cases with $H = \{1\}$ and $H = \{2\}$ achieve the same diversity order, which is equal to one. However, when only R_1 is able to switch between active and silent mode, the system achieves a better outage performance than the system where only R_2 has dual-mode operations. This
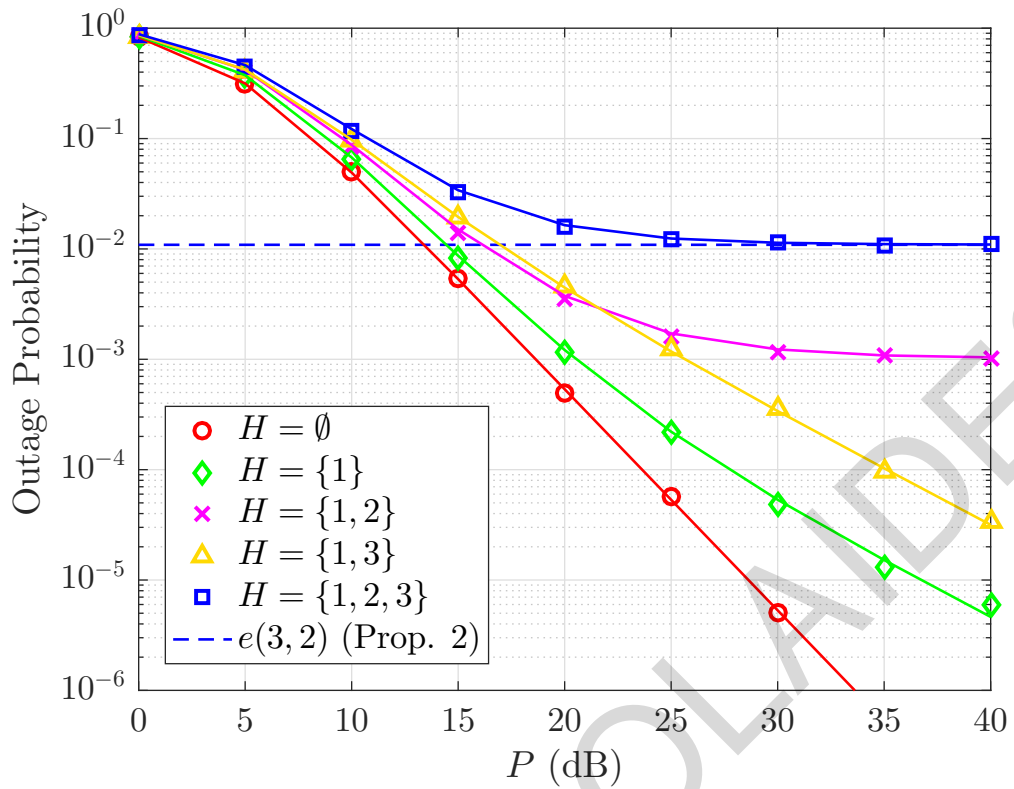
Figure 3.7: Outage probability versus P for different sets of dual-mode relays; $N = 3$ relays, $k = 2$ hops, $q = 0.1$, $\gamma = 0$ dB and $d = 0.75$ m.

is expected, since R_2 is closer to D, which is also its only receiver, and so R_2 being silent has a higher impact to the system's outage probability. Again, in this figure we show that our simulation results (markers) validate our analysis (lines). In Fig. 3.7, it can be seen that if only R_1 is dual-mode, the achieved diversity order is decreased to one. Moreover, in the case of $H = \{1, 3\}$ the same diversity order can be achieved, even though more dual-mode relays are used, since there is still a possible path from S to D which does not depend on the dual-mode operations ($S \rightarrow R_2 \rightarrow D$). On the contrary, the performance of the topology considering $H = \{1, 2\}$ converges to an outage floor, due to the consecutive order of the two dual-mode relays. Therefore, the selection of which relays will operate in dual-mode is critical for the network's performance, and especially the achieved diversity gain, and this observation follows our discussion in Section 3.5.1.

Finally, Fig. 3.8 depicts the outage probability versus P for different number of branches and various combinations of dual-mode relays, where each branch deploys a network setting with $N = 2$ relays and $k = 2$ hops. First of all, we can see that an increase in the number of branches results in the improvement of the system's
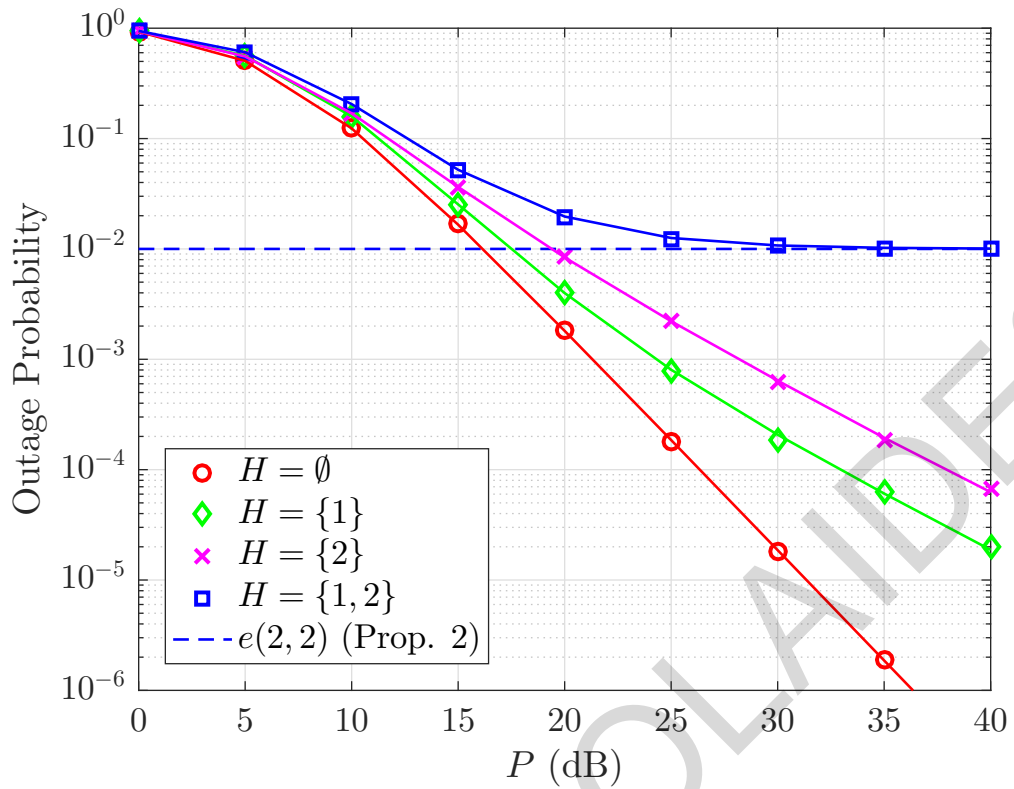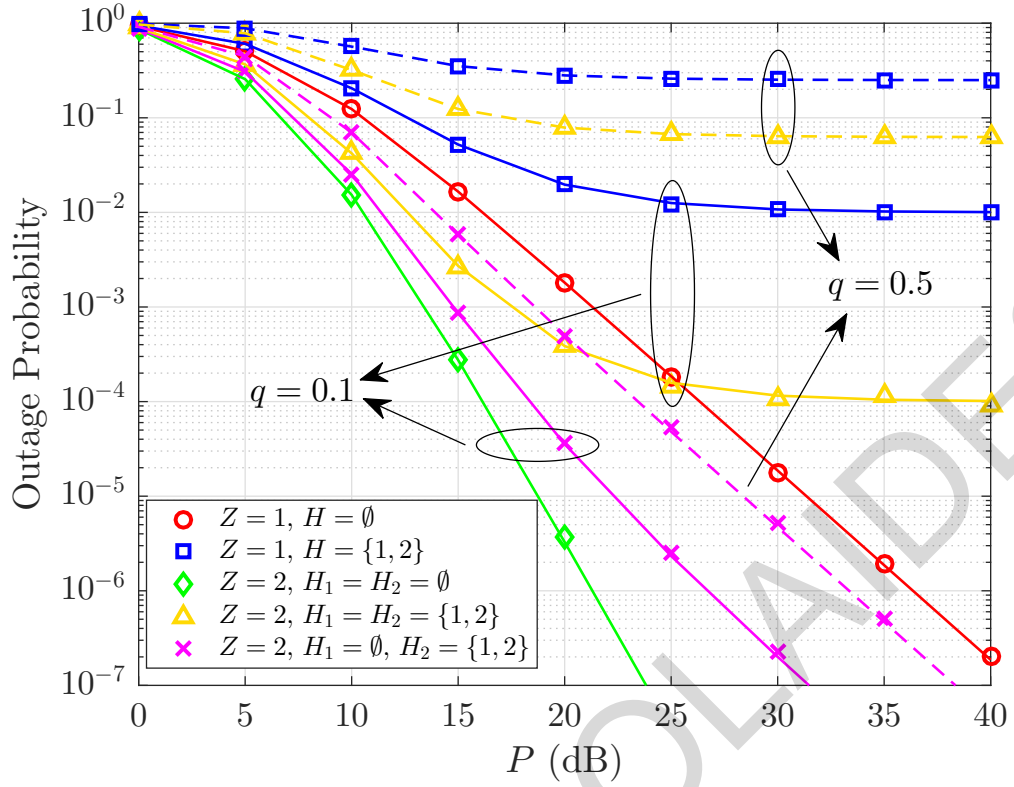
Figure 3.8: Outage probability versus P for different number of branches; $N = 2$ relays, $k = 2$ hops, $\gamma = 0$ dB and $d = 1$ m.

outage probability. Specifically, compared to the single branch with only active relays scenario, doubling the branches will also double the achieved diversity gain, while if the second branch has only dual-mode relays, the system will not achieve higher diversity gain but its outage performance will still be enhanced. Similarly, if we consider a single branch network with only dual-mode relays, doubling the branches will significantly decrease the outage floor value. The aforementioned scenarios are also presented for different values of q, i.e., the probability of a dual-mode relay to be silent. As expected, as this probability increases the system's outage probability increases as well, since the dual-mode relays will remain silent for a larger number of time-slots. However, the system's performance remains unaffected in terms of diversity gain.

To summarize, based on the presented results it can be observed that the myopic-based scheme can have a performance close to the full-cooperation scenario for low to medium transmit power values, while in the high SNR regime the maximum achieved performance is dominated by the number of hops. On the other hand, although the full-cooperation scheme achieves the optimal performance, in practice

as we increase the number of hops the implementation complexity increases (higher system's overhead, more complicated power management and hardware equipment etc.). In this case the number of hops can be used to adapt the myopic strategy to the available resources. Moreover, for optimizing the performance of the system, the selection of which relays will operate in dual-mode needs to be carefully designed.

3.7 Conclusions

In this chapter, we presented a new protocol over a multi-hop cooperative network, based on the myopic strategy, where the relays have buffers of finite size and can operate in two communication modes, namely the active and silent mode. A general methodology that captures how the contents of each relay's buffer and the communication operation of each relay evolve with time was proposed by using a MC formulation. Under this framework, we derived the outage probability of the system and a general expression for the resulting DMT, and we investigated the maximum diversity order that can be achieved, based on different topology scenarios. The proposed protocol was also generalized for multi-branch networks with orthogonal branches. We demonstrated that as the number of hops in the proposed protocol increases, the system's performance is enhanced in terms of outage probability, while the achieved diversity gain depends on both the number of hops and the group of relays that have dual-mode operations.

Chapter 4

Outage and DMT Analysis of Partition-based Schemes for RIS-aided MIMO Fading Channels

Recently, RIS has been proposed as a promising technology for controlling the wireless propagation environment in an efficient and intelligent manner to improve the efficiency and increase the coverage of wireless systems. However, most of the available solutions assume perfect CSI knowledge for their implementation. In this chapter, we investigate the performance of MIMO fading channels assisted by an RIS, through the employment of partition-based RIS schemes. The proposed schemes are implemented without requiring any CSI knowledge at the transmitter side; this characteristic makes them attractive for practical applications. In particular, the RIS elements are partitioned into sub-surfaces, which are periodically modified in an efficient way to assist the communication. Under this framework, we propose two low-complexity partition-based schemes, where each sub-surface is adjusted by following an amplitude-based or a phase-based approach. Specifically, the *activate-reflect* (AR) scheme activates each sub-surface consecutively, by changing the reflection amplitude of the corresponding elements. On the other hand, the *flip-reflect* (FR) scheme adjusts periodically the phase shift of the elements at each sub-surface. Through the sequential reconfiguration of each sub-surface, an equivalent parallel channel in the time domain is produced. We analyze the performance of each scheme in terms of outage probability and provide expressions for the achieved DMT.

4.1 Introduction

The development of future generations of wireless communications is envisioned to satisfy the constantly increasing demands in the number of devices that need to communicate, with extremely high data rates and ultra-reliable connectivity capabilities [15]. In particular, recent research advances towards the realization of the 6G era suggest that, by successfully controlling the wireless propagation environment in an efficient and intelligent manner, the performance of wireless networks could be enhanced beyond the current limits [69]. Towards this direction, RIS has been proposed as an appealing low-cost solution which can improve energy efficiency, due to the passive operation of the elements, and spectral efficiency, since they operate in ideal full-duplex mode, as well as increase the coverage of wireless networks [21,71]. Driven by the relative benefits of this technology, the employment of RISs to support the communication in wireless systems has been widely considered in the literature, while it has also been integrated with other promising candidate technologies for the next-generation systems, e.g., NOMA and THz communications [84,92]. Moreover, numerous studies investigate the performance of both SISO and MIMO networks assisted by the use of an RIS, focusing on various performance metrics, such as the ergodic capacity, the outage probability, the energy efficiency and the diversity gain [83,85,87,88,93].

Most of the aforementioned works assume that perfect CSI knowledge is available for the implementation of the proposed schemes. However, this assumption can be impractical, especially for a large number of RIS elements, due to the high implementation complexity or limited resources. Recently, some channel estimation protocols for RIS-aided networks have been proposed by considering several techniques, such as channel decomposition [112] and discrete Fourier transform (DFT) training [113]. It can be observed that the training time of the proposed solutions increases proportionally with the size of the RIS, which could induce large feedback overhead and compromise the expected performance gains. Moreover, several works claim that by increasing the number of elements, the performance of RIS-aided networks is enhanced. However, this highly depends on the information that is available in the system, as well as the considered communication scenario. In particular, in [96] it was shown that, when only statistical CSI is available, larger RISs improve the throughput of the system, but the gain diminishes quickly by increasing

the RIS elements. In addition, the authors in [154] considered an UAV-based system, where an RIS is mounted to the UAV, and demonstrated that increasing the RIS size may lead to reduced data collection from the UAV.

It is, therefore, an important and challenging task to provide efficient solutions, which can enhance the performance of RIS-aided networks with reduced implementation complexity. Motivated by this, in this chapter, we study the performance of RIS-assisted MIMO communications under partition-based RIS schemes. Specifically, by incorporating the idea of parallel partitions in multi-hop MIMO channels [47], we create a parallel channel in the time domain by intelligently adjusting different subsets of RIS elements based on a fixed reconfiguration pattern. The presented schemes have low complexity and do not require any CSI knowledge at the transmitter or for the RIS design. Specifically, the main contributions of this chapter are summarized as follows:

- A general framework for RIS-aided MIMO systems is presented, where the RIS is partitioned into non-overlapping sub-surfaces, which are sequentially reconfigured to assist the communication. Based on this framework, we propose two low-complexity schemes, by considering an amplitude-based or a phase-based approach. In particular, the AR scheme activates each sub-surface in sequential order, by changing the reflection amplitude of the corresponding elements. On the other hand, the FR scheme creates an equivalent time-varying channel, by modifying periodically the phase shift of the elements at each sub-surface between two discrete values. The proposed schemes can be easily implemented since, in contrast to other works, channel training is not required for adjusting the reflection coefficients of the RIS elements, and a fixed reflection sequence is considered for the reconfiguration of the sub-surfaces, based on a binary state control.

- A complete analytical methodology for the performance of the partition-based schemes is provided. Based on the channel statistics, we derive analytical expressions which characterize the outage probability of each of the proposed schemes. Moreover, under specific practical assumptions, a more tractable methodology on the outage analysis is provided. We also study the asymptotic performance gains of the presented schemes and provide expressions for the achieved DMT. Through this analysis, we show how the idea of partitioning
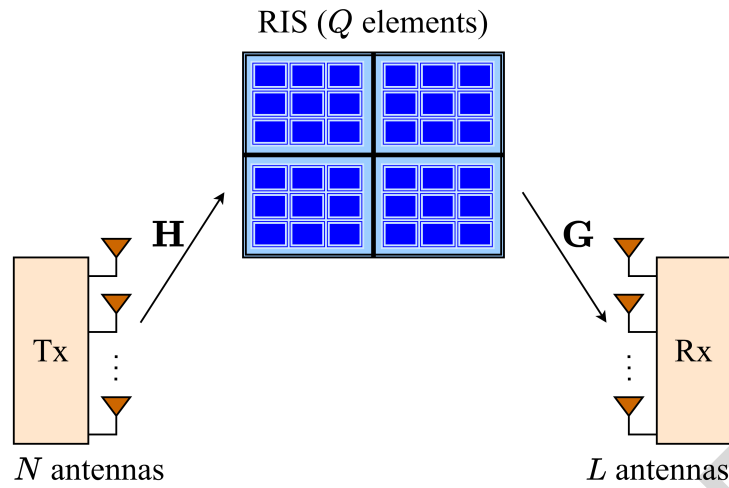
Figure 4.1: The considered RIS-aided channel model.

boosts the performance of the considered system and obtain useful insights into how some key parameters affect the performance gains.

- Our results demonstrate that, by employing the partition-based schemes, the outage performance of the considered system can be significantly improved compared to the conventional case, where all the RIS elements belong to a single partition and randomly rotate the signals. Moreover, both the proposed schemes achieve the same diversity gain. In particular, the achieved diversity gain is enhanced, compared to the conventional case, and this improvement is proportional to the number of partitions. Finally, it is shown that the RIS-aided MIMO system under the FR scheme always achieves the maximum multiplexing gain, while in the AR scheme the maximum multiplexing gain is obtained if certain conditions are satisfied, regarding the number of elements in each sub-surface.

4.2 System Model

We consider a topology where a transmitter (Tx) communicates with a receiver (Rx) through the employment of an RIS, as shown in Fig. 4.1. The Tx and the Rx are equipped with N and L antennas respectively, and the RIS consists of Q reflecting elements connected to a smart controller. Note that a direct link between

the Tx and the Rx is not available[1] (e.g. due to high path-loss or deep shadowing) [85, 86]. Moreover, we consider that adjacent elements are uncorrelated, i.e., a half-wavelength of spacing exists between them [88]. Let $\mathbf{H} \in \mathbb{C}^{Q \times N}$ denote the channel matrix from the Tx to the RIS, and $\mathbf{G} \in \mathbb{C}^{L \times Q}$ the channel matrix from the RIS to the Rx. We assume a frequency-flat Rayleigh block fading channel, in which the channel coefficients remain constant during one time slot, but change independently between different time slots [155, 156]. Moreover, each channel coefficient follows a circularly symmetric complex Gaussian distribution with zero mean and unit variance, i.e., $h_{i,j}, g_{i,j} \sim \mathcal{CN}(0, 1)$. For the rest of this chapter, the channel under this topology will be referred to as the (N, Q, L) channel.

At an arbitrary time slot, the Tx sends a signal vector $\mathbf{x} \in \mathbb{C}^{N \times 1}$. We assume that CSI is perfectly known at the Rx, while CSI knowledge is not available at the Tx and the RIS. Therefore, if $\mathbf{x}$ is transmitted with a constant power P, the power is uniformly allocated to the N transmit antennas. In the considered scenario, every time slot is divided into K sub-slots of equal duration. We denote by

$$\mathbf{\Phi}_k = \text{diag}[a_{1,k}e^{j\phi_{1,k}} \ a_{2,k}e^{j\phi_{2,k}} \ \dots \ a_{Q,k}e^{j\phi_{Q,k}}], \tag{4.1}$$

the diagonal reflection matrix of the RIS, where $a_{i,k} \in [0, 1]$ and $\phi_{i,k} \in [0, 2\pi)$ are the reflection amplitude and the phase shift of the i-th RIS element at the k-th time sub-slot, respectively. Thus, the end-to-end channel matrix during one sub-slot is written as

$$\mathcal{H}_k = \mathbf{G}\mathbf{\Phi}_k\mathbf{H}, \tag{4.2}$$

and the received signal vector at the k-th sub-slot is given by

$$\mathbf{y}_k = \sqrt{\frac{P}{N}}\mathcal{H}_k\mathbf{x} + \mathbf{n}_k, \tag{4.3}$$

where $\mathbf{n}_k \in \mathbb{C}^{L \times 1}$ is the AWGN vector with entries of variance σ^2, i.e., $n_{i,k} \sim \mathcal{CN}(0, \sigma^2)$. As such, the mutual information between the Tx and the Rx over one time slot is equal to

$$I = \frac{1}{K}\sum_{k=1}^{K}\log_2\left[\det\left(\mathbf{I}_L + \frac{\rho}{N}\mathcal{H}_k\mathcal{H}_k^\dagger\right)\right], \tag{4.4}$$

where $\rho = P/\sigma^2$ is the average SNR.

---

[1]This assumption is not restrictive and the proposed RIS schemes can also be implemented when a direct link between the Tx and the Rx exists, but our focus is to highlight the gains provided by these schemes.

4.3 Partition-based RIS schemes

In this section, we describe our proposed partition-based RIS schemes and analytically evaluate their performance. The proposed schemes are inspired by the idea of parallel partitions in multi-hop MIMO channels, which have been introduced in [47]. The main objective of these schemes is to incorporate the temporal processing into the RIS-aided channels by partitioning in a proper way the RIS elements, in order to enhance the performance of such networks. In particular, we assume that the RIS is partitioned into K non-overlapping sub-surfaces $\mathcal{S}_k$, $1 \leq k \leq K$ [157]. This partitioning into sub-surfaces is not restricted by any specific method. Hence, for simplicity and without loss of generality, we assume that K is a divisor of Q so that each sub-surface has an equal number of elements[2] m, i.e., $Km = Q$. An example of the considered scenario is demonstrated in Fig. 4.1, with $K = 4$ and $m = 9$, and where the sub-surfaces are defined by the black solid lines.

At each time sub-slot k, $1 \leq k \leq K$, the reflection configuration of the sub-surface $\mathcal{S}_k$ (i.e. the phase shifts and reflection amplitudes of the corresponding elements) is adjusted, according to the scheme that is deployed at the RIS. By using this approach, the information is transmitted at the destination by creating a set of K parallel sub-channels in the time domain [158]. It is important to note that the number of partitions, the resulting sub-surfaces as well as the configuration sequence are determined in advance. Moreover, this information remains fixed throughout the transmission procedure and therefore can be provided to the Rx *a-priori* [158].

In the following sub-sections, we present two partition-based schemes: the AR scheme, where each sub-surface is sequentially activated to assist the communication by changing the reflection amplitude of the respective elements, and the FR scheme, which modifies the phase shift of the RIS elements at each sub-surface. For these schemes, we focus on the performance evaluation in terms of outage probability. Recall that, the outage probability is defined as the probability that the mutual information is below a non-negative predefined target rate of R bits per channel use (bps/Hz). The general expression for the outage probability is given by

$$\Pi(R, K) = \mathbb{P}\{I < R\} = \mathbb{P}\left\{\sum_{k=1}^{K} I_k < RK\right\}, \tag{4.5}$$

---

[2]The results of the proposed scheme can be readily extended to the case where the defined sub-surfaces may contain different number of elements.

where I is given by (4.4) and

$$I_k = \log_2 \left[\det \left(\mathbf{I}_L + \frac{\rho}{N} \mathcal{H}_k \mathcal{H}_k^\dagger \right) \right], \tag{4.6}$$

is the mutual information of the k-th sub-channel. Next, we introduce the design framework that is considered for the implementation of the AR scheme.

4.3.1 Activate-Reflect scheme

For the AR scheme, we assume that each RIS element can be reconfigured between two possible states, either to be turned ON or OFF [114, 159]. If an element is ON, it can rotate the phase of the incident signals by a specific value, while in the OFF state, the transmitted signals cannot be reflected by the element. In other words, the reflection amplitude of the ON elements is set to one (full reflection), otherwise it is set to zero (full absorption). Without loss of generality, we assume that the induced phase shift by every element is equal to zero[3], i.e., $\phi_{i,k} = 0 \ \forall i, k$ [159].

For the implementation of the AR scheme, a design framework is considered by following the steps below:

- Before transmission, all the elements of each sub-surface are set to the OFF state, i.e., $a_i = 0 \ \forall i$. This is considered as the default configuration of each element.

- Then, each sub-surface is sequentially switched to the ON state to assist the communication of the considered network. Specifically, at each sub-slot k, $1 \leq k \leq K$, the sub-surface $\mathcal{S}_k$ is activated by turning ON only the elements that belong to the specific sub-surface. Note that any other element that does not belong to $\mathcal{S}_k$ will be reset to the default configuration. Therefore, the reflection amplitude of each RIS element at the k-th sub-slot is given by

$$a_{i,k} = \begin{cases} 1, & i\text{-th element} \in \mathcal{S}_k; \\ 0, & \text{otherwise.} \end{cases} \tag{4.7}$$

- The end-to-end channel is then composed of K parallel sub-channels, where each sub-channel can be represented by an equivalent (N, m, L) channel by considering only the activated RIS elements at each time sub-slot.
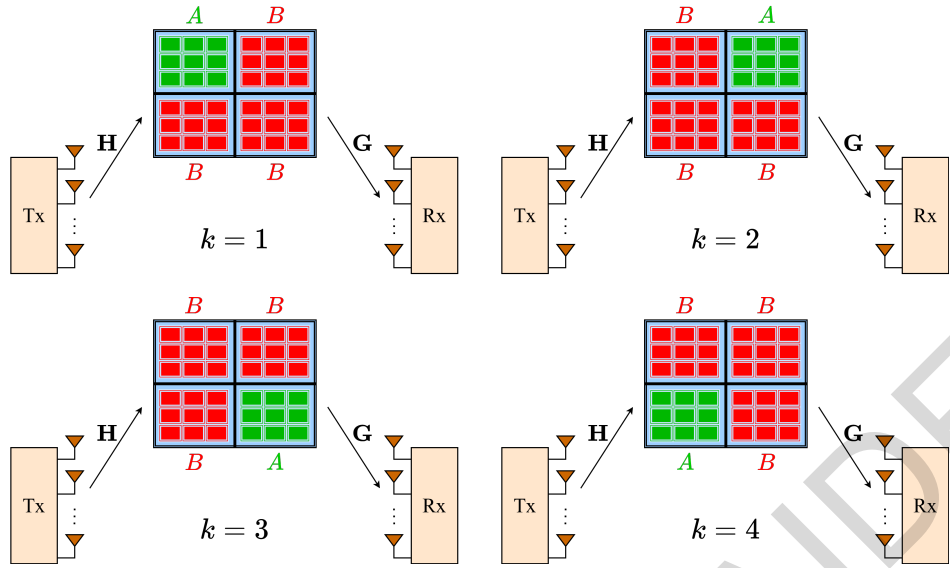
Figure 4.2: The different instances of the RIS configuration over one time slot for a system with $Q = 36$ and $K = 4$; under the AR scheme, $A = $ ON and $B = $ OFF (expression (4.7)); under the FR scheme, $A = \pi$ and $B = 0$ (expression (4.16)).

Note that the above configuration pattern corresponds to an ideal phase shift model, where the reflection amplitude of each element is independent from its corresponding phase shift; however, the AR scheme can be also employed when the reflection amplitude and the phase shift of each element are correlated [160]. An example of the above procedure is shown in Fig. 4.2, where we consider the same RIS-aided channel as in Fig. 4.1. Specifically, Fig. 4.2 depicts how the RIS configuration changes during an arbitrary time slot, by indicating the activated elements at each sub-slot. The proposed AR scheme could be implemented by following the approach presented in [161], where each element is connected to an RF switch, which tunes the reflection amplitude of the element as either zero or one, resulting in a two-level reflection amplitude control. It is apparent that, apart from requiring no CSI knowledge, this scheme has low design complexity and is cost-effective, since we only need a two-level amplitude control for the implementation, which significantly simplifies the RIS hardware. Moreover, although the expected rate decreases, as only m out of the Q elements are activated at each time sub-slot, the power consumption at the RIS is reduced compared to the conventional case. Below, we present two mathematical expressions that can be used to evaluate the

---

[3]The resulting channel gain is statistically equivalent to the case of random phase shifts at the RIS, i.e., each $\phi_{i,k}$ uniformly distributed in $[0, 2\pi)$ [85].

outage performance of the AR scheme. Specifically,

- In Proposition 4.1, the outage probability achieved by this scheme is derived numerically for an arbitrary number of transmit and receive antennas, by using the Gil-Pelaez inversion theorem [134].

- Theorem 4.1 derives the outage probability for the special case of the SISO channel, i.e., $N = L = 1$, by using the CLT, which approximates the channel $\mathcal{H}_k$ as a complex Gaussian random variable.

We first provide a preliminary result in the following lemma for the conventional case of $K = 1$, representing the *pure reflection* (PR) scheme, where all the elements randomly rotate the phase of the incident signals over an arbitrary time slot. This result will assist in the derivation of the analytical results for the presented schemes; the PR scheme will also be used as a performance benchmark for comparison purposes.

Lemma 4.1. *The characteristic function of the mutual information of the (N, Q, L) channel given in (4.4) under random reflections is given by*

$$\varphi(Q, t) = \frac{1}{\prod_{z=1}^{n_0} \prod_{\theta=0}^{2} \Gamma(z + \nu_\theta)} \det\left[\frac{1}{\Gamma(-\jmath t/\ln 2)}\right.$$
$$\left. \times G_{1,3}^{3,1}\left(\begin{array}{c} 1 \\ -\jmath t/\ln 2, \nu_2 + i, \nu_1 + i + j - 1 \end{array} \middle| \frac{N}{\rho}\right)\right]_{i,j}^{n_0}, \quad (4.8)$$

where (n_0, n_1, n_2) is the ordered version of the (N, Q, L) channel and $\nu_i \triangleq n_i - n_0, 0 \le i \le 2$.

Proof. Since $K = 1$, all the RIS elements belong to the same (single) sub-surface and are reconfigured only at the beginning of each time slot. Due to the random rotations at the elements, the induced phase shifts do not have any effect on the channel gain [85]. Therefore, without loss of generality, we can equivalently consider the case where $\phi_{i,1} = 0$, with $1 \le i \le Q$. The reflection matrix of the RIS is then equal to the $Q \times Q$ identity matrix, $\Phi = \mathbf{I}_Q$, and the resulting (N, Q, L) channel can be interpreted as a Rayleigh product channel, i.e., $\mathcal{H}_1 = \mathbf{GH}$. The mutual information of the channel is thus equal to

$$I = \log_2\left[\det\left(\mathbf{I}_L + \frac{\rho}{N} \mathcal{H}_1 \mathcal{H}_1^\dagger\right)\right] = \sum_{i=1}^{n_0} \log_2\left(1 + \frac{\rho}{N} \lambda_i\right), \quad (4.9)$$

where $\lambda_i, 1 \le i \le n_0$, are the eigenvalues of $\mathcal{H}_1 \mathcal{H}_1^\dagger$ and their joint pdf is given by [162]. The characteristic function of the mutual information is defined as

$$\varphi(Q, t) = \mathbb{E}\left\{\exp(\jmath t I)\right\} = \mathbb{E}\left\{\prod_{i=1}^{n_0}\left(1 + \frac{\rho}{N} \lambda_i\right)^{\jmath t/\ln 2}\right\}. \quad (4.10)$$

80

By using the analytical results of [162, Section II.B] for the evaluation of the moment generating function of the mutual information of a multi-hop MIMO channel, the final expression of $\varphi(Q, t)$ is obtained. $\qquad\square$

Next, by using the above lemma, the outage probability of the AR scheme is derived as follows.

Proposition 4.1. *The outage probability of the AR scheme is given by*

$$\Pi_{AR}(R, K, m) = \frac{1}{2} - \frac{1}{\pi} \int_0^\infty \frac{1}{t} \Im \left\{ \left[e^{-jtR} \varphi(m, t) \right]^K \right\} dt, \qquad (4.11)$$

where $\varphi(m, t)$ is the characteristic function of the mutual information of the (N, m, L) channel given by Lemma 4.1.

Recall that, at each time sub-slot, only m elements of the RIS are activated. The above result can be easily derived by considering that the random variables I_k are independent and the characteristic function of the sum $\sum_{k=1}^{K} I_k$ is calculated by the product of the characteristic functions of each I_k. It is also clear that, for $K = 1$, the above proposition provides a numerical expression for the outage probability of the (N, Q, L) channel under the conventional PR scheme. We next provide an approximation of the outage probability for the RIS-aided SISO channel.

Theorem 4.1. *The outage probability achieved by the RIS-assisted SISO channel employing the AR scheme, under the CLT, is approximated by*

$$\Pi_{AR}(R, K, m) \approx 1 - \exp\left(\frac{K}{\rho m}\right)$$

$$\times H_{1,K+1}^{K+1,0} \left[\begin{array}{c} (1,1,0) \\ (0,1,0), \left(1,1,\dfrac{1}{\rho m}\right), \dots, \left(1,1,\dfrac{1}{\rho m}\right) \end{array} \middle| \Theta \right], \quad (4.12)$$

where $\Theta = (2^R/\rho m)^K$.

Proof. By considering the SISO channel, the end-to-end channel matrix given in (4.2) is simplified to a scalar value which, under the AR scheme, is given by

$$\mathcal{H}_k = \sum_{i=1}^{Q} h_i g_i a_{i,k}, \qquad (4.13)$$

where $a_{i,k}$ is provided according to the framework of the AR scheme in (4.7). It has been proved in [85] that by applying the CLT, the distribution of the end-to-end channel $\mathcal{H}_k$ converges to a complex Gaussian distribution with zero mean and

variance m, since at sub-slot k only the m elements that correspond to the sub-surface $\mathcal{S}_k$ are turned ON. Therefore, the channel gain $W_k = \left|\mathcal{H}_k\right|^2$ is exponentially distributed with parameter $1/m$. Recall that the sub-surfaces $\mathcal{S}_k$ do not overlap, so the random variables W_k are mutually independent. The outage probability is then calculated as follows

$$
\begin{aligned}
\Pi_{\text{AR}}^{\text{CLT}}(R, K, m) &= \mathbb{P}\left\{ \frac{1}{K} \sum_{k=1}^{K} \log_2 (1 + \rho W_k) < R \right\} \\
&= \mathbb{P}\left\{ \prod_{k=1}^{K} (1 + \rho W_k) < 2^{RK} \right\},
\end{aligned}
\tag{4.14}
$$

which follows from the logarithmic identity $\log_2(x) + \log_2(y) = \log_2(xy)$. The final expression of the outage probability in (4.12) is eventually derived by obtaining the cdf of the product of K independent shifted exponential random variables, which is given in [132, Corollary 2]. $\qquad\square$

The above expression can be easily evaluated by using computational software tools, such as Matlab or Mathematica [132], while in Section V, we show that the provided approximation becomes very tight, even for a small number of elements in each sub-surface. The above approximation can be also considered for the PR scheme by setting $K = 1$. In this case, the expression is simplified to

$$
\Pi_{\text{PR}}(R) \approx 1 - \exp\left(-\frac{2^R - 1}{\rho Q} \right).
\tag{4.15}
$$

4.3.2 Flip-Reflect scheme

We now consider a partition-based scheme, where the reconfiguration of each sub-surface $\mathcal{S}_k$ occurs on the phase shift of the selected elements. For the FR scheme, in particular, all the elements of the RIS are always turned ON and are thus able to reflect the incident signals, i.e., $a_{i,k} = 1 \; \forall i, k$. At every sub-slot k, the RIS controller can modify the induced phase shift of each element between 0 or π. For the implementation of the FR scheme, we adopt a similar framework as for the AR scheme. Specifically, we consider the following procedure:

- Initially, the phase shift of all the RIS elements is set to zero. This setting is considered as the default configuration of each element for the FR scheme.

82

- Regarding the number of partitions, we consider the cases[4] $K = 2$ and $K > 2$. If $K = 2$, at the first time sub-slot all the elements remain at the default configuration and simply reflect the signals, i.e., $\phi_{i,1} = 0$ $\forall i$. At the second sub-slot, the elements of $\mathcal{S}_2$ are reconfigured by setting their phase shift into π. On the other hand, for $K > 2$, at the k-th sub-slot, the sub-surface $\mathcal{S}_k$ flips the signals by changing the phase shift of the corresponding elements into π. As such, the phase shift of each RIS element at the k-th sub-slot is equal to

$$\phi_{i,k} = \begin{cases} \pi, & (K > 2 \cup (K = 2 \cap k > 1)) \cap i \in \mathcal{S}_k; \\ 0, & \text{otherwise.} \end{cases} \tag{4.16}$$

- Therefore, the (N, Q, L) channel under the FR scheme is a time-varying channel consisting of K parallel sub-channels, where for each sub-channel a different flipping matrix Φ_k is used [33, 163].

Similarly to the AR scheme, we assume that the reflection amplitude and phase shift of each element can be independently modified, while the proposed design framework can be generalized to the case where the reflection amplitude and the phase shift of each element are coupled [160]. Fig. 4.2 depicts an example of the above procedure, by indicating the value of the phase shift for the elements of every sub-surface at each time sub-slot. The 1-bit phase-shift control presented in this framework could be implemented based on the binary programmable metasurface fabricated in [164], where each RIS element is connected to a PIN diode that can be switched between two states, resulting in a phase shift difference of π. Therefore, similar to the AR scheme, this scheme has low complexity in terms of RIS hardware requirements, as the proposed configuration patterns can be obtained with low-cost binary-state elements.

Based on the presented framework, we can now analyze the performance of the FR scheme in terms of outage probability. Note that, since all the RIS elements are always activated in this scheme, the instantaneous channel gains between different sub-slots are time-correlated. Thus, in this case, the derivation of the outage probability becomes challenging. As such, we present two approximations that can sufficiently describe the performance of the proposed scheme. In particular,

---

[4]By considering the above cases for the flipping pattern, we ensure that the RIS reflection matrices are linearly independent, so that the maximum performance gains can be achieved.

- In Theorem 4.2, we derive a numerical expression for the outage probability of an RIS-aided SISO channel by approximating the cascaded channels $\mathcal{H}_k$ with time-correlated Rayleigh fading channels.

- For the general case of RIS-aided MIMO channels, we provide a lower bound by assuming that the channels $\mathcal{H}_k$ are mutually independent.

In what follows, we analytically evaluate the correlation coefficient of the channel gains over different sub-slots for the SISO case, i.e., for $N = L = 1$, by using the Pearson correlation formula [135].

Lemma 4.2. *The correlation coefficient of the channel gains over different sub-slots $k \neq l$ under the FR scheme is given by*

$$\zeta = \frac{(Q - 2b)^2 + 2Q}{Q(Q + 2)}, \tag{4.17}$$

where

$$b = \begin{cases} m, & K = 2; \\ 2m, & K > 2. \end{cases} \tag{4.18}$$

Proof. Since $N = L = 1$, the channel $\mathcal{H}_k$ is a scalar value given by

$$\mathcal{H}_k = \sum_{i=1}^{Q} h_i g_i \exp j\phi_{i,k}, \tag{4.19}$$

where $\phi_{i,k}$ is provided in (4.16) by employing the FR scheme. The random variables $W_k = |\mathcal{H}_k|^2$ are correlated since the channel coefficients h_i and g_i remain constant during one time slot, i.e., over K sub-slots. In order to calculate the correlation coefficient between W_k and W_l, $k \neq l$, we consider the Pearson correlation formula which is given by

$$\zeta = \frac{\mathbb{E}\{W_k W_l\} - \mathbb{E}\{W_k\}\mathbb{E}\{W_l\}}{\sigma_{W_k}\sigma_{W_l}}, \tag{4.20}$$

where $\sigma_{W_i} = \sqrt{\mathbb{E}\{W_i^2\} - \mathbb{E}\{W_i\}^2}$. We find that $\mathbb{E}\{W_i\} = Q$, $\mathbb{E}\{W_i^2\} = 2Q(Q + 1)$ and $\mathbb{E}\{W_k W_l\} = Q(Q + 3) + (Q - b)(Q - 3b - 1) + b(b - 1)$, where b is given by (4.18). By substituting the previous results in (4.20), and after some trivial algebraic manipulations, we get the final expression of ζ as in (4.17). $\square$

It can be easily verified that when $Q \to \infty$, the correlation coefficient converges to

$$\zeta \to \begin{cases} 0, & K = 2; \\ 1 - \frac{8(K - 2)}{K^2}, & K > 2. \end{cases} \tag{4.21}$$
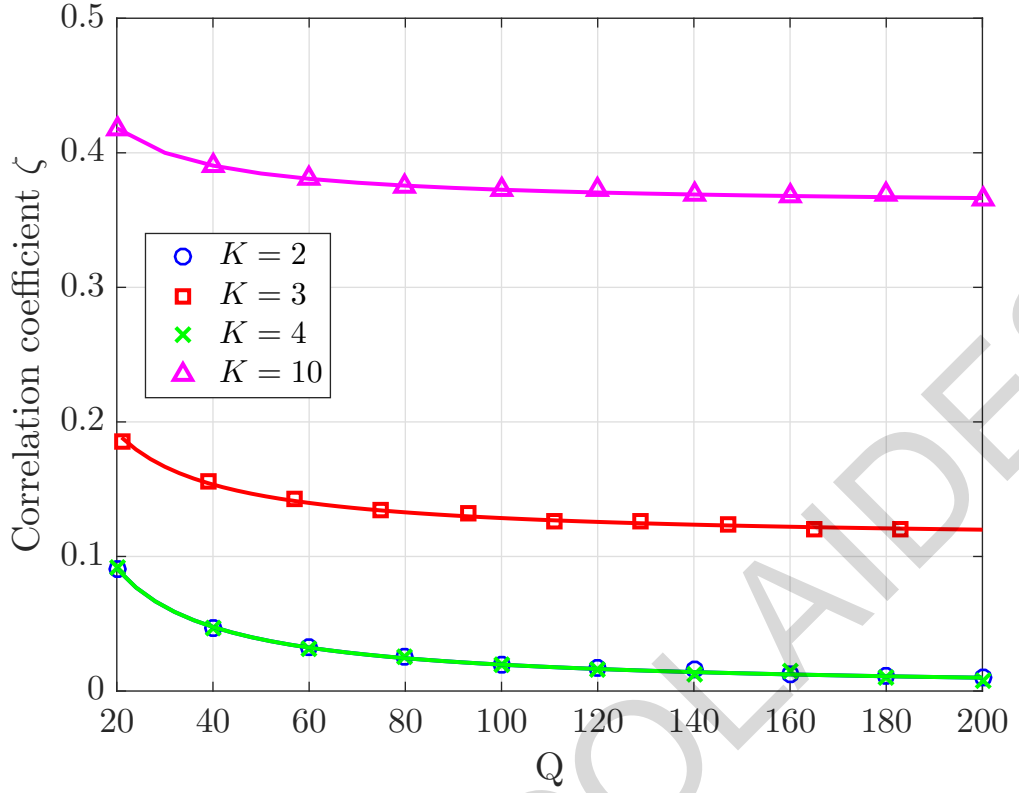
Figure 4.3: Correlation coefficient ζ versus number of elements Q; the theoretical results are depicted with lines and the simulation results with markers.

From the above expression, we can deduce that, the correlation between the channel gains is relatively small for small partition sizes. In particular, we observe that when $K = 2$ or 4 the correlation coefficient converges to zero. On the other hand, as K increases, ζ converges to one, i.e., full correlation. These results are also depicted in Fig. 4.3.

We can now focus on the derivation of the approximated expression of the outage probability for the RIS-aided SISO networks. Since the considered channels are time-correlated, we adopt a correlated Rayleigh fading channel model to approximate their distribution, and incorporate the correlation coefficients provided in the above lemma. Specifically, the approximated channel can be written as [165]

$$\tilde{\mathcal{H}}_k = \begin{cases} \sigma_k X_1, & k = 1; \\ \sigma_k(\sqrt{1-\zeta}X_k + \sqrt{\zeta}X_1), & 2 \le k \le K, \end{cases} \tag{4.22}$$

where X_k, $1 \le k \le K$, are independent complex Gaussian random variables with zero mean and unit variance and $\sigma_k^2 = \mathbb{E}\left\{\left|\tilde{\mathcal{H}}_k\right|^2\right\} = Q$. Let $W_k = \left|\tilde{\mathcal{H}}_k\right|^2$ denote the channel gain at the k-th sub-slot. Based on the definition of $\tilde{\mathcal{H}}_k$, we deduce that W_1 is

exponentially distributed with parameter $1/Q$, where the associated pdf is given by

$$f_{W_1}(x) = \frac{1}{Q}\exp\left(-\frac{x}{Q}\right). \tag{4.23}$$

Conditioned on W_1, the remaining terms W_k, $2 \leq k \leq K$, follow an independent non-central chi-squared distribution with two degrees of freedom. Therefore, the conditional PDF of W_k, given $W_1 = y$, is written as [166, Theorem 1.3.4]

$$f_{W_k|W_1}(x|y) = \frac{\exp\left(-\dfrac{x + \zeta y}{\Omega}\right)}{\Omega} I_0\left(2\frac{\sqrt{\zeta xy}}{\Omega}\right), \tag{4.24}$$

where $\Omega \triangleq Q(1 - \zeta)$. As such, the approximated outage expression is given as follows.

Theorem 4.2. *The outage probability of the SISO channel, under the FR scheme, is approximated by*

$$\Pi_{\mathrm{FR}}(R, K, m) \approx \left(\frac{1}{\rho}\right)^{K-1} \int_1^{c_1} \int_1^{c_2} \cdots \int_1^{c_{K-1}} \left[1 - Q_1\left(\sqrt{\frac{2\zeta(\tau_1 - 1)}{\rho\Omega}}, \sqrt{2\Theta}\right)\right]$$
$$\times f_{W_1}\left(\frac{\tau_1 - 1}{\rho}\right) \prod_{k=2}^{K-1} f_{W_k|W_1}\left(\frac{\tau_k - 1}{\rho} \bigg| \frac{\tau_1 - 1}{\rho}\right) d\tau_{K-1} \cdots d\tau_1, \tag{4.25}$$

where $c_i \triangleq 2^{RK} / \prod_{k=1}^{i-1} \tau_k$, $1 \leq i \leq K - 1$ and

$$\Theta \triangleq \frac{1}{\rho\Omega}\left(\frac{2^{RK}}{\prod_{k=1}^{K-1} \tau_k} - 1\right). \tag{4.26}$$

Proof. By using the approximated channel $\tilde{\mathcal{H}}_k$ defined in (4.22) and by setting $W_k = |\tilde{\mathcal{H}}_k|^2$, the outage probability under the FR scheme is evaluated as

$$\Pi_{\mathrm{FR}}(R, K, m) = \mathbb{P}\left\{\frac{1}{K}\sum_{k=1}^{K} \log_2(1 + \rho W_k) < R\right\}$$
$$= \mathbb{P}\left\{\prod_{k=1}^{K}(1 + \rho W_k) < 2^{RK}\right\} \tag{4.27}$$
$$= \mathbb{E}_{W_k}\left\{F_{W_K}\left[\frac{1}{\rho}\left(\frac{2^{RK}}{\prod_{k=1}^{K-1}(1 + \rho W_k)} - 1\right)\right]\right\}, \tag{4.28}$$

which follows by solving the inequality in (4.27) for W_K. The conditional cdf of W_K, given W_1, is derived by taking the integral of (4.24), which is equal to

$$F_{W_K|W_1}(x|y) = 1 - Q_1\left(\sqrt{\frac{2\zeta y}{\Omega}}, \sqrt{\frac{2x}{\Omega}}\right). \tag{4.29}$$

Since the random variables W_k, conditioned on W_1, are all independent between each others, we have

$$\Pi_{\text{FR}}(R, K, m) = \int_{w_1} \cdots \int_{w_{K-1}} f_{W_1}(w_1)$$
$$\times \prod_{k=2}^{K-1} f_{W_k|W_1}(w_k|w_1) F_{W_K|W_1}(\vartheta|w_1) \, dw_{K-1} \cdots dw_1, \quad (4.30)$$

where

$$\vartheta \triangleq \frac{1}{\rho} \left(\frac{2^{RK}}{\prod_{k=1}^{K-1} (1 + \rho w_k)} - 1 \right), \quad (4.31)$$

while $f_{W_1}(w_1)$ and $f_{W_k|W_1}(w_k|w_1)$ are given by (4.23) and (4.24), respectively. Regarding the integration limits, we need to ensure that the inequality

$$\frac{2^{RK}}{\prod_{k=1}^{K-1} (1 + \rho w_k)} - 1 > 0, \quad (4.32)$$

is satisfied sequentially for each w_k from $K - 1$ to 1. The final expression is derived by using the integral transformation $\tau_k \rightarrow 1 + \rho w_k$. $\quad\square$

We show that the presented approach provides a very tight approximation of the outage performance under the FR scheme, and can adequately describe the system's behavior, even for small values of Q.

Finally, for the general case where $N, L \geq 1$, we point out some remarks on the performance of the considered RIS-aided networks under the FR scheme. For this case, specifically, we provide a lower bound on the outage probability by assuming that all the resulting parallel channel matrices $\mathcal{H}_k$ are mutually independent. Under this assumption, the (N, Q, L) channel, by using the FR scheme, achieves the same performance as the (N, KQ, L) channel under the AR scheme with the same partition size K. The outage probability of the FR scheme is therefore lower bounded by

$$\Pi_{\text{FR}}(R, K, m) \geq \Pi_{\text{AR}}(R, K, Q), \quad (4.33)$$

where $\Pi_{\text{AR}}(R, K, Q)$ is given by (4.11). The above performance bound becomes tight when m (and therefore Q) is sufficiently large and the number of partitions K is relatively small, since the correlation of the channel gains between different sub-slots remains low. Moreover, based on this result, we can conclude that the AR scheme requires the employment of an RIS with K times more elements to outperform the outage probability achieved by the FR scheme.

4.4 Diversity-multiplexing tradeoff analysis

We now turn our attention to the DMT achieved by the proposed schemes, which gives the performance limit for uncoded transmission. Recall that, a scheme achieves multiplexing gain r and diversity gain $d(r)$ if the target data rate $R(\rho) \sim r \log \rho$ and the outage probability of the scheme $\Pi(\rho)$ satisfy the conditions [133]

$$\lim_{\rho \to \infty} \frac{R(\rho)}{\log \rho} = r,$$

and

$$\lim_{\rho \to \infty} -\frac{\log \Pi(\rho)}{\log \rho} = d(r). \tag{4.34}$$

By following the definitions of [47], if the achieved DMT of the end-to-end channels for any two schemes is the same, then these channels are said to be *DMT-equivalent*. Let (n_0, n_1, n_2) be the ordered version of the (N, Q, L) channel, with $n_0 \leq n_1 \leq n_2$. An ordered (l_0, l_1, l_2) channel is a *vertical reduction* of the considered channel, if both are DMT-equivalent and satisfy the condition $l_i \leq n_i \ \forall i$. Finally, according to the information theoretic cut-set bound [151], the DMT achieved by any RIS scheme is upper bounded as

$$d_{(N,Q,L)}(r) \leq \min\{d_{(N,Q)}(r), d_{(Q,L)}(r)\}, \tag{4.35}$$

where the maximum diversity and multiplexing gain are given by

$$d_{\max} = \min\{N, L\} \times Q, \tag{4.36}$$

and

$$r_{\max} = \min\{N, Q, L\}. \tag{4.37}$$

Before deriving the DMT achieved by the presented schemes, we need to provide the DMT expression for the conventional PR scheme, which is given below. The (N, Q, L) channel under the PR scheme is DMT-equivalent to the Rayleigh product channel. Therefore, the achieved DMT is a piecewise-linear function defined by the points $(r, d_{\mathrm{PR}}(r)), r = 0, ..., n_0$ with [167, Theorem 2]

$$d_{(N,Q,L)}^{\mathrm{PR}}(r) = (n_0 - r)(n_1 - r) - \left\lfloor \frac{[(n_0 + n_1 - n_2 - r)^+]^2}{4} \right\rfloor. \tag{4.38}$$

Based on the above expression, some important remarks can be extracted about the DMT performance of an RIS-aided network operating under the PR scheme. Specifically,

- The DMT achieved by the PR scheme depends only on the ordered version of the (N, Q, L) channel.

- The DMT of the (N, Q, L) channel under the PR scheme is limited by the DMT performance of the $N \times L$ channel if the number of RIS elements satisfies the condition $Q \geq N + L - 1$. This can be easily proven since, under this condition, the last term of (4.38) is equal to zero.

- The (N, Q, L) channel can be vertically reduced to any $(N, \tilde{Q}, L)$ channel, with $Q > \tilde{Q} \geq Q_{min} = N + L - 1$, and still achieve the same DMT.

It is therefore easily observed that the PR scheme is suboptimal in terms of diversity gain, compared to the maximum diversity gain associated with the theoretical cut-set bound. In typical RIS-assisted networks, the number of RIS elements is usually much larger than the number of transmit and receive antennas. Therefore, the DMT achieved by this scheme is limited by the "bottleneck" ordered channel. For $Q > Q_{min}$ the performance of the (N, Q, L) channel can only be improved in terms of coding gain. However, the achieved coding gain decreases as the number of elements increases. This can be easily proven for the RIS-aided SISO channel, by using the approximated expression in (4.15). In this case, by using the definition of [124], the coding gain is given by

$$\mathcal{G} = \lim_{\rho \to \infty} \Pi_{\mathrm{PR}}(R) \rho^{d_{(1,Q,1)}(0)} = \lim_{\rho \to \infty} \left[1 - \exp\left(-\frac{2^R - 1}{\rho Q} \right) \right] \rho \approx \frac{2^R - 1}{Q}, \qquad (4.39)$$

where we used the approximation $\exp(-x) \approx 1 - x$ for $x \to 0$. Apparently, when $Q \to \infty$, the coding gain converges to zero. We next evaluate the DMT of the proposed AR scheme.

Corollary 4.1. *The DMT achieved by the (N, Q, L) channel under the AR scheme is equal to*

$$d^{\mathrm{AR}}_{(N,Q,L)}(r) = K d^{\mathrm{PR}}_{(N,m,L)}(r), \qquad (4.40)$$

where K is the number of sub-surfaces with m elements.

The above result is derived by considering that in the proposed scheme, the end-to-end channel consists of K independent parallel sub-channels, and each sub-channel achieves the same DMT given in (4.38) with $Q = m$. It is apparent that the AR scheme can significantly enhance the performance of the (N, Q, L) channel in terms

of diversity gain compared to the PR scheme, especially for a large number of RIS elements. In particular, this scheme can achieve both the maximum diversity and multiplexing gain associated with the cut-set bound, if the RIS is divided into K sub-surfaces of m elements with [47]

$$\min\{N, L\} \leq m \leq |N - L| + 1, \tag{4.41}$$

and m is a divisor[5] of Q. If the above bounds cannot be simultaneously satisfied, then the AR scheme can achieve either $d_{\max}$ or $r_{\max}$ given by (4.36) and (4.37), respectively.

It can be seen that, despite the improvement achieved in diversity gain by the employment of the AR scheme, the end-to-end channel suffers from rate-deficiency, while the maximum multiplexing gain is no longer guaranteed. On the other hand, this issue is resolved with the FR scheme. In this case, the exact DMT is difficult to be obtained for the FR scheme, so we provide a lower bound instead, which is given in the following proposition.

Proposition 4.2. *The DMT achieved by the (N, Q, L) channel under the FR scheme is lower bounded by*

$$d^{\mathrm{FR}}_{(N,Q,L)}(r) \geq \max\left\{d^{\mathrm{AR}}_{(N,Q,L)}(r), d^{\mathrm{PR}}_{(N,Q,L)}(r)\right\}. \tag{4.42}$$

Proof. We first prove that the FR scheme achieves the same diversity order as the AR scheme, i.e.,

$$d^{\mathrm{FR}}_{(N,Q,L)}(0) = d^{\mathrm{AR}}_{(N,Q,L)}(0) = Kd^{\mathrm{PR}}_{(N,m,L)}(0). \tag{4.43}$$

Let us denote by $\mathcal{H}'_k$ the k-th sub-channel created under the FR scheme, and by $\mathcal{H}_k$ the respective sub-channel resulting from the AR scheme. Based on the description of each scheme, the set of matrices $\left\{\mathcal{H}'_k\right\}_{k=1}^{K}$ is derived from $\{\mathcal{H}_k\}_{k=1}^{K}$ by using the transformation

$$\left[\mathcal{H}'_1 \ \mathcal{H}'_2 \ \ldots \mathcal{H}'_K\right] = [\mathcal{H}_1 \ \mathcal{H}_2 \ \ldots \mathcal{H}_K] \, \mathbf{T}, \tag{4.44}$$

where $\mathbf{T}$ is a $KN \times KN$ matrix composed of $K \times K$ sub-matrices and each sub-matrix $\mathbf{T}_{i,j}$ is equal to

$$\mathbf{T}_{i,j} = \begin{cases} -\mathbf{I}_N, & (i = j, K > 2) \text{ or } (i = j > 1, K = 2); \\ \mathbf{I}_N, & \text{otherwise.} \end{cases} \tag{4.45}$$

---

[5]In the generalized case of an RIS divided into sub-surfaces with different number of elements, m_i, $1 \leq i \leq K$, just needs to be an integer number within the defined region (see (4.41)).

90

We can easily verify that **T** is invertible, constant and linear. Therefore, the two schemes achieve the same diversity order since

$$\sum_{k=1}^{K} \left\| \mathcal{H}'_k \right\|_F^2 \geq \lambda_{\min} \left(\mathbf{T} \mathbf{T}^\dagger \right) \sum_{k=1}^{K} \left\| \mathcal{H}_k \right\|_F^2 = K \sum_{k=1}^{K} \left\| \mathcal{H}_k \right\|_F^2$$

$$\doteq \sum_{k=1}^{K} \left\| \mathcal{H}_k \right\|_F^2, \tag{4.46}$$

where $\lambda_{\min}(\cdot)$ denotes the minimum eigenvalue of a matrix and the relation $a \doteq b^c$ means $\lim_{b \to \infty} \frac{\log a}{\log b} = c$.

The next step is to prove that the FR scheme can achieve at least the DMT of the AR scheme for $r = 0, ..., \min\{N, m, L\}$. In the considered channel, the multiplexing gain r can be achieved if an (r, r, r) sub-channel is reserved for spatial multiplexing at each time sub-slot. According to Corollary 4.1 and by using the DMT characterization of a Rayleigh product channel given in [47, Theorem 3.4], we have

$$d_{(N,Q,L)}^{\mathrm{AR}}(r) = K d_{(N-r,m-r,L-r)}^{\mathrm{PR}}(0) = d_{(N-r,Q-Kr,L-r)}^{\mathrm{AR}}(0). \tag{4.47}$$

Similar to (4.43), the $(N - r, Q - Kr, L - r)$ channel achieves the same diversity order under both the FR and the AR scheme. Besides, one can show that $d_{(N,Q,L)}^{\mathrm{FR}}(r) \geq d_{(N-r,Q-Kr,L-r)}^{\mathrm{FR}}(0)$, since all the elements are activated in the FR scheme and the multiplexing gain r can be achieved with less than Kr elements. It follows that

$$d_{(N,Q,L)}^{\mathrm{FR}}(r) \geq d_{(N,Q,L)}^{\mathrm{AR}}(r). \tag{4.48}$$

Finally, the parallel channel under the FR scheme is in outage if $\sum_{k=1}^{K} I_k < Kr \log \rho$, which implies that at least one of the sub-channels is in outage with the corresponding random variable I_k below the target rate $r \log \rho$. Therefore, the FR scheme can achieve at least the DMT of the conventional case, i.e.,

$$d_{(N,Q,L)}^{\mathrm{FR}}(r) \geq d_{(N,Q,L)}^{\mathrm{PR}}(r). \tag{4.49}$$

By combining (4.43), (4.48) and (4.49) we get the lower bound for the DMT of the FR scheme as (4.42). □

We can observe that the FR scheme is superior to both the AR and the PR schemes. Based on the framework of the FR scheme, all the RIS elements are always activated and assist the communication, so the maximum multiplexing gain is ensured. At the same time, through the temporal processing pattern presented in Section 4.3.2,
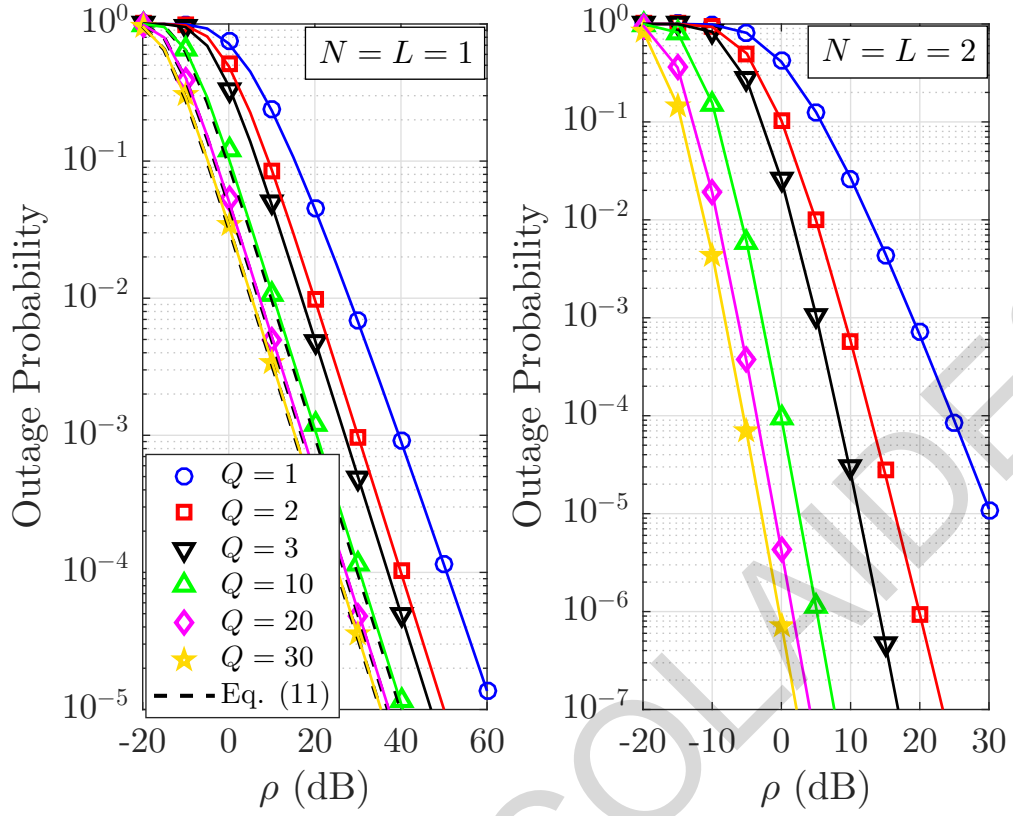
Figure 4.4: Outage probability versus average SNR for the PR scheme ($K = 1$).

we can increase the achieved diversity gain. Therefore, while the AR and the PR schemes can achieve the maximum diversity and multiplexing gain respectively, the FR scheme achieves both extremes. Moreover, the (N, Q, L) channel under the FR scheme can achieve both d_{max} and r_{max}, by considering only the upper bound condition of (4.41).

4.5 Numerical Results

We provide numerical results to demonstrate the performance of the presented RIS schemes and validate our theoretical analysis. For the simulations, we consider that the rate threshold is equal to $R = 1$ bps/Hz throughout the simulations, while the variance of each entry at the AWGN vector is normalized to $\sigma^2 = 1$. Note that, the considered set of parameter values is used for the sake of presentation. A different set of values will affect the performance but will lead to similar observations. Moreover, in the following results, the proposed schemes are compared with the conventional PR scheme, i.e., the case of $K = 1$. Unless otherwise stated, the analytical results are illustrated with lines (solid, dashed or dotted) and the simulation results with
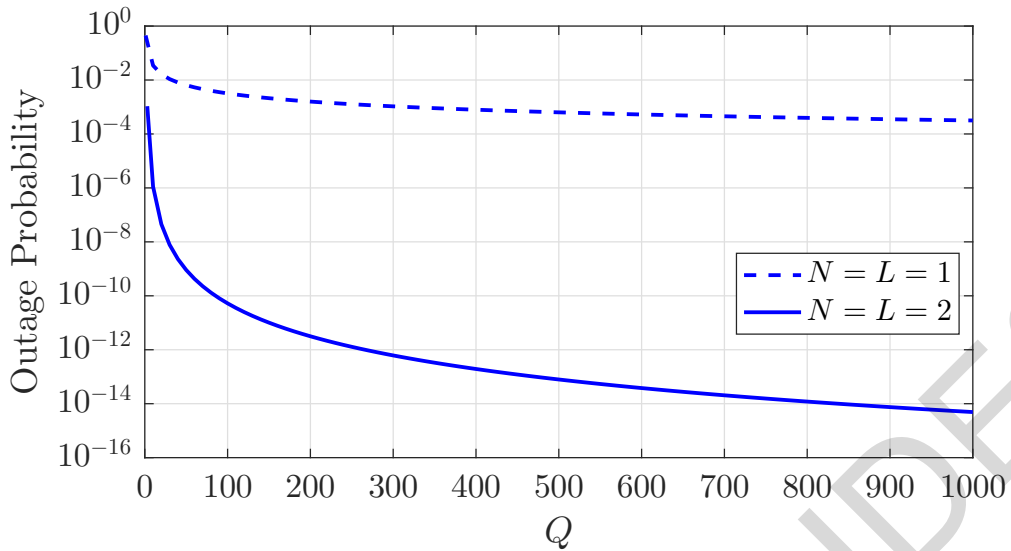
Figure 4.5: Outage probability versus Q under the PR scheme for $\rho = 5$ dB.

markers.

Fig. 4.4 illustrates the system's outage probability with respect to the average SNR under the PR scheme for different values of RIS elements. We show the results of two different cases: the first case considers a SISO network setting, i.e., $N = L = 1$ antenna, while in the second case we have a MIMO setting with $N = L = 2$ antennas. We can see that the outage performance is improved, by increasing the number of RIS elements. Specifically, for the RIS-aided SISO channel we observe that for all values of Q a diversity order equal to one is achieved and the system's performance is improved in terms of coding gain. On the other hand, the performance in the MIMO setting is enhanced in terms of diversity gain until the RIS elements reach the value of $Q_{min} = N + L - 1 = 3$, where $d(0) = NL = 4$. After this threshold, the diversity order remains the same as we increase Q, so the outage probability can be only improved in terms of coding gain. This observation is in accordance with our remark that the asymptotic performance of the PR scheme is limited by the $N \times L$ channel. Finally, the presented results validate the accuracy of our theoretical analysis. Specifically, we observe that in both cases the simulation results (markers) perfectly match with the theoretical values (solid lines) of Proposition 4.1 for $K = 1$. In addition, the expression in (4.15) provides an exceptional approximation (dashed lines) of the achieved outage probability, even for small values of Q, while as Q increases the approximation becomes tighter.

As noted previously in Fig. 4.4, for $Q > Q_{min}$ the outage performance is improved only in terms of coding gain. However, this gain gradually diminishes as the number
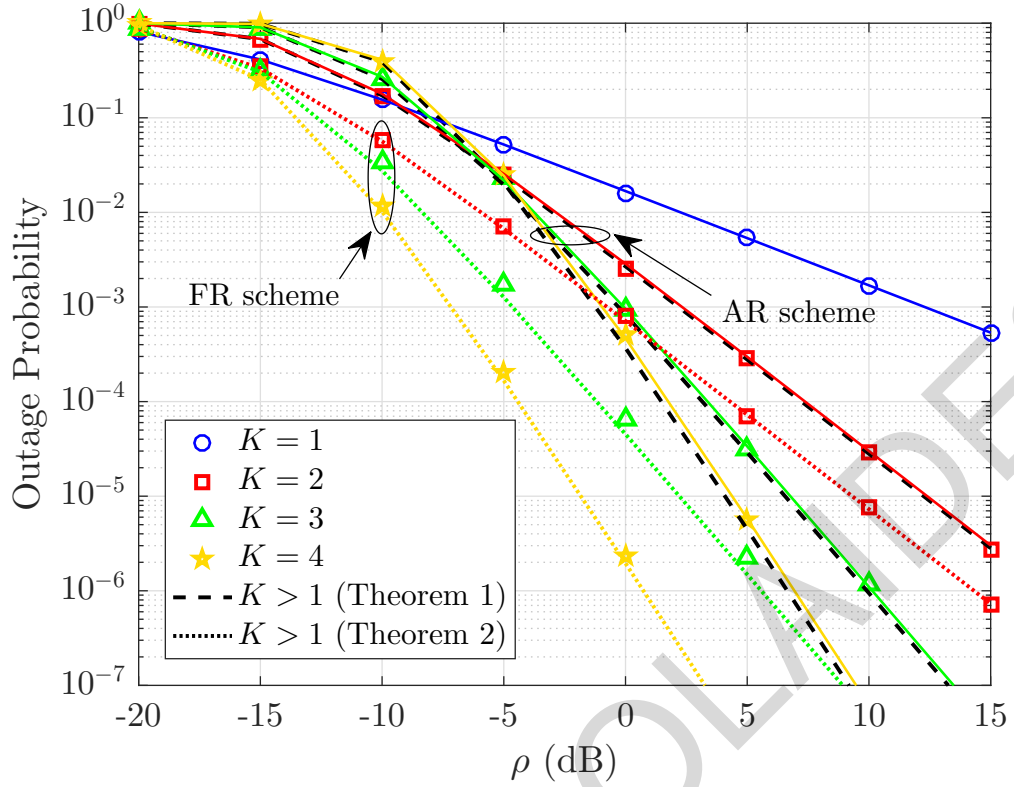
Figure 4.6: Outage probability versus average SNR for the partition-based schemes; $N = L = 1$ antenna and $Q = 60$.

of elements increases. This observation is more evident in Fig. 4.5, where the outage probability is shown against the number of elements for the same channel settings at $\rho = 5$ dB, and is consistent with the conclusions derived in [96]. We can therefore deduce that under the PR scheme, employing a larger RIS does not necessarily provide significant gains to the outage probability of the RIS-aided network.

Figs. 4.6 and 4.7 illustrate the achieved outage probability of the considered RIS-aided system under the proposed partition-based schemes (AR and FR schemes), for a network topology with $N = L = 1$ and 2 antennas, respectively, $Q = 60$ elements and different partition sizes. The performance of the proposed schemes is also compared to the PR scheme ($K = 1$). In addition, Fig. 4.6 shows the numerical expression of Proposition 4.1 for the AR scheme, as well as the approximation for a SISO channel provided by Theorem 4.1, while for the FR scheme the approximated numerical expression of Theorem 4.2 is depicted. The theoretical results of Proposition 4.1 regarding the AR scheme (solid lines) are in agreement with the simulations (markers), which validates our analysis. Moreover, the derived expressions of Theorems 4.1 and 4.2 provide a very tight approximation of the actual performance of the
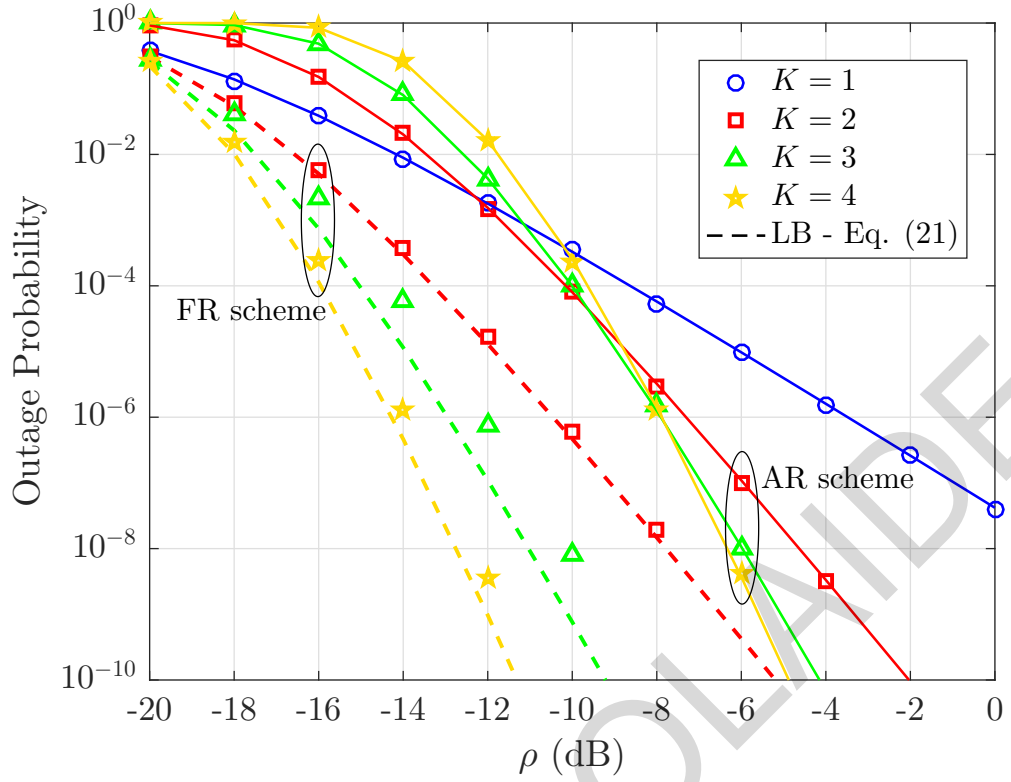
Figure 4.7: Outage probability versus average SNR for the partition-based schemes; $N = L = 2$ antennas and $Q = 60$.

system. In Fig. 4.7, apart from the numerical expression of Proposition 4.1 for the AR scheme, the lower bound of the FR scheme given in (4.33) is shown, assuming mutually independent channel matrices $\mathcal{H}_k$. It can be seen that, for $Q \gg K$ the lower bound is close to the performance achieved by the FR scheme, which validates its consideration.

In both figures, it can be seen that for high SNR values, both the AR scheme and the FR scheme outperform the conventional PR scheme. Specifically, by increasing the number of partitions, the asymptotic performance of the presented schemes is improved in terms of diversity gain. We can also clearly see that the proposed schemes achieve the same diversity order, which is in accordance with our results in Section 4.4. However, the FR scheme outperforms the AR scheme in terms of coding gain. This is due to the fact that in the FR scheme, during each time sub-slot all the RIS elements are always activated, while in the AR scheme at each sub-slot only the elements of the selected sub-surface are turned ON. Moreover, we observe that, as the number of partitions increases, the gain achieved by the FR scheme over the AR scheme increases as well. In particular, in both figures, it can be seen that partitioning the RIS into 4 sub-surfaces almost doubles the coding gain between the
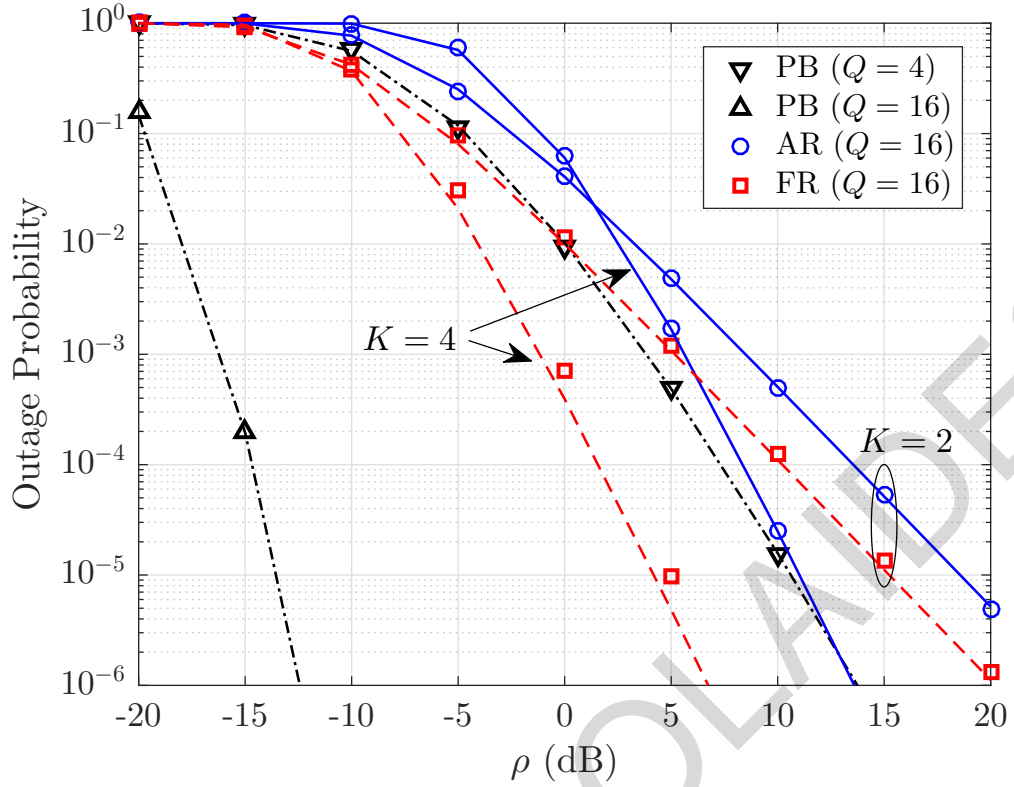
Figure 4.8: Outage probability comparison of the partition-based schemes and the passive beamforming case for a network topology with $N = L = 1$.

two schemes, compared to the case of $K = 2$. On the contrary, in the low SNR regime only the FR scheme outperforms the PR scheme. This is expected since, according to the framework of the AR scheme, by increasing the number of partitions each time-slot is divided in more sub-slots and at each time sub-slot only Q/K elements are activated, resulting in a deteriorated spectral efficiency.

In Fig. 4.8, we compare the outage performance of the proposed schemes with the case of passive beamforming at the RIS, by considering a RIS-aided SISO channel. In the passive beamforming case, the Tx estimates the cascaded channel through a channel estimation method, e.g., [114], and aligns the phase shifts of the RIS elements, i.e., $\phi_i = -\angle h_i g_i$, with $1 \leq i \leq Q$. We consider an ideal scenario where no errors are derived from the channel estimation, so we have perfect CSI knowledge. The outage probability achieved by the passive beamforming is obtained in [85, Theorem 3]. Fig. 4.8 depicts the outage probability of the passive beamforming for $Q = 4$ and 16 elements, and the outage probability of the AR and FR schemes for $Q = 16$ and different partition sizes. As expected, the passive beamforming case outperforms the proposed schemes. On the other hand, it can be seen that, by increasing the
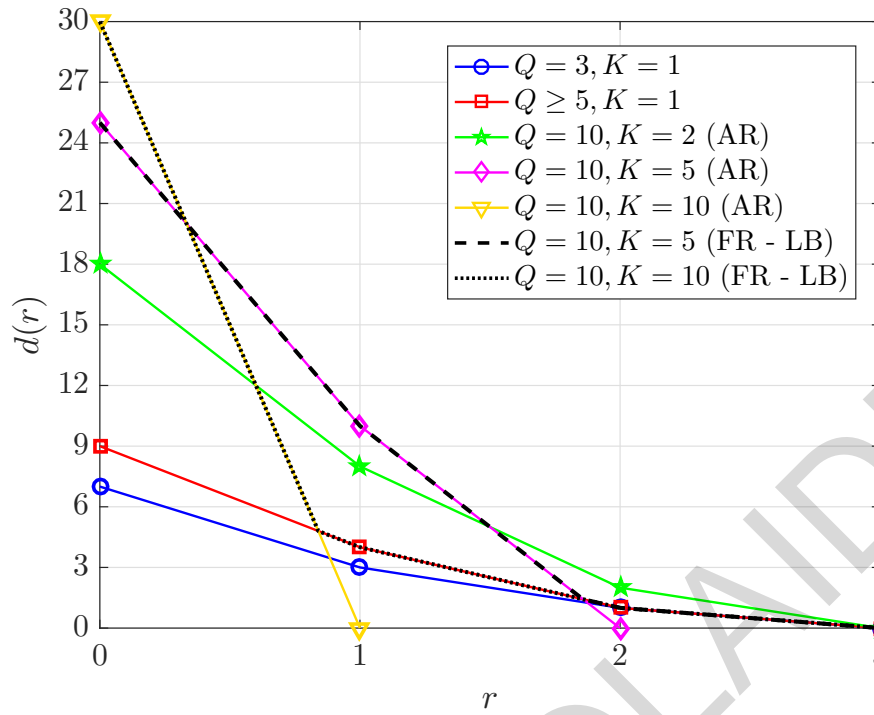
Figure 4.9: DMT comparison of the PR scheme and the partition-based schemes for a network topology with $N = L = 3$.

number of partitions at the RIS, the difference between the outage performance of the proposed schemes and the passive beamforming decreases. Moreover, a fair comparison in terms of power consumption at the RIS is considered, i.e., same number of activated elements, between the AR scheme, with $Q = 16$ elements and $K = 4$ partitions, and the passive beamforming case with $Q = 4$. In this case, we observe that the performance of the two scenarios is comparable. This shows that the proposed schemes have low implementation complexity and conserve the available resources at the RIS, but can still achieve significant performance gains.

Finally, a comparison of the achieved DMT between the PR scheme and the partition-based RIS schemes is depicted in Fig. 4.9, for a network setting with $N = L = 3$ antennas. We can see that for the PR scheme ($K = 1$) the optimum DMT is achieved when $Q = N + L - 1 = 5$, which is denoted by the red solid line. Any other topology with $Q > 5$ can be vertically reduced to the $(3, 5, 3)$ channel, since it will be DMT-equivalent. By employing the AR scheme, we observe that the DMT can be significantly improved in terms of diversity gain. Moreover, the proposed scheme achieves the maximum multiplexing gain, if the number of partitions satisfies the lower bound of (4.41), i.e., $m \geq \min\{N, L\}$. However, under the AR scheme, the considered channel setting cannot achieve both $d_{\max}$ and $r_{\max}$ provided by the cut-set

bound with a single value of K, since (4.41) cannot be fully satisfied with any partition size. Therefore, if a larger number of partitions is considered so that $m < \min\{N, L\}$, the presented scheme can still increase the achieved diversity gain, but it becomes suboptimal in terms of multiplexing gain. This remark is illustrated in Fig. 4.9, by considering an RIS with $Q = 10$ and a partition size of 5 or 10 sub-surfaces. Fig. 4.9 also shows the provided lower bound on the DMT achieved by the FR scheme. It can be seen that the FR scheme outperforms both the PR and the AR scheme. In particular, with the FR scheme, the RIS-aided channel achieves the same diversity order obtained by the AR scheme, and remains optimal in terms of multiplexing gain, for all partition sizes. Finally, for the considered network topology, only the FR scheme achieves both $d_{\max}$ and $r_{\max}$ with a single value of K, which is depicted with the black dotted line for the case with $Q = K = 10$.

Overall, it is observed that the proposed schemes can provide significant performance gains for RIS-aided systems with low design complexity since, apart from requiring no CSI knowledge for their implementation, they can be easily realized with low-cost binary-state elements. Compared to the conventional PR scheme, both the AR and FR schemes provide higher diversity gains, which are proportional to the number of partitions at the RIS. Although both schemes achieve the same diversity order, the FR scheme is beneficial in terms of coding gain, since all the elements are always activated, while the AR scheme could be preferred in scenarios where the available power resources at the RIS are limited. On the other hand, although the passive beamforming case outperforms the proposed solutions, the optimal performance gains can be achieved assuming that perfect CSI is already known, which significantly increases its implementation complexity and incurs high training overhead.

4.6 Conclusions

In this chapter, we studied the performance of RIS-assisted MIMO communications by employing two low-complexity partition-based schemes, that do not require any CSI knowledge at the transmitter side for their implementation. Specifically, the RIS elements are partitioned into sub-surfaces, which are reconfigured periodically in an efficient manner, creating a parallel channel in the time domain. We first proposed the AR scheme, which activates each sub-surface in a consecutive order.

Next, we presented the FR scheme, where each sub-surface sequentially flips the incident signals through a phase shift adjustment. Theoretical expressions of the outage probability and the DMT were provided, while the considered schemes were compared to the conventional PR scheme. We demonstrated that, by considering the proposed schemes, we can increase the diversity order achieved by the RIS-aided system and improve the performance beyond the limit of the MIMO channel, while at the same time we keep the implementation complexity low.

Chapter 5

A Hybrid Scheme for Reconfigurable Intelligent Surfaces: How Many Elements Should be Estimated?

Several studies in the literature have shown that by optimizing the elements' reflection coefficients of an RIS assisting a wireless network, can yield high performance gains, given that CSI is known. However, channel training in RIS-aided systems is a non-trivial and resource consuming task. In this work, a low-complexity hybrid scheme is presented for a wireless network assisted by an RIS, where channel estimation is required for only a subset of the elements. Specifically, in order to reduce the channel training overhead and boost the performance of the RIS-aided network, the RIS is partitioned in two sub-surfaces, which are sequentially activated to assist the communication. The elements of the first sub-surface align their phase shifts, based on the acquired CSI from a channel training period, whereas the elements of the second sub-surface randomly rotate the phase of the incident signals. The performance of the proposed scheme is investigated under the effect of imperfect CSI at the RIS. Analytical expressions for the outage probability are derived and useful insights on the optimal configuration of the RIS are provided.

5.1   Introduction

Following the discussion of the previous chapters, RIS is an appealing technology for the deployment of future 6G communications, which can support massive con-

nectivity networks with high data rates, enhanced reliability and low latency [21]. Due to the controllable nature of this technology, several works have recently investigated RIS-aided networks for various communication scenarios [88, 89, 120]. As previously mentioned, most of the existing works base their proposed solutions on the assumption that perfect knowledge of the CSI is available. However, channel estimation in RIS-assisted systems is not a trivial task, due to the passive nature of the reflecting elements and the fact that the RIS does not have signal processing capabilities [21]. Towards this direction, several channel estimation methods for RIS-aided networks have been suggested. In [114], the cascaded transmitter-RIS-receiver channels are estimated by individually activating one-by-one the elements at the RIS. Moreover, in [168], a DFT-based method has been proposed for estimating the cascaded channels. In this case, the RIS training states are given as the columns of a DFT matrix, resulting in higher estimation accuracy [113].

Nevertheless, for a large number of elements, performing channel estimation for all the RIS elements becomes impractical, since the incurred training overhead is prohibitively large and causes significant performance degradation, while the resources are usually limited. To avoid the above limitations, some efforts have been made to reduce the training requirements of such systems. Specifically, in [169] the authors suggest to reduce channel estimation overhead through an element-grouping method. Moreover, a low-overhead RIS reconfiguration scheme is proposed in [170] which, instead of acquiring full CSI for configuring the RIS, requires only the estimation of the mobile user's position. Finally, various low-complexity RIS schemes are proposed in [85], which induce random phase shifts to the incident signal in order to enhance the performance of RIS-aided systems, resulting in low-to-zero CSI requirements.

Motivated by this, in this work we study the performance of a low-complexity hybrid scheme for an RIS-aided network, where only a subset of the elements are used for channel estimation, and we investigate how the performance is affected under an imperfect CSI scenario at the RIS. In particular, this scheme partitions the RIS into two sub-surfaces, where the elements of the first sub-surface optimize their phase shifts through a coherent beamforming (CB) design, based on the estimated CSI, while the remaining elements induce random rotations (RR). By sequentially activating each sub-surface, a time-varying channel is produced, which can boost the performance of the considered network. The proposed scheme can significantly

reduce the channel training overhead for the RIS configuration and can be easily adapted to several channel estimation methods that have been proposed for RIS-aided systems. Through this approach, we aim to provide a tradeoff between the number of RIS elements that need to be considered for channel estimation in order to optimize the performance of the considered system. Therefore, we present a complete analytical framework in terms of outage probability and we provide useful insights on the effect of the number of elements used for channel estimation and the consideration of imperfect CSI. Our results show that the proposed scheme can provide higher coding gain, compared to the case where all the elements induce RR, and overcomes the performance limitations caused by the imperfect CSI in the full channel estimation scenario.

5.2   System Model

We consider an RIS-aided communication system shown in Fig. 5.1, where the communication between a single-antenna transmitter (Tx) and a single-antenna receiver (Rx) is assisted by the employment of an RIS equipped with Q reflecting elements. We assume a scenario where a direct link between the Tx and the Rx does not exist (e.g. due to path blockages or heavy shadowing); hence the communication is achieved only through the RIS [85,87]. Let $\mathbf{h} = \begin{bmatrix} h_1\, h_2 \cdots h_Q \end{bmatrix}^\top$ and $\mathbf{g} = \begin{bmatrix} g_1\, g_2 \cdots g_Q \end{bmatrix}^\top$ denote the channel vectors from the Tx to the RIS and from the RIS to the Rx, respectively. We consider that all wireless links exhibit fading which follows a flat quasi-static Rayleigh block fading model[1] [87]; the channel coefficients remain invariant during a coherence interval of T channel uses, but change independently between different coherence intervals, by following a circularly symmetric complex Gaussian distribution with zero mean and unit variance, i.e., h_i and $g_i \sim \mathcal{CN}(0,1)$.

At an arbitrary time instance t, the reflection amplitude and the phase shift of each RIS element are modified, according to the proposed scheme that will be presented in Section 5.3. We denote by

$$\boldsymbol{\phi}_t = [a_{1,t}e^{J\phi_{1,t}}\ \ a_{2,t}e^{J\phi_{2,t}}\ \ \ldots\ \ a_{Q,t}e^{J\phi_{Q,t}}], \tag{5.1}$$

the reflection vector of the RIS at the t-th time instance, where $a_{i,t} \in [0,1]$ is the

---

[1]We consider Rayleigh fading for simplicity but this work could also be extended with other models.
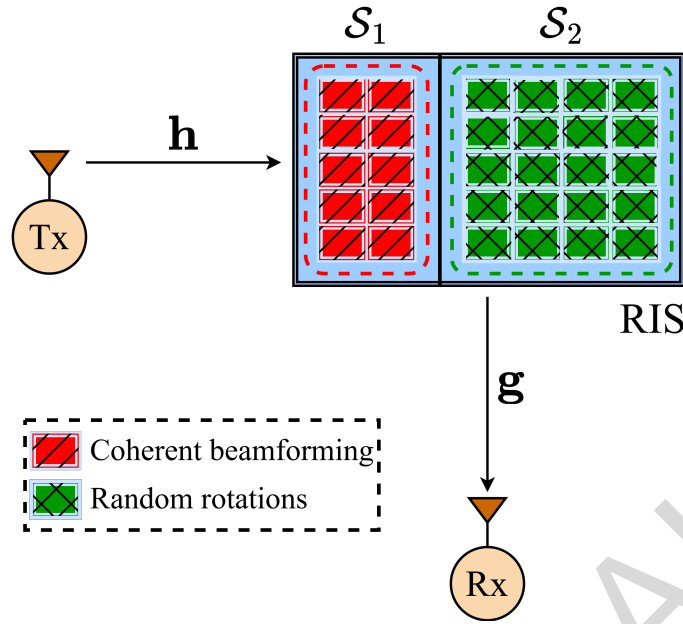
Figure 5.1: The considered RIS-aided communication system.

reflection amplitude of the i-th RIS element and $\phi_{i,t} \in [0, 2\pi)$ is the induced phase shift. In this setup, we consider an RIS hardware implementation where, at every time instance, each reflecting element can be found in two possible states, either to be turned ON or OFF [114,120]. Once an element is at the ON state, its reflection amplitude is set to 1 (full reflection) and we can only control its phase shift; conversely, at the OFF state the reflection amplitude is set to 0 (no reflection[2]) and the element cannot assist the communication. Finally, we assume that at the beginning of each coherence interval we have no prior knowledge of the CSI at the RIS. The received signal at the Rx at the t-th time instance is expressed as

$$
\begin{aligned}
y_t &= \sqrt{P_t}\mathbf{h}^\top \mathrm{diag}(\boldsymbol{\phi}_t)\mathbf{g}x_t + n_t \\
&= \sqrt{P_t}\sum_{i=1}^{Q} v_i a_{i,t} e^{j\phi_{i,t}} x_t + n_t,
\end{aligned} \tag{5.2}
$$

where $n_t \sim \mathcal{CN}(0, \sigma^2)$ is the AWGN with variance σ^2, x_t is the signal transmitted by the Tx with transmit power P_t and $v_i \triangleq h_i g_i$, $1 \leq i \leq Q$, denotes the product channel corresponding to the i-th RIS element.

---

[2]When an element is OFF, it does not act as a scattering object; this can be ensured by assuming that an OFF element fully absorbs the electromagnetic waves impinging its surface [81].
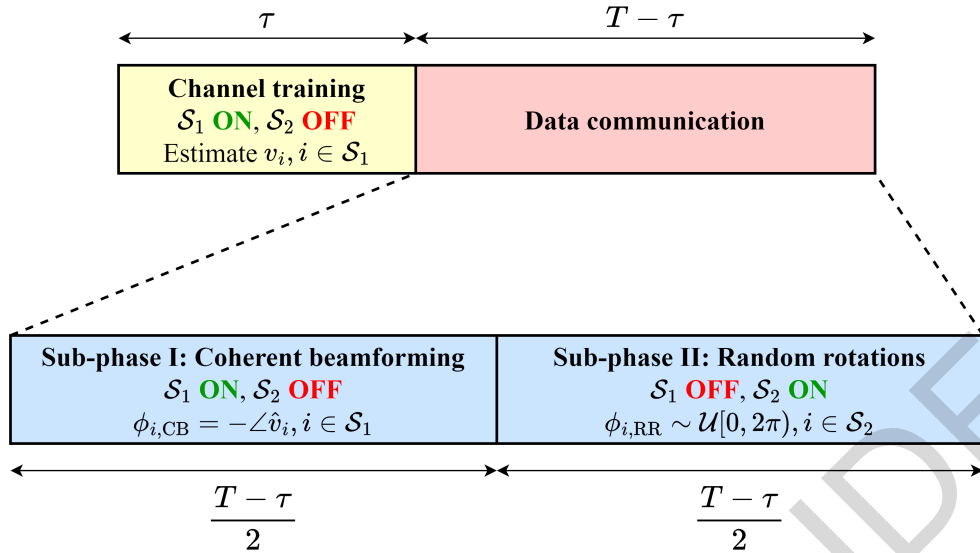
Figure 5.2: The phases of the transmission procedure and the RIS reconfiguration for the proposed scheme.

5.3 Hybrid CB/RR RIS Scheme

We now proceed to the description of the proposed hybrid CB/RR RIS scheme, which implements a temporal processing strategy for the reconfiguration of the RIS elements, in order to increase the achieved rate of the considered system. For the implementation of the proposed scheme, we assume that the RIS is partitioned into two non-overlapping sub-surfaces $\mathcal{S}_1$ and $\mathcal{S}_2$, consisting of Q_e and $Q_r = Q - Q_e$ elements, respectively. The elements of $\mathcal{S}_1$ are configured based on a CB design, i.e., the phase shifts are aligned to the phases of the corresponding channel coefficients, while the remaining elements follow an RR approach by inducing random phase shifts to the incident signals. An example of this approach is shown in Fig. 5.1, where the two sub-surfaces $\mathcal{S}_1$ and $\mathcal{S}_2$ (containing $Q_e = 10$ and $Q_r = 20$ elements, respectively) are indicated by the black solid line.

In order to optimize the phase shift parameters of the elements that belong to $\mathcal{S}_1$, the knowledge of the related product channels v_i is required. Since in the considered scenario prior CSI knowledge at the RIS is not available, a training period needs to be allocated for the required CSI acquisition. Therefore, each coherence interval is divided into two phases, as shown in Fig. 5.2: the *channel training phase* of duration $\tau \leq T$, where the product channels v_i corresponding to the elements of $\mathcal{S}_1$ are estimated, and the *data transmission phase* occuring for the remaining period

$T - \tau$, where the two sub-surfaces are sequentially activated to assist the transmission of the desired signals from the Tx to the Rx. In the following, we provide a more detailed description of each phase.

Channel training phase

The first phase is dedicated for the estimation of the channels associated with the elements of $\mathcal{S}_1$. During this phase, the elements that belong to $\mathcal{S}_2$ are set to the OFF state. The remaining elements switch their reflection coefficients, based on the RIS training states of the adopted channel training method. Without loss of generality, we consider a DFT-based training method for estimating the product channels [168]. Specifically, during the training period τ a pilot signal $x_p = 1$ is transmitted with fixed power P_o. This period is further divided into Q_e sub-phases of equal duration. During the j-th sub-phase, all the elements of $\mathcal{S}_1$ are turned ON and their phase shifts are set equal to the values of the j-th column of a $Q_e \times Q_e$ DFT matrix. Note that the columns of the DFT matrix are mutually orthogonal. The cascaded channels $\hat{v}_i$, $i \in \mathcal{S}_1$, are estimated by using a minimum mean square error approach [113]. In the considered scenario we assume imperfect CSI, where the variance of the channel estimation error is given by [113, 171]

$$\sigma_e^2 = \frac{1}{1 + \tau P_o}. \tag{5.3}$$

Data transmission phase

In the second phase, the desired data signals are sent with transmit power P from the Tx to the Rx. During this phase, the RIS controller activates $\mathcal{S}_1$ and $\mathcal{S}_2$ sequentially to assist the communication procedure. In particular, the data transmission phase is divided into two sub-phases of equal duration[3], i.e., $(T - \tau)/2$. In the first sub-phase, the elements of $\mathcal{S}_1$ are ON and the elements of $\mathcal{S}_2$ remain at the OFF state. The phase shifts of the activated elements are adjusted to align the phases of the product channels, based on the estimated CSI from the channel training phase, in order to yield the CB gains and maximize the achieved rate [113]. The design parameters for

---

[3]We consider equal duration of the two sub-phases for simplicity; the duration of each sub-phase can be adjusted to optimize the performance of the proposed scheme.

the RIS elements during the first sub-phase are summarized below

$$a_{i,\text{CB}} = \begin{cases} 1, & i\text{-th element} \in \mathcal{S}_1; \\ 0, & \text{otherwise}, \end{cases}$$

$$\phi_{i,\text{CB}} = -\angle\hat{v}_i, i\text{-th element} \in \mathcal{S}_1. \tag{5.4}$$

Finally, in the second sub-phase of data transmission, the communication is assisted only by $\mathcal{S}_2$. Specifically, in this sub-phase, the elements of $\mathcal{S}_2$ are now activated, while the elements of $\mathcal{S}_1$ are turned OFF. Each activated element randomly rotates the phase of the incident signal, by following a uniform distribution in $[0, 2\pi)$. The reflection coefficients are therefore given by

$$a_{i,\text{RR}} = \begin{cases} 1, & i\text{-th element} \in \mathcal{S}_2; \\ 0, & \text{otherwise}, \end{cases}$$

$$\phi_{i,\text{RR}} \sim \mathcal{U}\left[0, 2\pi\right), i\text{-th element} \in \mathcal{S}_2. \tag{5.5}$$

As a result, the end-to-end channel over a coherence interval is composed of two independent parallel sub-channels in the time domain, where for each sub-channel only the activated elements in each sub-phase need to be considered. It is worth noting that with the proposed scheme, we are able to reduce the channel training overhead, since channel estimation is required for only a subset of elements. In the following section, we evaluate the performance of the proposed scheme in terms of outage probability. Moreover, we compare our scheme with two benchmark scenarios: the *RR-only* scenario, where all the elements randomly rotate the phase of the incident signals ($Q_e = 0$ and $\tau = 0$), and the conventional *full-CB* scheme, where all the elements align their phase shifts based on the estimated CSI ($Q_e = Q$) [113]. Note that, in both cases, all the elements of the RIS are activated for the whole data transmission phase.

5.4 Outage probability analysis

In this section, we present our main analytical results for the performance of the considered scheme. Specifically, we derive the achieved outage probability, which is defined as the probability that the achieved rate over a coherence interval is not above a predefined threshold r. Based on the presented RIS scheme, the outage

probability can be written as

$$\Pi(Q_e, T) = \mathbb{P}\{R_{CB} + R_{RR} < r\}, \tag{5.6}$$

where

$$R_{CB} = \frac{T - \tau}{2T} \log_2\left(1 + \rho\left(\sum_{i \in \mathcal{S}_1} |\hat{v}_i|\right)^2\right), \tag{5.7}$$

is the sum-rate achieved over the CB sub-phase of the data transmission phase with $\rho = P(\sigma^2 + Q_e P \sigma_e^2)^{-1}$, and

$$R_{RR} = \frac{T - \tau}{2T} \log_2\left(1 + \frac{P}{\sigma^2}\left|\sum_{i \in \mathcal{S}_2} v_i \exp(\jmath\phi_{i,RR})\right|^2\right), \tag{5.8}$$

is the achieved sum-rate of the RR sub-phase. In what follows, we provide an approximation that can sufficiently describe the outage performance of the proposed scheme, by using the moment matching method and the CLT.

Theorem 5.1. *The outage probability of the proposed hybrid CB/RR scheme is approximated by*

$$\Pi(Q_e, T) \approx \frac{1}{Q_r P} \int_1^\theta \frac{1}{\Gamma(Q_e \kappa)} \gamma\left(Q_e \kappa, \frac{\sqrt{\Theta}}{\xi}\right) \exp\left(-\frac{y - 1}{Q_r P}\right) dy, \tag{5.9}$$

where

$$\kappa = \frac{\pi^2}{16 - \pi^2}, \quad \xi = \frac{16 - \pi^2}{4\pi} \sqrt{1 - \sigma_e^2}, \tag{5.10}$$

$$\theta \triangleq 2^{\frac{2rT}{T - \tau}}, \tag{5.11}$$

and

$$\Theta \triangleq \frac{1}{\rho}\left(\frac{\theta}{y} - 1\right). \tag{5.12}$$

Proof. Let $W_{CB} = \sum_{i \in \mathcal{S}_1} |\hat{v}_i|$. Recall that the channel coefficients h_i and g_i are independent and identically distributed (i.i.d) complex Gaussian random variables with variance one. By taking into account the errors induced at the channel training phase, the mean and variance of $|\hat{v}_i|$ are equal to

$$\mathbb{E}\{|\hat{v}_i|\} = \frac{\pi\sqrt{1 - \sigma_e^2}}{4}, \tag{5.13}$$

and

$$\text{Var}\{|\hat{v}_i|\} = \frac{16 - \pi^2}{16}\left(1 - \sigma_e^2\right). \tag{5.14}$$

By applying the moment matching method, $|\hat{v}_i|$ is approximated as a Gamma random variable [87], where the shape parameter κ and scale parameter ξ are calculated as

$$\kappa = \frac{\mathbb{E}\{\|\hat{v}_i\|\}^2}{\mathrm{Var}\{\|\hat{v}_i\|\}} \text{ and } \xi = \frac{\mathrm{Var}\{\|\hat{v}_i\|\}}{\mathbb{E}\{\|\hat{v}_i\|\}}, \tag{5.15}$$

and are given by (5.10). Since W_{CB} is the sum of Q_e i.i.d. Gamma random variables with the same parameters, it is also Gamma distributed with parameters $Q_e\kappa$ and ξ. We now let

$$W_{\mathrm{RR}} = \sum_{i \in \mathcal{S}_2} v_i \exp(\jmath\phi_{i,\mathrm{RR}}). \tag{5.16}$$

It has been proved in [85] that by applying the CLT, the distribution of W_{RR} converges to a complex Gaussian distribution with zero mean and variance Q_r. Therefore, the channel gain $H_{\mathrm{RR}} = |W_{\mathrm{RR}}|^2$ is exponentially distributed with parameter $1/Q_r$. We can now evaluate the outage probability as

$$\begin{aligned}
\Pi(Q_e, T) &= \mathbb{P}\left\{R_{\mathrm{CB}} + R_{\mathrm{RR}} < \frac{2Tr}{T-\tau}\right\} \\
&= \mathbb{E}_{H_{\mathrm{RR}}}\left\{F_{W_{\mathrm{CB}}}\left(\sqrt{\frac{1}{\rho}\left(\frac{\theta}{1 + \frac{PH_{\mathrm{RR}}}{\sigma^2}} - 1\right)}\right)\right\} \\
&= \int_z F_{W_{\mathrm{CB}}}\left(\sqrt{\frac{1}{\rho}\left(\frac{\theta}{1 + \frac{Pz}{\sigma^2}} - 1\right)}\right) f_{H_{\mathrm{RR}}}(z)dz,
\end{aligned} \tag{5.17}$$

where the cdf of W_{CB} and the pdf of H_{RR} are given by

$$F_{W_{\mathrm{CB}}}(x) = \frac{1}{\Gamma(Q_e\kappa)}\gamma\left(Q_e\kappa, \frac{x}{\xi}\right), \tag{5.18}$$

and

$$f_{H_{\mathrm{RR}}}(z) = \frac{1}{Q_r}\exp\left(-\frac{z}{Q_r}\right), \tag{5.19}$$

respectively. The integration limits are evaluated by ensuring that

$$\frac{\theta}{1 + Pz/\sigma^2} - 1 > 0, \tag{5.20}$$

and the final expression is derived by using the transformation $y \to 1 + Pz/\sigma^2$. $\quad\square$

It is clear that under the RR-only scenario, i.e., $Q_e = 0$, a channel training phase is not required ($\tau = 0$), and so the whole coherence interval is used for data transmission. Therefore, we need to consider only (5.8) for the achieved rate of the RIS-aided system and the approximated outage expression is simplified to

$$\Pi(0, T) \approx 1 - \exp\left(-\frac{(2^r - 1)\sigma^2}{QP\|\hat{v}_i\|}\right). \tag{5.21}$$

108

On the other hand, by considering the benchmark scenario of the conventional full-CB scheme, where $Q_e = Q$, the outage probability can be expressed as

$$\Pi(Q, T) \approx \frac{1}{\Gamma(Q\kappa)} \gamma \left(Q\kappa, \sqrt{\frac{1}{\xi^2 \rho} (\vartheta - 1)} \right), \qquad (5.22)$$

with

$$\vartheta = 2^{\frac{rT}{T-\tau}}. \qquad (5.23)$$

It can be easily observed that the outage performance of the considered RIS-aided system is significantly affected by the size of each RIS sub-surface. Although the employment of the CB design at the RIS can provide high performance gains, estimating the channels for a large number of elements incurs high training overhead, which inevitably degrades the system's performance. Thus, in this work, we aim to find the optimal number of elements in each sub-surface in order to minimize the outage probability, i.e.,

$$Q_e^\star = \arg \min_{0 \leq Q_e \leq Q} \Pi(Q_e, T). \qquad (5.24)$$

By using the derived theoretical expressions for $\Pi(Q_e, T)$, the above optimal value can be easily obtained through an exhaustive search method on the number of elements that should be estimated.

We now turn our attention to the asymptotic outage performance of the system as P increases. When $P \to \infty$ then the instantaneous SNR over the CB sub-phase converges to

$$\lim_{P \to \infty} \rho \left(\sum_{i \in S_1} |\hat{v}_i| \right)^2 \to \frac{1}{Q_e \sigma_e^2} \left(\sum_{i \in} |\hat{v}_i| \right)^2. \qquad (5.25)$$

Then, by using that $\exp(-x) \approx 1 - x$ for $x \approx 0$ and by taking the smallest order term of (5.9) as the dominant term, we observe that the outage probability decreases with the rate of $1/P$, i.e.,

$$\lim_{P \to \infty} \Pi(Q_e, T) \to \frac{1}{Q_r P \Gamma(Q_e \kappa)} \int_1^\theta \gamma \left(Q_e \kappa, \sqrt{\frac{Q_e \sigma_e^2}{\xi^2} \left(\frac{\theta}{y} - 1 \right)} \right) dy. \qquad (5.26)$$

Note that, under the RR-only scenario ($Q_e = 0$) the achieved outage probability follows a similar behavior, since asymptotically it converges to

$$\lim_{P \to \infty} \Pi(0, T) \to \frac{(2^r - 1)\sigma^2}{QP}. \qquad (5.27)$$

On the other hand, when employing the full-CB scheme, due to the channel estimation error imposed by the imperfect CSI the outage probability converges to a
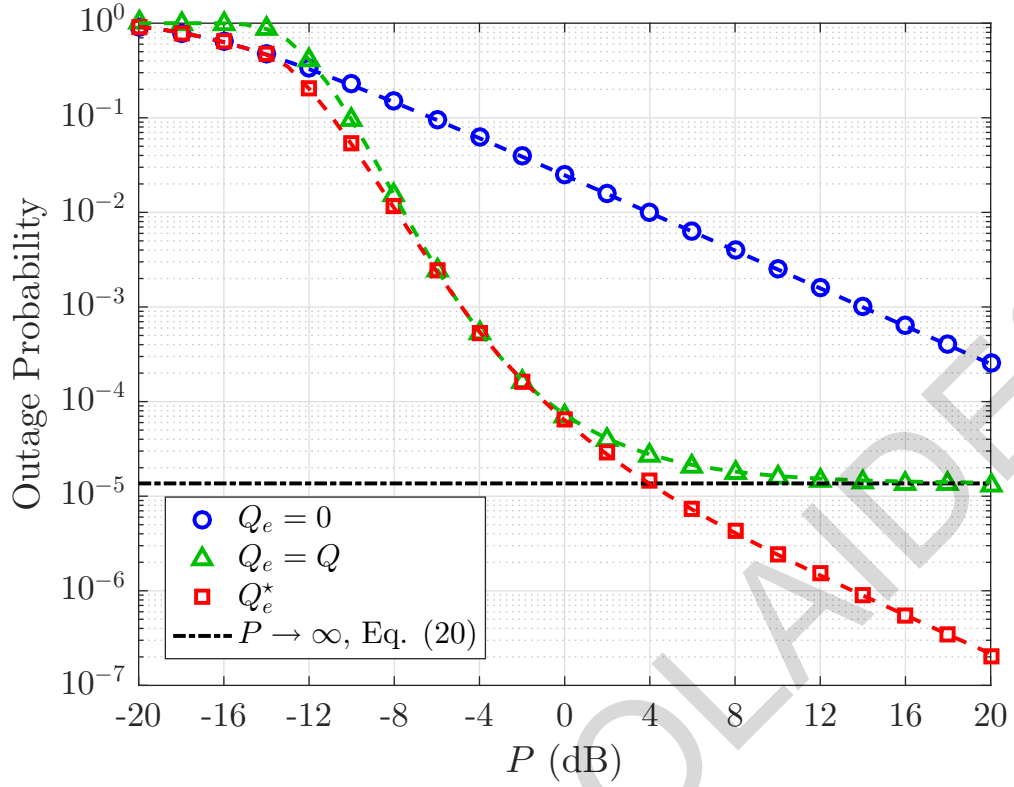
Figure 5.3: Outage probability versus transmit power P; $Q = 40$ and $T = 50$ channel uses.

constant floor given by

$$\lim_{P \to \infty} \Pi(Q, T) \to \frac{1}{\Gamma(Q\kappa)} \gamma \left(Q\kappa, \sqrt{\frac{Q\sigma_e^2}{\xi^2} (\vartheta - 1)} \right). \tag{5.28}$$

It is therefore deduced that, at high SNR the CB/RR scheme overcomes the outage floor that limits the performance of the full-CB case due to imperfect CSI, since in the proposed scheme the two sub-surfaces are sequentially activated and the channel estimation error affects only the elements of $\mathcal{S}_1$. In particular, when $P \to \infty$ both the RR-only scenario and the CB/RR scheme outperform the full-CB case, while the optimal performance is obtained by the partition size $Q_e^\star$ that achieves the highest coding gain.

5.5 Numerical Results

In this section, we validate our analytical framework and main observations with Monte Carlo simulations. For the sake of presentation, we consider $r = 1$ bps/Hz and $\sigma^2 = 1$. Moreover, for the channel training we assume that $\tau = Q_e$ channel uses
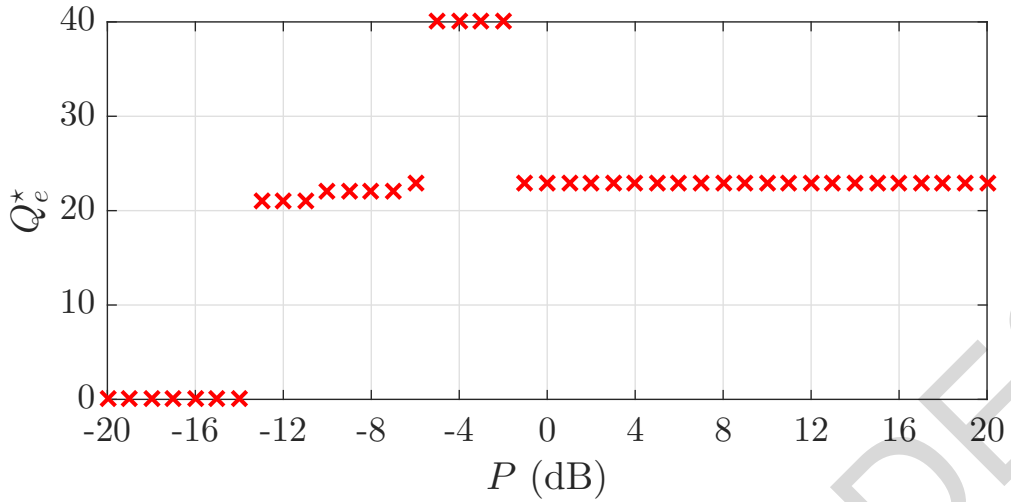
Figure 5.4: Optimal partition size versus transmit power P; $Q = 40$ and $T = 50$ channel uses.

and $P_o = -10$ dB. The proposed scheme is compared with the conventional RR-only scenario ($Q_e = 0$) and the full-CB case ($Q_e = Q$). The simulation results have been obtained after 10^8 simulation runs. Unless otherwise stated, analytical results are depicted with lines and simulation results with markers.

In Fig. 5.3, we illustrate the achieved outage probability in terms of the transmit power P for an RIS with $Q = 40$ elements and a coherence interval of $T = 50$ channel uses. In particular, Fig. 5.3 shows the achieved outage probability for the conventional cases of $Q_e = 0$ and $Q_e = Q$, and the optimal partition size of the RIS $Q_e^\star$. It is observed that for very low values of P, dedicating part of the coherence interval for channel estimation does not provide any significant performance gains. Therefore, the best option is to employ the RR-only scenario at the RIS in order to make full use of the available time for data transmission. On the other hand, in the high SNR regime it is clear that the hybrid CB/RR RIS scheme can significantly outperform the conventional scenarios. Specifically, we observe that for both the RR-only case and the proposed scheme, the outage probability decreases with the rate of $1/P$, while in the full-CB scenario the outage probability converges to the floor value calculated in (5.28). However, the proposed scheme, under optimal partitioning, can achieve considerably higher coding gain compared to the RR-only case. Finally, we note that the theoretical lines approximate the simulation results exceptionally well, validating the accuracy of the presented analysis.

The optimal partition size that achieves the best outage performance, as indicated

111
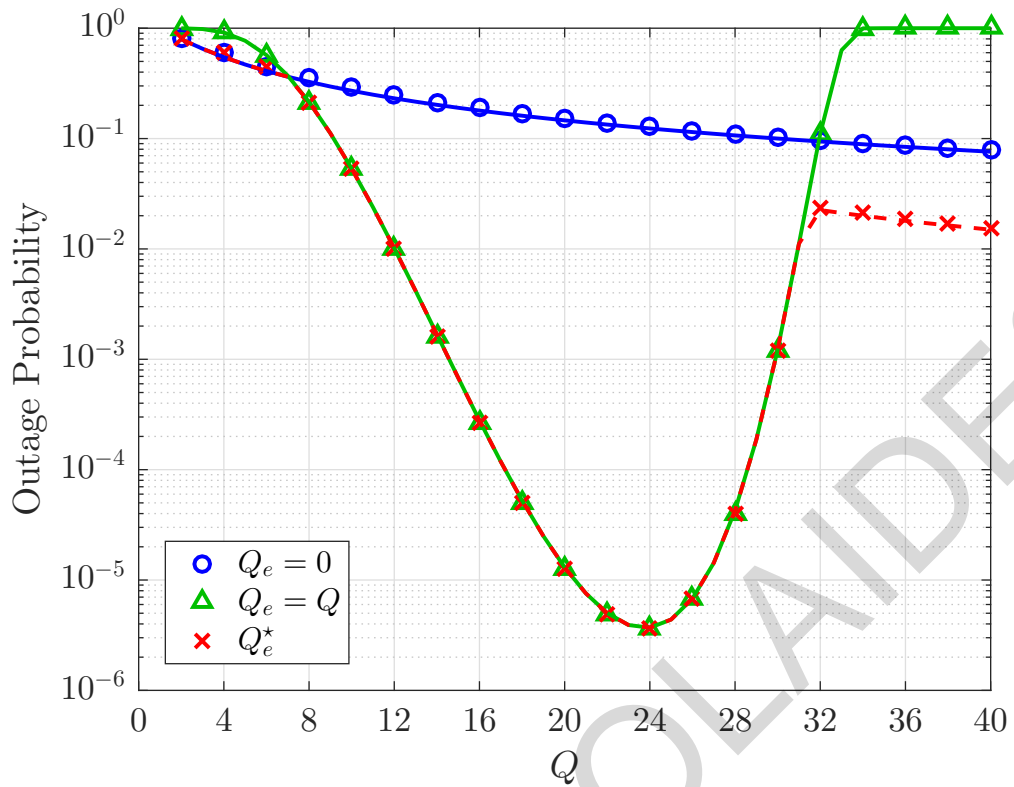
Figure 5.5: Outage probability versus number of elements Q; $T = 40$ channel uses and $P = -5$ dB.

by the red dotted line in Fig. 5.3, is provided in Fig. 5.4. It can be seen that for most of the transmit power values the outage probability is minimized by using around half of the total RIS elements for CB. In particular, in the high SNR region the optimal partition size becomes constant at $Q_e^\star = 23$ elements, since this value overcomes the outage floor of the full-CB scenario and the achieved coding gain is maximized. Note that, the sudden changes in the optimal partition size between $Q_e^\star = 0$, $Q_e^\star = Q$ and around half of the elements occur due to the fixed and equal duration of the two sub-phases of the data transmission phase.

Fig. 5.5 depicts the outage probability with respect to the total number of RIS elements Q for $T = 40$ channel uses and transmit power $P = -5$ dB. We observe that, for $Q \ll T$ the RR-only case provides the best outage performance, as the expected gains from the CB design are insufficient for such low number of elements. As the number of RIS elements increases, the full-CB scenario becomes optimal, since the optimization of the RIS phase shifts yields high performance gains. However, when the number of elements approaches the total channel uses, i.e., $Q \to T$, the training overhead becomes large under the full-CB case and the outage probability is significantly deteriorated. On the other hand, the proposed scheme overcomes

the above limitations by reducing the required training overhead, since the channel training is performed for only a subset of elements; hence it outperforms the conventional scenarios and provides the best outage performance when the partition size is optimized.

Therefore, based on the presented analysis and associated results, it can be deduced that the proposed scheme is a promising solution to compensate for the training overhead required for the channel estimation and the performance gains that can be achieved. In particular, the hybrid scheme can be implemented with low design complexity, since only a subset of elements is considered for channel estimation, while the sequential activation of each subsurface can be realized with low-cost elements. Moreover, in cases where the available resources (number of elements, channel uses per coherence interval etc.) do not favor full estimation of the channels, the considered scheme is a potential alternative solution to overcome the performance limitations occurred by the available resources and imperfect CSI.

5.6 Conclusions

In this chapter, we proposed a hybrid CB/RR scheme for an RIS-assisted network, which requires channel estimation for only a subset of the elements. The presented scheme splits the RIS into two sub-surfaces, which are sequentially activated and employ a CB-based and an RR-based design, respectively, resulting in reduced channel training overhead. The performance of the proposed scheme was investigated under imperfect CSI. We derived analytical expressions for the outage probability and we showed that, by optimizing the number of estimated elements, the proposed scheme can still benefit from the performance gains obtained by the channel training and can improve the performance beyond the limits imposed by the imperfect CSI at the RIS.

Chapter 6

An RIS-enabled Time Reversal Scheme for Multipath Near-Field Channels

Time reversal is a promising technique that exploits multipaths for achieving energy focusing in high-frequency wideband communications. In this chapter, we focus on a TR scheme facilitated by an RIS which, due to the higher frequency and large array aperture, operates in the near-field region. The proposed scheme enriches the propagation environment for the TR in such weak scattering conditions and does not need channel knowledge for the RIS configuration. Specifically, the RIS is employed to create multiple virtual propagation paths that are required to efficiently apply the TR. We derive a performance bound for the proposed scheme under near-field modeling through the received SNR. Moreover, we present numerical results to showcase the potential gains of the proposed scheme over the conventional CSI-based passive beamforming at the RIS and provide important insights on how various system design parameters affect the performance.

6.1 Introduction

The rapid surge in wireless devices has led to an unprecedented amount of data traffic that the upcoming 6G networks need to efficiently handle. In order to address these challenges, a paradigm shift towards higher-frequency communications with wider bandwidths has been proposed [125]. However, as bandwidth increases, more

multipaths are resolved, which may cause destructive interference at the receiver [124]. As previously mentioned in Chapter 2, TR is signal processing technique suitable for high-frequency wideband communications, which can achieve high energy focusing in both space and time domains by using the time-reversed impulse response of the multipath channel as a prefilter at the transmitter. Due to its potential performance benefits in wireless communications, TR has received considerable attention by the research community in both academia and industry [127, 129, 130].

However, it has been shown that the TR-based networks can only provide sufficient performance gains within a rich scattering environment [130]. Under weak propagation conditions, e.g., due to severe path loss or high blockage sensitivity, the employment of an RIS is an appealing solution to overcome this bottleneck, as it is able to individually reflect the incident signals, essentially creating multiple virtual paths in a controllable manner. Nevertheless, due to the shift of future 6G networks towards higher frequencies, a large RIS needs to be utilized to obtain sufficient performance gains. As such, the operating regime of the RIS changes from the traditional far-field to the near-field region, which affects the modeling of the wireless channel [172, 173].

Motivated by the above, in this chapter we propose a low-complexity *RIS-enabled TR scheme*, where an RIS, operating in the near-field region, artificially enriches the scattering environment for the efficient application of the TR. To our best knowledge, this is the first work considering the utilization of an RIS for facilitating the TR technique. Apart from providing sufficient propagation paths for the TR, the proposed scheme is mutually beneficial to the RIS since accurate CSI knowledge is not required for its configuration. By considering near-field channels, we study the fundamental limits of the RIS-based TR scheme, through the achieved SNR at the receiver, and we provide useful insights on the effect of several design parameters on the system's performance. It is observed that, under a linear RIS topology the system provides maximum virtual paths. We also highlight, through numerical results, the performance gains that can be obtained by the proposed scheme. It is shown that for a large number of elements the proposed scheme achieves higher SNR gain, compared to the passive beamforming counterpart.
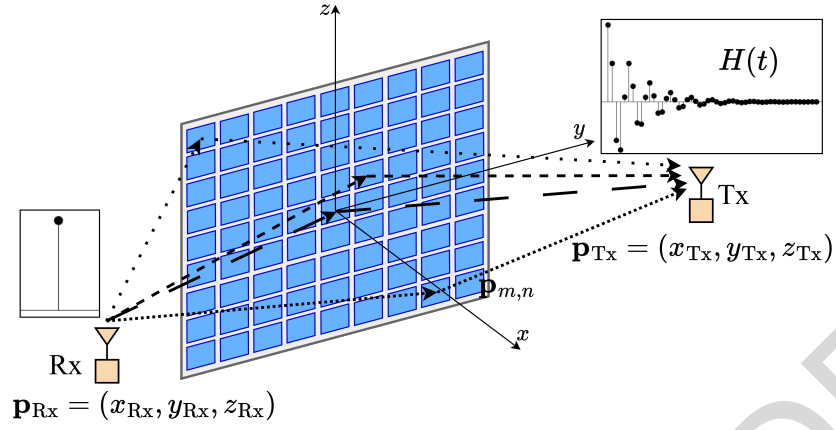
(a) Channel probing phase
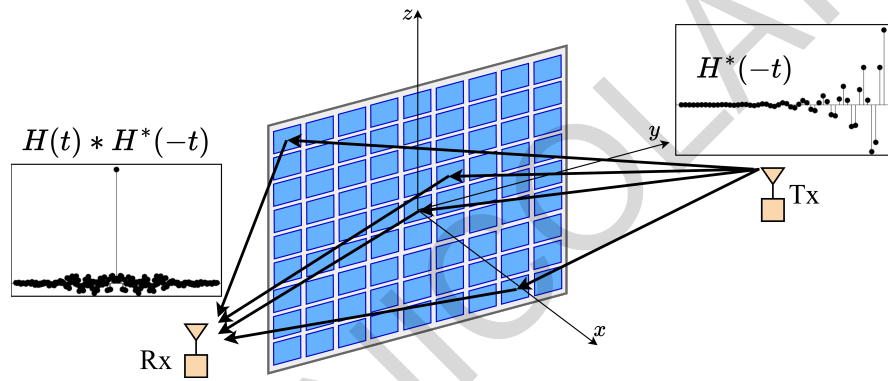
(b) Data transmission phase

Figure 6.1: Network topology and communication procedure of the considered RIS-enabled TR scheme.

6.2 System Model

We consider an RIS-aided communication system shown in Fig. 6.1, where the communication between a single-antenna transmitter (Tx) and a single-antenna receiver (Rx) is assisted by the employment of an RIS. The communication occurs in the near-field communication regime of the RIS, where the wireless links are typically considered to be predominantly LoS [172]. We assume that the direct LoS link between the Tx and Rx is not available (e.g., is blocked by obstacles [172]).

The RIS is placed in the yz-plane of a Cartesian coordinate system with its geometric center at the origin and consists of Q elements distributed in M rows and N columns, i.e., $Q = MN$. For the sake of symmetry, and without loss of generality, we assume the parameters M and N to be odd numbers. In this way, the center element of the RIS corresponds to the origin of the Cartesian system with coordi-

nates $(0, 0, 0)$. Moreover, the distance between two adjacent elements is considered to be $d = \frac{\lambda}{2} = \frac{c_0}{2f_c}$, where λ is the signal wavelength, f_c is the carrier frequency and c_0 denotes the speed of light. Therefore, the coordinates of the element located in the m-th row and n-th column of the RIS are denoted by $\mathbf{p}_{m,n} = (0, nd, md)$, where $m = 0, \pm 1, \ldots, \pm(M - 1)/2$ and $n = 0, \pm 1, \ldots, \pm(N - 1)/2$, respectively. We denote by

$$\Phi_{m,n} = a_{m,n} \exp\left(\jmath \phi_{m,n}\right), \tag{6.1}$$

the reflection coefficient of the (m, n)-th RIS element, where $a_{m,n} \in [0, 1]$ is the reflection amplitude and $\phi_{m,n} \in [0, 2\pi)$ is the induced phase shift.

The Tx transmits a passband signal $x_p(t)$ derived from the baseband equivalent signal [124]

$$x(t) = \sum_{k=0}^{\infty} x[k] g\left(t - \frac{k}{W}\right), \tag{6.2}$$

where $x[k] \in \mathbb{C}$ denotes the sequence of symbols to be transmitted with constant power P, and $g(t)$ is a pulse shaping filter limited by a finite bandwidth W. The Tx and Rx are located in the positive direction of the x axis at positions $\mathbf{p}_{\mathrm{Tx}} = (x_{\mathrm{Tx}}, y_{\mathrm{Tx}}, z_{\mathrm{Tx}})$ and $\mathbf{p}_{\mathrm{Rx}} = (x_{\mathrm{Rx}}, y_{\mathrm{Rx}}, z_{\mathrm{Rx}})$ respectively, with their corresponding Euclidean distances from the origin given by $\left\| \mathbf{p}_i \right\| = \sqrt{x_i^2 + y_i^2 + z_i^2}$, $i \in \{\mathrm{Tx}, \mathrm{Rx}\}$. Accordingly, the Euclidean distance between the Tx or the Rx and the (m, n)-th element is equal to

$$\begin{aligned} r_{i,m,n} &\triangleq \left\| \mathbf{p}_i - \mathbf{p}_{m,n} \right\| \\ &= \sqrt{x_i^2 + (y_i - nd)^2 + (z_i - md)^2}. \end{aligned} \tag{6.3}$$

Note that, since we focus on a near-field communication scenario, the distance of the Tx and Rx from the center of the RIS is upper bounded by the Rayleigh distance $d_{\mathrm{R}} = \frac{2D^2}{\lambda}$ [172, 173], where D denotes the largest distance between two elements of the RIS, i.e., $D = d\sqrt{(M-1)^2 + (N-1)^2}$. Hence, for $i \in \{\mathrm{Tx}, \mathrm{Rx}\}$ we have

$$r_{i,0,0} = \left\| \mathbf{p}_i \right\| \leq d\left[(M-1)^2 + (N-1)^2\right]. \tag{6.4}$$

Finally, we assume that in the considered scenario the near-field LoS channel follows the uniform spherical wave (USW) model [173]. Under this model, the channel coefficients of the system have uniform channel gains based on the free-space path loss. Specifically, the channel coefficient between the Tx or the Rx and the (m, n)-th element of the RIS is given by

$$h_{i,m,n} = \frac{1}{\left\| \mathbf{p}_i \right\| \sqrt{4\pi}} \exp\left(-\jmath \frac{2\pi r_{i,m,n}}{\lambda}\right). \tag{6.5}$$

117

In what follows, we demonstrate how the RIS can be utilized as an enabler of the TR scheme, by generating a multipath propagation environment.

6.3 RIS-enabled TR scheme

We now proceed to the description of the proposed RIS-enabled TR scheme and evaluate its performance in terms of the SINR. As previously mentioned, the main idea of the TR technique is to exploit the scattering environment in such a way that will allow focusing the power of electromagnetic signals in both time and space domains. In order to efficiently apply the TR in the near-field region, we first need to guarantee that a rich scattering environment is available [130]. In such weak scattering conditions, the RIS can be employed to enrich the propagation environment. In principle, the TR scheme consists of two phases as shown in Fig. 6.1: (1) the *channel probing phase*, which is required to provide knowledge regarding the system's multipath environment to the Tx, and (2) the *data transmission phase*, which is dedicated to the transmission of the information signal from the Tx to the Rx, taking into consideration the acquired knowledge [127]. In the following subsections, we present how the TR scheme could be implemented in the context of the considered RIS-aided near-field communication system, by providing a detailed description of each phase.

6.3.1 RIS-based Tapped Delay Channel

According to the TR scheme, during the channel probing phase, the Rx sends an impulse-like pilot signal [127], which is propagated towards the Tx through the RIS (Fig. 6.1a). The resulting channel impulse response (CIR) $H(t)$ is then received by the Tx. Note that, this phase is necessary so that the Tx can obtain some knowledge regarding the propagation environment, which is indirectly provided through the received CIR. Assuming that in the considered near-field communication scenario the non-LoS paths provide negligible gains compared to the LoS propagation, the transmitted signal is reflected towards the Rx only by the Q elements of the RIS. These elements can equivalently be seen as scatterers providing a total of Q different propagation paths, each of them generating a delayed and attenuated copy of the transmitted waveform. The multipath CIR ensued from the RIS can therefore be

expressed by

$$H(t) = \sum_{m,n} h_{m,n} \delta(t - \tau_{m,n}), \tag{6.6}$$

where $h_{m,n}$ and $\tau_{m,n}$ denote the end-to-end channel coefficient and time delay, respectively, of the path occurred by the (m, n)-th element. Based on the USW model, the end-to-end channel coefficient of the (m, n)-th path is given by

$$\begin{aligned} h_{m,n} &= h_{\text{Tx},m,n} h_{\text{Rx},m,n} \Phi_{m,n} \\ &= \frac{a_{m,n}}{4\pi \left\| \mathbf{p}_{\text{Tx}} \right\| \left\| \mathbf{p}_{\text{Rx}} \right\|} \exp \left[\jmath \left(\phi_{m,n} - \frac{2\pi \left(r_{\text{Tx},m,n} + r_{\text{Rx},m,n} \right)}{\lambda} \right) \right]. \end{aligned} \tag{6.7}$$

Furthermore, the time delay of the (m, n)-th path is equal to

$$\begin{aligned} \tau_{m,n} &= \frac{1}{c_0} \left(r_{\text{Tx},m,n} + r_{\text{Rx},m,n} + \frac{\lambda \phi_{m,n}}{2\pi} \right) \\ &\approx \frac{1}{c_0} \left(r_{\text{Tx},m,n} + r_{\text{Rx},m,n} \right). \end{aligned} \tag{6.8}$$

The approximated expression holds since the delay induced by the phase shift of the RIS element is much smaller than the propagation delay of the corresponding path, hence its impact is negligible.

However, it is generally hard to retrieve the multipath CIR shown in (6.6), since the communication system is limited by the available bandwidth W, which affects the time delay resolution of the system [124]. Specifically, the resolution to distinguish two propagation paths with different time delays is limited to $1/W$, as shown in Fig. 6.2. The propagation paths whose time delays are within a symbol duration $1/W$ are merged into a single tap. Therefore, the equivalent CIR of the considered system can be modeled as a tapped delay channel with L taps, where each tap corresponds to a group of closely spaced paths that cannot be resolved [124]. Let $\tau_{min} = \min_{m,n} \tau_{m,n}$ and $\tau_{max} = \max_{m,n} \tau_{m,n}$ denote the minimum and maximum time delay occurred by the RIS-enabled propagation paths, respectively. Also let T_l denote the set of paths (m, n) that belong to the l-th tap, $l = 1, \ldots, L$, defined as

$$T_l = \left\{ (m, n) : \frac{l-1}{W} \leq \tau_{m,n} - \tau_o < \frac{l}{W} \right\}, \tag{6.9}$$

where $\tau_o = \lfloor \tau_{min} W \rfloor / W$ indicates the initial time instance of the first tap containing at least one propagation path. The equivalent CIR with limited bandwidth W can therefore be expressed in a simplified discrete time form as

$$H_{eq}[k] = \sum_{l=1}^{L} h_{eq,l} \delta[k - l], k = 1, \ldots, L, \tag{6.10}$$

119

Figure 6.2: The RIS-based tapped delay channel.

where the total number of taps is $L = \lceil (\tau_{max} - \tau_o)W \rceil$, and $h_{eq,l}$ contains the channel coefficients of all the paths included in the l-th tap, which is equal to

$$h_{eq,l} = \sum_{(m,n) \in T_l} h_{m,n}. \tag{6.11}$$

Note that, if the total delay spread is within a symbol duration, the equivalent CIR is frequency-flat; otherwise, H_{eq} becomes frequency-selective with $L > 1$. After receiving the CIR, the system proceeds to the data transmission phase, which will be presented in the next section, along with the analysis for the achieved SINR.

6.3.2 Data Transmission and Achieved SINR

In the second phase of the TR scheme, the Tx incorporates the channel knowledge acquired from the channel probing phase into the data sequence in such a way that will enable spatial and temporal focusing of the power at the Rx location. In particular, the Tx time-reverses (and conjugates) the received CIR, and uses the resulting normalized waveform as a prefilter for the information signal (Fig. 6.1b) [127]. Based on the RIS-enabled equivalent CIR derived in (6.10) for a finite bandwidth W, the normalized, time-reversed and conjugate CIR generated by the Tx is given by

$$\hat{H}_{eq}[k] = \frac{H_{eq}^*[L-k]}{\sqrt{\sum_{l=1}^{L} \left| H_{eq}[l] \right|^2}}, k = 1, \dots, L. \tag{6.12}$$

By embedding the above waveform into the sequence of data symbols $\{x[k]\}$, the transmitted signal can be expressed as the convolution of the time-reversed CIR with the information signal, i.e.,

$$s[k] = \sqrt{P}\left(x * \hat{H}_{eq}\right)[k]. \tag{6.13}$$

Due to the channel reciprocity, the RIS-based multipath channel acts as a natural matched filter to $\hat{H}_{eq}[k], k = 1, \ldots, L$. As a result, the convolution of the time-reversed CIR with the multipath channel provides a unique peak at the receiver's location. Note that, the maximum-power peak of the autocorrelation function of the CIR occurs when $k = L$.

We can now proceed to the performance analysis of the TR scheme for the considered system in terms of SINR. The signal received at the Rx at the end of the data transmission phase can be written as the sum of the useful signal and an inter-symbol interference (ISI) term as follows

$$
\begin{aligned}
y[k] &= \sqrt{P}\left(x * \hat{H}_{eq} * H_{eq}\right)[k] + n[k] \\
&= \underbrace{\sqrt{P}\left(\hat{H}_{eq} * H_{eq}\right)[L]x[k - L]}_{\text{Useful signal}} \\
&\quad + \underbrace{\sqrt{P}\sum_{l=1, l \neq L}^{2L-1}\left(\hat{H}_{eq} * H_{eq}\right)[l]x[k - l]}_{\text{ISI}} + n[k],
\end{aligned} \tag{6.14}
$$

where $n[k] \sim \mathcal{CN}(0, \sigma^2)$ is the AWGN with variance σ^2. The SINR can be expressed as

$$\gamma_{\text{TR}} = \frac{P_{\text{U}}}{P_{\text{ISI}} + \sigma^2}, \tag{6.15}$$

where P_{U} is the power of the useful signal which, by combining (6.7) and (6.11), is equal to

$$
\begin{aligned}
P_{\text{U}} &= P\left|\left(\hat{H}_{eq} * H_{eq}\right)[L]\right|^2 = P\sum_{l=1}^{L}\left|h_{eq,l}\right|^2 \\
&= \frac{P}{16\pi^2\|\mathbf{p}_{\text{Tx}}\|^2\|\mathbf{p}_{\text{Rx}}\|^2}\sum_{l=1}^{L}\left|\sum_{(m,n)\in T_l} a_{m,n} \right. \\
&\quad \left. \times \exp\left[\jmath\left(\phi_{m,n} - \frac{2\pi\left(r_{\text{Tx},m,n} + r_{\text{Rx},m,n}\right)}{\lambda}\right)\right]\right|^2,
\end{aligned} \tag{6.16}
$$

and P_{ISI} is the ISI power given by

$$P_{\text{ISI}} = P\sum_{l=1, l \neq L}^{2L-1}\left|\left(\hat{H}_{eq} * H_{eq}\right)[l]\right|^2. \tag{6.17}$$

121

Since we focus on the potential of employing the RIS for the efficient implementation of the TR technique, we consider an ideal scenario where the ISI can be successfully eliminated; ISI mitigation in TR-based systems can be achieved through sophisticated signal processing and equalization techniques [127, 130]. Thus, we can focus only on the achieved SNR $\tilde{\gamma}_{TR}$, which serves as a useful communication theory bound, i.e.,

$$\gamma_{TR} \leq \tilde{\gamma}_{TR} = \frac{P_U}{\sigma^2}. \tag{6.18}$$

Based on the above expressions, we observe that the performance of the considered RIS-enabled TR system depends on the number of observable taps L, as well as the cardinality of the sets $T_l, 1 \leq l \leq L$,, i.e., the number of elements within each tap. In what follows, we provide a discussion on how various aspects of the system deployment can affect these parameters, and therefore the SNR achieved by the proposed scheme.

6.3.3 Insights into System Design Effects

Since the presented RIS-based TR scheme is highly sensitive to several system design parameters, it is of particular interest to examine how the RIS should be deployed in order to maximize the potential gains provided by the application of this technique in wireless systems. Based on how the RIS-enabled tapped delay channel is generated in Section 6.3.1, the number of taps and the number of non-resolvable paths considered in each tap can be controlled either by modifying the RIS configuration, that is, the total number of elements Q and their deployment into M rows and N columns, or by changing the value of the available bandwidth W. In particular, as the number of elements at the RIS increases, the number of observable taps can be increased as well, resulting in an improvement of the obtained SNR. On the other hand, for a fixed number of elements, the RIS topology and the available bandwidth could still affect the system's channel resolution.

For the sake of presentation, Table 6.1 shows the number of resolvable taps that are recorded in an indicative RIS-aided system operating at $f_c = 10$ GHz with $Q = 1225$ elements over various bandwidth values and for different RIS topologies. We observe that,

- As the RIS structure changes from the square-shaped RIS towards a stripe-like RIS with $M \ll N$, the resulting channel can be resolved into more taps. In

Table 6.1: Number of resolvable taps L

$\mathbf{p}_{Tx} = (2, 2, 0), \mathbf{p}_{Rx} = (2, -2, 0), Q = 1225, f_c = 10 \text{ GHz}$			
$W = 2 \text{ GHz}$		$W = 4 \text{ GHz}$	
$M \times N$	Number of taps (L)	$M \times N$	Number of taps (L)
35×35	1	35×35	1
7×175	3	7×175	5
5×245	6	5×245	10
1×1225	89	1×1225	176

particular, we observe from Table 6.1 that by deploying the RIS as a linear array of elements ($M = 1$), L becomes significantly larger compared to other RIS configurations.

- For a given RIS topology, increasing the available bandwidth W can also lead to a larger number of taps. However, it is important to note that a larger number of taps does not always improve the achieved SNR. Specifically, although a higher value of W will provide more taps, for a given RIS configuration the number of non-resolvable paths in each tap will decrease, and so the channel gains of the taps will be reduced.

It is therefore deduced that, although the proposed scheme can be applied for any system configuration, the deployment of a linear RIS (or stripe-like RIS [174]) is beneficial for the efficient application of the TR, since this topology can significantly enrich the scattering environment, by maximizing the number of generated propagation paths. The adoption of this topology has several advantages, such as easier deployment in indoor scenarios, e.g., along the perimeter of a large conference room or a shopping mall, while it is also more robust to the presence of obstacles compared to a square-shaped RIS [174, 175].

6.4 Numerical Results

Based on the discussion provided in Section 6.3.3, in the following figures we focus on the performance of the proposed scheme under a linear RIS topology deployed horizontally ($M = 1, N = Q$), in order to maximize the number of obtained paths. For
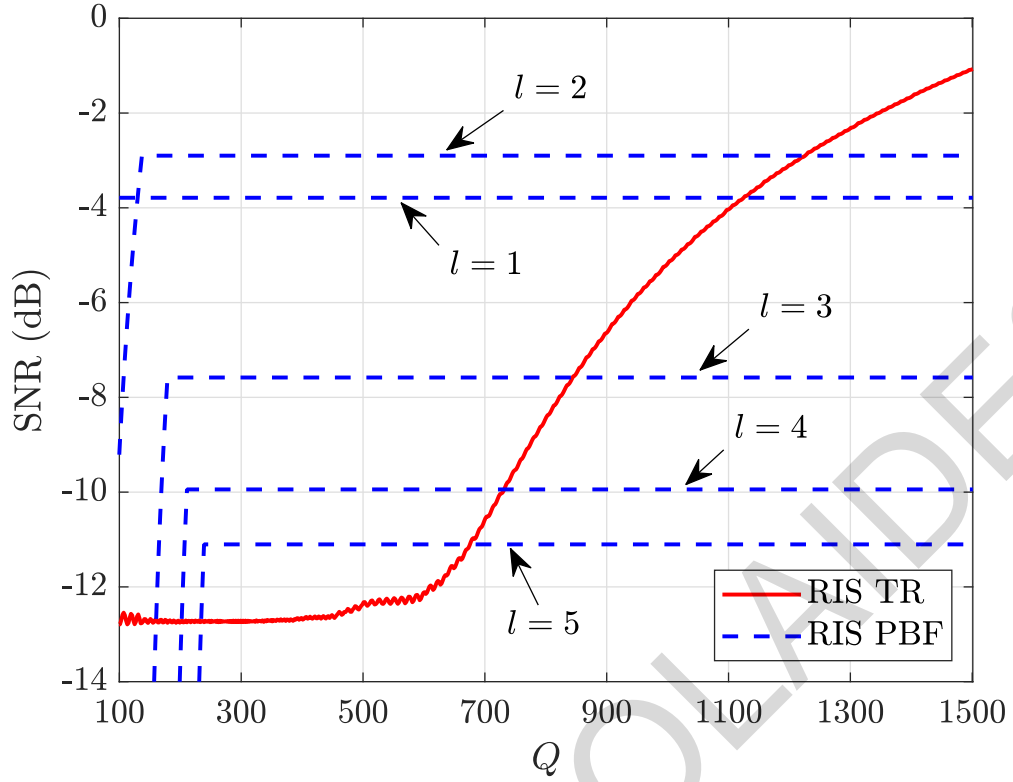
Figure 6.3: Comparison of achieved SNR under RIS-enabled TR versus RIS passive beamforming for $W = 2$ GHz.

the sake of presentation, we consider a system operating at $f_c = 10$ GHz (and thus $d = 1.5$ cm), with the positions of the Tx/Rx set to $\mathbf{p}_{\text{Tx}} = (2, 2, 0)$ and $\mathbf{p}_{\text{Rx}} = (2, -2, 0)$, respectively. Moreover, we set $P = 30$ dBm and $\sigma^2 = 1$. Since our focus in the proposed scheme is to employ the RIS for increasing the number of paths and the reflection coefficients of the RIS elements have negligible impact on the derived time delays, we assume $a_{m,n} = 1$ and $\phi_{m,n} = 0$, $\forall m, n$.

Fig. 6.3 shows the achieved SNR of the RIS-enabled TR scheme with respect to the number of elements. The performance of the proposed scheme is also compared to the case where the RIS performs (CSI-based) passive beamforming. Similar to the proposed scheme, we assume ideally that the ISI can be fully eliminated [176]. By setting the phase shifts of the elements corresponding to the l-th tap as $\phi_{m,n} = 2\pi \left(r_{\text{Tx},m,n} + r_{\text{Rx},m,n} \right) / \lambda$, the SNR for the l-th tap is

$$\tilde{\gamma}_{l,\text{PBF}} = \frac{P |T_l|^2}{16\pi^2 \left\| \mathbf{p}_{\text{Tx}} \right\|^2 \left\| \mathbf{p}_{\text{Rx}} \right\|^2 \sigma^2}, \tag{6.19}$$

where $|T_l|$ denotes the cardinality of the set of paths corresponding to the l-th tap. It can be seen that as the number of elements increases, the performance of the proposed scheme is improved, while for a large number of elements it outperforms
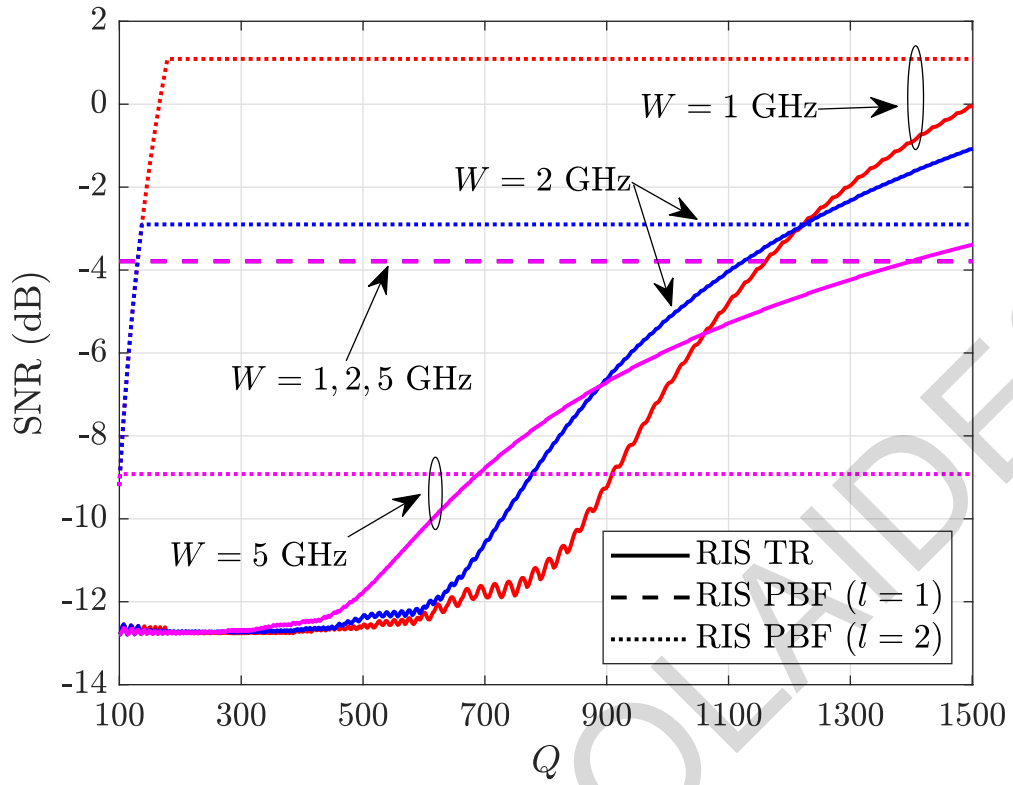
Figure 6.4: Achieved SNR versus Q for different values of bandwidth W.

the highest SNR gain achieved with RIS passive beamforming. This is due to the fact that by increasing the elements of the RIS, the number of generated taps is also increased, providing a rich scattering environment for the efficient implementation of the TR scheme. On the other hand, under the RIS passive beamforming the SNR for the l-th tap depends only on the propagation paths within the specific tap, so further increase of the elements will not improve the performance. Note that, the slight ripple effect observed at the achieved SNR of the proposed scheme is due to the non-monotonic nature of (6.16), which as expected disappears in the passive beamforming case.

In Fig. 6.4, we show how the available bandwidth W affects the performance of the RIS-enabled TR and the RIS passive beamforming with respect to the number of elements. It is observed that, under the RIS-enabled TR, for a moderate number of elements, a larger bandwidth provides a higher SNR gain. As previously mentioned, by considering a larger bandwidth, we can obtain a larger number of taps. Thus, with a smaller number of elements the scattering environment is sufficiently enriched, and the gains of the TR technique can be obtained. However, for a large number of elements, by increasing the bandwidth the performance is deteriorated. Note that, in this case the number of generated taps is sufficiently large under all the

considered values of W. On the other hand, for a larger bandwidth, each tap contains a smaller number of non-resolvable paths, and so the channel gain obtained for each tap is decreased. Therefore, for a very large number of elements increasing the bandwidth reduces the achieved SNR. Finally, we observe that the SNR obtained under the RIS passive beamforming can be significantly degraded when the available bandwidth is increased. In this case, the proposed scheme can outperform the passive beamforming scenario with a smaller number of elements.

Overall, it can be seen that the proposed RIS-enabled TR scheme is an appealing solution for enhancing the performance of high-frequency wideband communications. In particular, it can provide sufficient propagation paths for the efficient application of the TR and at the same time it avoids the complicated task of the CSI acquisition per propagation path for the RIS configuration, resulting in low implementation complexity. Moreover, it is observed that as the number of observable paths that can be obtained by the system increases, by increasing the number of elements or the available bandwidth, the proposed scheme becomes the preferred option compared to the conventional CSI-based passive beamforming case.

6.5 Conclusions

In this chapter, we investigated the performance of a a low-complexity RIS-enabled TR scheme applied in high-frequency wideband communications. Specifically, in order to satisfy the fundamental requirement of a rich scattering environment for the TR, the proposed scheme employs an RIS operating in the near-field region, due to the higher frequency and large array aperture, to generate multiple artificial propagation paths. In such weak scattering conditions, the RIS is able to enrich the propagation environment, while CSI knowledge is not required for the RIS configuration. Under a near-field channel model, we studied the performance limits of the proposed scheme by deriving the achieved SNR at the Rx, and examined how various system design parameters affect the performance. We observed that a linear RIS topology maximizes the number of resolvable paths. It was also demonstrated that the proposed scheme improves the SNR, while for a large number of elements it can outperform the conventional CSI-based passive beamforming at the RIS.

Chapter 7

Conclusion and Future Work

Within the past decade, the exponential increase of wireless devices has led to an unprecedented growth in data traffic demands. Recent predictions have witnessed that this trend is likely to persist. Future generations of wireless communications are committed to provide efficient solutions to satisfy these demands and exceed the performance limits of current wireless systems. Towards this direction, the wireless propagation environment is a critical factor for the efficient system design, which can impact the performance significantly. Multi-hop relaying networks and RISs are considered as key enabling technologies that can assist the communication and meet the requirements of next-generation networks. In particular, the integration of these technologies in the deployment of wireless networks can provide ubiquitous connectivity for a massive number of devices simultaneously, increase the coverage and improve the reliability of wireless networks. Moreover, due to their scalability, flexibility, adaptability and easy deployment, these technologies are regarded as appealing solutions for the implementation of low-cost and energy efficient networks. However, the use of these technologies in the deployment of wireless systems is not a trivial task and features several challenges that need to be efficiently addressed. As such, this thesis focused on the potentials of integrating multi-hop relaying networks and RISs in wireless networks, as well as the challenges associated with their implementation.

7.1 Concluding remarks

In this thesis, we proposed novel and flexible protocols and communication schemes for the design of efficient wireless networks assisted by the employment of the aforementioned communication paradigms, aiming to reduce their computational complexity and improve their performance. By leveraging tools from information theory, probability theory and signal processing we established complete analytical frameworks for the performance analysis of the proposed solutions that can be easily adapted to the parameters of the considered systems. Moreover, tractable theoretical expressions for fundamental network performance metrics were derived, such as the achieved SNR, the outage probability or the DMT. Through our analysis, we provided fundamental insights towards the deployment of relay-assisted and RIS-assisted wireless networks, and we demonstrated how key design parameters affect their performance. We showed that the proposed solutions can yield high performance gains, by exploiting the space and time domain for efficiently conveying information to the end users. In what follows, we refer to the main conclusions extracted from each chapter of the thesis. In particular,

- In Chapter 3, we presented of a novel cooperative protocol over a multi-hop network, based on the myopic strategy, where each node of the network cooperates with a limited number of neighboring nodes for the transmission of the signals. The network consists of relays with buffers of finite size to store the successfully decoded signals and can operate in two communication modes, namely the active and silent mode. A general and flexible methodology to model the evolution of the buffers' status and the transitions at the operations of each relay was proposed by using an MC formulation. Under this elegant framework, we studied the performance of the proposed protocol in terms of the outage probability and the achieved DMT. We demonstrated that the outage performance of the system is improved as the number of hops in the myopic protocol increases, while the achieved diversity gain depends on both the number of hops and the set of relays that have dual-mode operations.

- In Chapter 4, we focused on the performance of an RIS-aided MIMO system, where the elements are partitioned into non-overlapping sub-surfaces and are sequentially reconfigured to assist the communication, by following an

amplitude-based or a phase-based approach. The proposed schemes have low implementation complexity and can be applied without requiring CSI knowledge at the transmitter or for the RIS reconfiguration. Under this framework, we explored the fundamental performance limits of the proposed schemes and derived tractable theoretical expressions of the outage probability and the DMT. Moreover, we derived useful insights on the achieved diversity and multiplexing gains of each scheme and we showed that, by considering the proposed schemes, the RIS-aided MIMO systems can overcome the performance limitations of the MIMO channel.

- In Chapter 5, we proposed a low-complexity hybrid scheme for an RIS-aided network, where channel estimation is required for only a subset of the elements. The presented scheme considers that the RIS is divided in two non-overlapping sub-surfaces, which are sequentially activated to support the communication in the system. The configuration of the elements in the first and second sub-surface follows a CB-based and an RR-based design, respectively; hence, the required channel training overhead is significantly reduced. The performance of the proposed scheme was investigated under imperfect CSI and we derived analytical expressions for the outage probability. We showed that, by optimizing the number of elements that need to be estimated, the proposed scheme provides significant performance gains and overcomes the limitations caused by imperfect CSI.

- Finally, in Chapter 6 we considered an alternative use of the RIS in wireless communications. Specifically, we studied the potential gains of employing an RIS for facilitating the TR technique applied in high-frequency wideband communications. The RIS, which due to the higher frequency and large array aperture, operates in the near-field region, is used to generate multiple propagation paths in a simple manner. Thus, it artificially enriches the scattering environment, which is required for the efficient application of the TR, while its configuration does not require CSI knowledge. We investigated the performance of the proposed scheme through the received SNR and provided important insights on the effect of some system design parameters on the system's performance.

7.2 Future Work

In the following we present possible future works:

- **Delay adjustable metasurface (DAM)-enabled TR scheme:** As it has been shown in Chapter 6, the employment of an RIS for facilitating the TR scheme by enriching the propagation environment is a promising solution for high-frequency wideband communications. However, in the considered scenario the time delays depend only on the relative distances between the transceivers and the elements of the RIS. Enabling the control of the time delays for each propagation path could be an interesting future research direction for this scheme. As such, our work in Chapter 6 can be extended to an advanced scenario, where the TR scheme is facilitated by the utilization of a DAM [177, 178]. In contrast to the existing RIS-based solutions, each element of the DAM is equipped with an additional time-delay unit that can induce an extra delay onto the impinging signals by storing and retrieving the EM waves [179]. Through this approach, the DAM can also control the delays of the signals and the resulting tapped delay channel can be decoupled from the topology of the RIS, which could provide even higher performance gains. On the other hand, the hardware constraints associated with the deployment of such metasurfaces, as well as their potential effects on the overall performance of the system, should be addressed properly.

- **RIS-aided optical wireless communications (OWC):** The concept of OWC is a promising candidate technology to support the high data rate requirements of future wireless networks [180]. In particular, OWC include the communication technologies that utilize the freely available optical band of the EM spectrum, such as the free-space optics and visible light communication. Compared to radio-frequency systems, OWC utilize larger bandwidth, that results in higher data rates, and transmit data with high directionality. On the other hand, OWC networks are very sensitive to changes of the propagation environment and exhibit high susceptibility to blockages. An interesting research direction that has very recently emerged is the integration of RISs in OWC systems to assist the communication and address the connectivity issues [181, 182]. However, one of the main challenges for the deployment of RIS in OWC systems is the

development of accurate channel models, taking into account the distinctive effects of optical wireless channels, as well as the impact of different optical RIS functionalities on the channel properties. Moreover, in order to obtain sufficient performance gains, a massive number of elements may need to be integrated within a limited surface, reducing their inter-element distances. This can result in the employment of approximately continuous aperture surfaces, where the mutual coupling effect i.e., the interaction between adjacent elements of the RIS, is no longer negligible and therefore needs to be taken into consideration in the RIS-aided OWC channel models. As such, the fundamental behavior and performance limits of such systems still need to be explored.

- **Combinatorial optimization in RIS-aided systems:** In the available litera-ture, there are several studies dealing with the optimization of the reflection coefficients at the RIS, so that the potential benefits of RIS-assisted networks can be fully reaped. For this, various optimization methods have been used, such as the semidefinite relaxation method and the minorize-maximization algorithm [94, 183]. Despite the extensive literature on RIS optimization, the majority of the proposed ideas focus on the scenario of continuous phase shifts at the RIS. However, the reflection coefficients of the elements are normally limited to a set of discrete values, due to hardware constraints. Finding the solution that will optimize the performance in such scenarios leads to the for-mulation of NP-hard combinatorial optimization problems over all the possible states of the RIS elements, which are very challenging to be solved. A promis-ing technology to solve such problems is the employment of physics-based quantum computing techniques, such as quantum annealing [184], which can be used to provide optimal solutions to difficult computational problems with significantly reduced implementation complexity compared to conventional optimization methods.

- **RIS-assisted underwater wireless communications (UWC):** In recent years, the advances in underwater activities, e.g., study of oceanic animals and moni-toring/surveillance applications, have increased active research on UWC. Com-pared to terrestrial networks, the propagation medium in UWC suffers from significantly higher path loss, as well as various underwater environmental conditions, such as turbidity and salinity. Although acoustic signals were

mainly used for UWC, recently the consideration of optical signals enabled the information transmission with higher data rates and much lower delays, but at the cost of reduced propagation distance. Moreover, underwater wireless optical communications are highly sensitive to changes in environmental conditions and random obstacles. Towards this direction, the employment of RISs in UWC could be a key solution to overcome the aforementioned propagation issues, as they can be used to facilitate the connectivity between underwater communication devices, such as sensors, submarines and ships, in a controllable manner [185]. However, existing EM RIS designs cannot be directly applied on RIS-aided UWC, due to the distinctive properties of the channels in underwater conditions. Therefore, novel RIS communication schemes need to be conceived for the utilization of this technology in UWC.

Bibliography

[1] Cisco, "Cisco annual internet report (2018–2023) white paper." [Online]. Available: https://www.cisco.com

[2] G. A. Akpakwu, B. J. Silva, G. P. Hancke, and A. M. Abu-Mahfouz, "A survey on 5G networks for the Internet of Things: Communication technologies and challenges," *IEEE Access*, vol. 6, pp. 3619–3647, Dec. 2017.

[3] International telecommunication union, radiocommunication sector, "IMT vision-framework and overall objectives of the future development of IMT for 2020 and beyond." [Online]. Available: https://www.itu.int/rec/R-REC-M.2083

[4] W. Jiang, B. Han, M. A. Habibi, and H. D. Schotten, "The road towards 6G: A comprehensive survey," *IEEE Open J. Commun. Soc.*, vol. 2, pp. 334–366, Feb. 2021.

[5] J. G. Andrews, S. Buzzi, W. Choi, S. V. Hanly, A. Lozano, A. C. K. Soong, and J. C. Zhang, "What will 5G be?" *IEEE J. Sel. Areas Commun.*, vol. 32, no. 6, pp. 1065–1082, Jun. 2014.

[6] N. Bhushan, J. Li, D. Malladi, R. Gilmore, D. Brenner, A. Damnjanovic, R. T. Sukhavasi, C. Patel, and S. Geirhofer, "Network densification: The dominant theme for wireless evolution into 5G," *IEEE Commun. Mag.*, vol. 52, no. 2, pp. 82–89, Feb. 2014.

[7] E. G. Larsson, O. Edfors, F. Tufvesson, and T. L. Marzetta, "Massive MIMO for next generation wireless systems," *IEEE Commun. Mag.*, vol. 52, no. 2, pp. 186–195, Feb. 2014.

[8] L. Lu, G. Y. Li, A. L. Swindlehurst, A. Ashikhmin, and R. Zhang, "An overview of massive MIMO: Benefits and challenges," *IEEE J. Sel. Topics Signal Process.*, vol. 8, no. 5, pp. 742–758, Oct. 2014.

[9] E. Björnson, J. Hoydis, and L. Sanguinetti, "Massive MIMO has unlimited capacity," *IEEE Trans. Wireless Commun.*, vol. 17, no. 1, pp. 574–590, Jan. 2018.

[10] I. A. Hemadeh, K. Satyanarayana, M. E. Hajjar, and L. Hanzo, "Millimeter-wave communications: Physical channel models, design considerations, antenna constructions, and link-budget," *IEEE Commun. Surveys Tuts.*, vol. 20, no. 2, pp. 870–913, Dec. 2017.

[11] T. S. Rappaport, Y. Xing, G. R. MacCartney, A. F. Molisch, E. Mellios, and J. Zhang, "Overview of millimeter wave communications for fifth-generation (5G) wireless networks-with a focus on propagation models," *IEEE Trans. Antennas Propag.*, vol. 65, no. 12, pp. 6213–6230, Dec. 2017.

[12] X. Ge, S. Tu, G. Mao, C. X. Wang, and T. Han, "5G ultra-dense cellular networks," *IEEE Wireless Commun.*, vol. 23, no. 1, pp. 72–79, Feb. 2016.

[13] M. Kamel, W. Hamouda, and A. Youssef, "Ultra-dense networks: A survey," *IEEE Commun. Surveys Tuts.*, vol. 18, no. 4, pp. 2522–2545, May 2016.

[14] F. Guo, F. R. Yu, H. Zhang, X. Li, H. Ji, and V. C. M. Leung, "Enabling massive IoT toward 6G: A comprehensive survey," *IEEE Internet Things J.*, vol. 8, no. 15, pp. 11 891–11 915, Aug. 2021.

[15] Z. Zhang, Y. Xiao, Z. Ma, M. Xiao, Z. Ding, X. Lei, G. K. Karagiannidis, and P. Fan, "6G wireless networks: Vision, requirements, architecture, and key technologies," *IEEE Veh. Technol. Mag.*, vol. 14, no. 3, pp. 28–41, Sep. 2019.

[16] M. Giordani, M. Polese, M. Mezzavilla, S. Rangan, and M. Zorzi, "Toward 6G networks: Use cases and technologies," *IEEE Commun. Mag.*, vol. 58, no. 3, pp. 55–61, Mar. 2020.

[17] F. Tariq, M. R. A. Khandaker, K. K. Wong, M. A. Imran, M. Bennis, and M. Debbah, "A speculative study on 6G," *IEEE Wireless Commun.*, vol. 27, no. 4, pp. 118–125, Aug. 2020.

[18] International telecommunication union, radiocommunication sector, "IMT traffic estimates for the years 2020 to 2030." [Online]. Available: https://www.itu.int/pub/R-REP-M.2370-2015

[19] M. Katz, M. M. Blue, and M. L. Aho, "6Genesis flagship program: Building the bridges towards 6G-enabled wireless smart society and ecosystem," in *Proc. Latin-American Conf. Commun.*, Guadalajara, Mexico, Nov. 2018, pp. 1–9.

[20] P. Mach and Z. Becvar, "Device-to-device relaying: Optimization, performance perspectives, and open challenges towards 6G networks," *IEEE Commun. Surveys Tuts.*, vol. 24, no. 3, pp. 1336–1393, Jun. 2022.

[21] C. Pan, H. Ren, K. Wang, J. F. Kolb, M. Elkashlan, M. Chen, M. D. Renzo, Y. Hao, J. Wang, A. L. Swindlehurst, X. You, and L. Hanzo, "Reconfigurable intelligent surfaces for 6G systems: Principles, applications, and research directions," *IEEE Commun. Mag.*, vol. 59, no. 6, pp. 14–20, Jun. 2021.

[22] E. C. van der Meulen, "Three-terminal communication channels," *Adv. Appl. Prob.*, vol. 3, no. 1, pp. 120–154, 1971.

[23] G. Noh, H. Chung, and I. Kim, "Mobile relay technology for 5G," *IEEE Wireless Commun.*, vol. 27, no. 3, pp. 6–7, Jun. 2020.

[24] A. A. Amin and S. Y. Shin, "Capacity analysis of cooperative NOMA-OAM-MIMO based full-duplex relaying for 6G," *IEEE Wireless Commun. Lett.*, vol. 10, no. 7, pp. 1395–1399, Jul. 2021.

[25] R. Atallah, M. Khabbaz, and C. Assi, "Multihop V2I communications: a feasibility study, modeling, and performance analysis," *IEEE Trans. Veh. Technol.*, vol. 66, no. 3, pp. 2801–2810, Mar. 2017.

[26] H. Nishiyama, M. Ito, and N. Kato, "Relay-by-smartphone: Realizing multihop device-to-device communications," *IEEE Commun. Mag.*, vol. 52, no. 4, pp. 56–65, Apr. 2014.

[27] J. N. Laneman, D. N. C. Tse, and G. W. Wornell, "Cooperative diversity in wireless networks: Efficient protocols and outage behavior," *IEEE Trans. Inf. Theory*, vol. 50, no. 12, pp. 3062–3080, Dec. 2004.

[28] A. Ribeiro, X. Cai, and G. B. Giannakis, "Symbol error probabilities for general cooperative links," *IEEE Trans. Wireless Commun.*, vol. 4, no. 3, pp. 1264–1273, May 2005.

[29] T. M. Cover and A. A. El-Gamal, "Capacity theorems for the relay channel," *IEEE Trans. Inf. Theory*, vol. 25, no. 5, pp. 474–584, Sep. 1979.

[30] G. Kramer, M. Gastpar, and P. Gupta, "Cooperative strategies and capacity theorems for relay networks," *IEEE Trans. Inf. Theory*, vol. 51, no. 9, pp. 3037–3063, Sep. 2005.

[31] G. Farhadi and N. Beaulieu, "On the ergodic capacity of multi-hop wireless relaying systems," *IEEE Trans. Wireless Commun.*, vol. 8, no. 5, pp. 2286–2291, May 2009.

[32] A. Wyner and J. Ziv, "The rate-distortion function for source coding with side information at the decoder," *IEEE Trans. Inf. Theory*, vol. 22, no. 1, pp. 1–10, Jan. 1976.

[33] S. Yang and J. C. Belfiore, "Distributed rotation recovers spatial diversity," in *Proc. IEEE Int. Symp. Inf. Theory*, Austin, TX, Jun. 2010, pp. 2158–2162.

[34] N. V. Shende, Ö. Gürbüz, and E. Erkip, "Half-duplex or full-duplex communications: Degrees of freedom analysis under self-interference," *IEEE Trans. Wireless Commun.*, vol. 17, no. 2, pp. 1081–1093, Feb. 2018.

[35] D. Korpi, M. Heino, C. Icheln, K. Haneda, and M. Valkama, "Compact inband full-duplex relays with beyond 100 dB self-interference suppression: Enabling techniques and field measurements," *IEEE Trans. Antennas Propag.*, vol. 65, no. 2, pp. 960–965, Feb. 2017.

[36] M. Duarte, C. Dick, and A. Sabharwal, "Experiment-driven characterization of full-duplex wireless systems," *IEEE Trans. Wireless Commun.*, vol. 11, no. 12, pp. 4296–4307, Dec. 2012.

[37] M. O. Hasna and M. S. Alouini, "A performance study of dual-hop transmissions with fixed gain relays," *IEEE Trans. Wireless Commun.*, vol. 3, no. 6, pp. 1963–1968, Nov. 2004.

[38] E. Bjornson, M. Matthaiou, and M. Debbah, "A new look at dual-hop relaying: Performance limits with hardware impairments," *IEEE Trans. Commun.*, vol. 61, no. 11, pp. 4512–4525, Nov. 2013.

[39] M. O. Hasna and M. S. Alouini, "Outage probability of multihop transmission over Nakagami fading channels," *IEEE Commun. Lett.*, vol. 7, no. 5, pp. 216–218, May 2003.

[40] V. Jamali, N. Zlatanov, H. Shoukry, and R. Schober, "Achievable rate of the half-duplex multi-hop buffer-aided relay channel with block fading," *IEEE Trans. Wireless Commun.*, vol. 14, no. 11, pp. 6240–6256, Nov. 2015.

[41] J. G. Rois, F. G. Cuba, R. M. Akdeniz, F. J. G. Castaño, J. C. Burguillo, S. Rangan, and B. Lorenzo, "On the analysis of scheduling in dynamic duplex multihop mmWave cellular systems," *IEEE Trans. Wireless Commun.*, vol. 14, no. 11, pp. 6028–6042, Nov. 2015.

[42] X. Lin and J. G. Andrews, "Connectivity of millimeter wave networks with multi-hop relaying," *IEEE Wireless Commun. Lett.*, vol. 4, no. 2, pp. 209–212, Apr. 2015.

[43] J. Boyer, D. D. Falconer, and H. Yanikomeroglu, "Multihop diversity in wireless relaying channels," *IEEE Trans. Commun.*, vol. 52, no. 10, pp. 1820–1830, Oct. 2004.

[44] A. K. Sadek, W. Su, and K. J. R. Liu, "Multinode cooperative communications in wireless networks," *IEEE Trans. Signal Process.*, vol. 55, no. 1, pp. 341–355, Jan. 2007.

[45] C. Dong, L. L. Yang, and L. Hanzo, "Performance analysis of multihop-diversity-aided multihop links," *IEEE Trans. Veh. Tech.*, vol. 61, no. 6, pp. 2504–2516, Jul. 2012.

[46] K. Sreeram, S. Birenjith, and P. V. Kumar, "DMT of multihop networks: End points and computational tools," *IEEE Trans. Inf. Theory*, vol. 58, no. 2, pp. 804–819, Feb. 2012.

[47] S. Yang and J. C. Belfiore, "Diversity of MIMO multihop relay channels," 2007. [Online]. Available: https://arxiv.org/abs/0708.0386

[48] B. Ying and A. Nayak, "A power-efficient and social-aware relay selection method for multi-hop D2D communications," *IEEE Commun. Lett.*, vol. 22, no. 7, pp. 1450–1453, Jul. 2018.

[49] T. S. Rappaport, Y. Xing, O. Kanhere, S. Ju, A. Madanayake, S. Mandal, A. Alkhateeb, and G. C. Trichopoulos, "Wireless communications and applications above 100 GHz: Opportunities and challenges for 6G and beyond," *IEEE Access*, vol. 7, pp. 78 729–78 757, Jun. 2019.

[50] S. Ju, Y. Xing, O. Kanhere, and T. S. Rappaport, "Millimeter wave and sub-terahertz spatial statistical channel model for an indoor office building," *IEEE J. Sel. Areas Commun.*, vol. 39, no. 6, pp. 1561–1575, Jun. 2021.

[51] Y. Wu, J. Kokkoniemi, C. Han, and M. Juntti, "Interference and coverage analysis for terahertz networks with indoor blockage effects and line-of-sight access point association," *IEEE Trans. Wireless Commun.*, vol. 20, no. 3, pp. 1472–1486, Mar. 2021.

[52] G. Stratidakis, E. N. Papasotiriou, H. Konstantinis, A. A. A. Boulogeorgos, and A. Alexiou, "Relay-based blockage and antenna misalignment mitigation in THz wireless communications," in *Proc. 6G Wireless Summit*, Levi, Finland, Mar. 2020, pp. 1–4.

[53] N. Saeed, A. Celik, M. S. Alouini, and T. Y. Al-Naffouri, "Performance analysis of connectivity and localization in multi-hop underwater optical wireless sensor networks," *IEEE Trans. Mobile Comput.*, vol. 18, no. 11, pp. 2604–2615, Nov. 2019.

[54] A. Celik, N. Saeed, B. Shihada, T. Y. Al-Naffouri, and M. S. Alouini, "Opportunistic routing for opto-acoustic internet of underwater things," *IEEE J. Internet Things*, vol. 9, no. 3, pp. 2165–2179, Feb. 2022.

[55] Y. Chen, N. Zhao, Z. Ding, and M. S. Alouini, "Multiple UAVs as relays: multi-hop single link versus multiple dual-hop links," *IEEE Trans. Wireless Commun.*, vol. 17, no. 9, pp. 6348–6359, Sep. 2018.

[56] X. Li, Y. Chen, P. Xue, G. Lv, and M. Shu, "Outage performance for satellite-assisted cooperative NOMA systems with coordinated direct and relay transmission," *IEEE Commun. Lett.*, vol. 24, no. 10, pp. 2285–2289, Oct. 2020.

[57] *Air Interface for Broadband Wireless Access Systems Amendment 1: Multihop Relay Specification*, IEEE Std. 802.16j, 2009.

[58] *Air Interface for Broadband Wireless Access Systems Amendment 3: Advanced Air Interface*, IEEE Std. 802.16m, 2011.

[59] 3GPP, "Overview of 3GPP Release 10."

[60] ——, "Overview of 3GPP Release 12."

[61] ——, "Overview of 3GPP Release 13."

[62] ——, "Overview of 3GPP Release 14."

[63] ——, "Overview of 3GPP Release 15."

[64] ——, "Overview of 3GPP Release 17."

[65] X. Wu, L. P. Barnes, and A. Özgür, ""The capacity of the relay channel": Solution to Cover's problem in the Gaussian case," *IEEE Trans. Inf. Theory*, vol. 65, no. 1, pp. 255–275, Jan. 2019.

[66] A. El Gamal, A. Gohari, and C. Nair, "A strengthened cutset upper bound on the capacity of the relay channel and applications," *IEEE Trans. Inf. Theory*, vol. 68, no. 8, pp. 5013–5043, Aug. 2022.

[67] J. Zhang, E. Björnson, M. Matthaiou, D. W. K. Ng, H. Yang, and D. J. Love, "Prospective multiple antenna technologies for beyond 5G," *IEEE J. Sel. Areas Commun.*, vol. 38, no. 8, pp. 1637–1660, Aug. 2020.

[68] M. D. Renzo, A. Zappone, M. Debbah, M. S. Alouini, C. Yuen, J. Rosny, and S. Tretyakov, "Smart radio environments empowered by reconfigurable intelligent surfaces: How it works, state of research, and the road ahead," *IEEE J. Sel. Areas Commun.*, vol. 38, no. 11, pp. 2450–2525, Nov. 2020.

[69] M. D. Renzo, M. Debbah, D. T. P. Huy, A. Zappone, M. S. Alouini, C. Yuen, V. Sciancalepore, G. C. Alexandropoulos, J. Hoydis, H. Gacanin, J. Rosny, A. Bounceur, G. Lerosey, and M. Fink, "Smart radio environments empowered by reconfigurable AI meta-surfaces: An idea whose time has come," *EURASIP J. Wireless Commun. Netw.*, vol. 2019, no. 1, pp. 1–20, Dec. 2019.

[70] Y. Liu, X. Liu, X. Mu, T. Hou, J. Xu, M. D. Renzo, and N. Al-Dhahir, "Reconfigurable intelligent surfaces: Principles and opportunities," *IEEE Commun. Surveys Tuts.*, vol. 23, no. 3, pp. 1546–1577, May 2021.

[71] Q. Wu, S. Zhang, B. Zheng, C. You, and R. Zhang, "Intelligent reflecting surface-aided wireless communications: A tutorial," *IEEE Trans. Commun.*, vol. 69, no. 5, pp. 3313–3351, May 2021.

[72] Q. Wu and R. Zhang, "Towards smart and reconfigurable environment: Intelligent reflecting surface aided wireless network," *IEEE Commun. Mag.*, vol. 58, no. 1, pp. 106–112, Jan. 2020.

[73] C. Liaskos, S. Nie, A. Tsioliaridou, A. Pitsillides, S. Ioannidis, and I. Akyildiz, "A new wireless communication paradigm through software-controlled metasurfaces," *IEEE Commun. Mag.*, vol. 56, no. 9, pp. 162–169, Sep. 2018.

[74] H. T. Chen, A. J. Taylor, and N. Yu, "A review of metasurfaces: Physics and applications," *Rep. Prog. Phys.*, vol. 79, no. 7, p. 076401, Jun. 2016.

[75] S. Gong, X. Lu, D. T. Hoang, D. Niyato, L. Shu, D. I. Kim, and Y. C. Liang, "Toward smart wireless communications via intelligent reflecting surfaces: A contemporary survey," *IEEE Commun. Surveys Tuts.*, vol. 22, no. 4, pp. 2283–2314, Jun. 2020.

[76] A. Pors, M. G. Nielsen, R. L. Eriksen, and S. I. Bozhevolnyi, "Broadband focusing flat mirrors based on plasmonic gradient metasurfaces," *Nano Lett.*, vol. 13, no. 2, pp. 829–834, Jan. 2013.

[77] D. H. Kwon, "Lossless scalar metasurfaces for anomalous reflection based on efficient surface field optimization," *IEEE Antennas Wireless Propag. Lett.*, vol. 17, no. 7, pp. 1149–1152, Jul. 2018.

[78] A. E. Olk, P. E. M. Macchi, and D. A. Powell, "High-efficiency refracting millimeter-wave metasurfaces," *IEEE Trans. Antennas Propag.*, vol. 68, no. 7, pp. 5453–5462, Jul. 2020.

[79] X. Wang, J. Ding, B. Zheng, S. An, G. Zhai, and H. Zhang, "Simultaneous realization of anomalous reflection and transmission at two frequencies using bi-functional metasurfaces," *Sci. Rep.*, vol. 8, p. 1876, Jan. 2018.

[80] S. Ghosh and K. V. Srivastava, "Polarization-insensitive single- and broadband switchable absorber/reflector and its realization using a novel biasing technique," *IEEE Trans. Antennas Propag.*, vol. 64, no. 8, pp. 3665–3670, Aug. 2016.

[81] H. Li, F. Costa, Y. Wang, Q. Cao, and A. Monorchio, "A wideband multifunctional absorber/reflector with polarization-insensitive performance," *IEEE Trans. Antennas Propag.*, vol. 68, no. 6, pp. 5033–5038, Jun. 2020.

[82] L. Zhang, X. Q. Chen, S. Liu, Q. Zhang, J. Zhao, J. Y. Dai, G. D. Bai, X. Wan, Q. Cheng, G. Castaldi, V. Galdi, and T. J. Cui, "Space-time-coding digital metasurfaces," *Nat. Commun.*, vol. 9, no. 1, p. 4334, Oct. 2018.

[83] Q. Tao, J. Wang, and C. Zhong, "Performance analysis of intelligent reflecting surface aided communication systems," *IEEE Commun. Lett.*, vol. 24, no. 11, pp. 2464–2468, Nov. 2020.

[84] Y. Cheng, K. H. Li, Y. Liu, K. C. Teh, and H. V. Poor, "Downlink and uplink intelligent reflecting surface aided networks: NOMA and OMA," *IEEE Trans. Wireless Commun.*, vol. 20, no. 6, pp. 3988–4000, Jun. 2021.

[85] C. Psomas and I. Krikidis, "Low-complexity random rotation-based schemes for intelligent reflecting surfaces," *IEEE Trans. Wireless Commun.*, vol. 20, no. 8, pp. 5212–5225, Aug. 2021.

[86] P. Xu, G. Chen, Z. Yang, and M. D. Renzo, "Reconfigurable intelligent surfaces-assisted communications with discrete phase shifts: How many quantization levels are required to achieve full diversity?" *IEEE Wireless Commun. Lett.*, vol. 10, no. 2, pp. 358–362, Feb. 2021.

[87] S. Atapattu, R. Fan, P. Dharmawansa, G. Wang, J. Evans, and T. A. Tsiftsis, "Reconfigurable intelligent surface assisted two–way communications: Performance analysis and optimization," *IEEE Trans. Commun.*, vol. 68, no. 10, pp. 6552–6567, Oct. 2020.

[88] Q. Wu and R. Zhang, "Intelligent reflecting surface enhanced wireless network via joint active and passive beamforming," *IEEE Trans. Wireless Commun.*, vol. 18, no. 11, pp. 5394–5409, Nov. 2019.

[89] Z. Ding and H. V. Poor, "A simple design of IRS-NOMA transmission," *IEEE Commun. Lett.*, vol. 24, no. 5, pp. 1119–1123, May 2020.

[90] S. Lin, B. Zheng, G. C. Alexandropoulos, M. Wen, M. D. Renzo, and F. Chen, "Reconfigurable intelligent surfaces with reflection pattern modulation: Beamforming design and performance analysis," *IEEE Trans. Wireless Commun.*, vol. 20, no. 2, pp. 741–754, Feb. 2021.

[91] S. Lin, F. Chen, M. Wen, Y. Feng, and M. D. Renzo, "Reconfigurable intelligent surface-aided quadrature reflection modulation for simultaneous passive beamforming and information transfer," *IEEE Trans. Wireless Commun.*, vol. 21, no. 3, pp. 1469–1481, Mar. 2022.

[92] C. Huang, Z. Yang, G. C. Alexandropoulos, K. Xiong, L. Wei, C. Yuen, Z. Zhang, and M. Debbah, "Multi-hop RIS-empowered terahertz communications: A DRL-based hybrid beamforming design," *IEEE J. Sel. Areas Commun.*, vol. 39, no. 6, pp. 1663–1677, Jun. 2021.

[93] S. Zhang and R. Zhang, "Capacity characterization for intelligent reflecting surface aided MIMO communication," *IEEE J. Sel. Areas Commun.*, vol. 38, no. 8, pp. 1823–1838, Aug. 2020.

[94] C. Pan, H. Ren, K. Wang, W. Xu, M. Elkashlan, A. Nallanathan, and L. Hanzo, "Multicell MIMO communications relying on intelligent reflecting surfaces," *IEEE Trans. Wireless Commun.*, vol. 19, no. 8, pp. 5218–5233, Aug. 2020.

[95] H. V. Cheng and W. Yu, "Multiplexing gain of modulating phases through reconfigurable intelligent surface," in *Proc. Int. Symp. Inf. Theory*, Melbourne, Australia, Jul. 2021, pp. 2346–2351.

[96] X. Zhang, X. Yu, and S. Song, "Outage probability and finite-SNR DMT analysis for IRS-aided MIMO systems: How large IRSs need to be?" *IEEE J. Sel. Topics Signal Process.*, vol. 16, no. 5, pp. 1070–1085, Aug. 2022.

[97] K. Weinberger and A. Sezgin, "Sacrificing CSI for a greater good: RIS-enabled opportunistic rate splitting," in *Proc. IEEE 12th Sensor Array Multichannel Signal Process. Workshop (SAM)*, Trondheim, Norway, Jun. 2022, pp. 281–285.

[98] J. Chen, P. Elia, and S. A. Jafar, "On the two-user MISO broadcast channel with alternating CSIT: A topological perspective," *IEEE Trans. Inf. Theory*, vol. 61, no. 8, pp. 4345–4366, Aug. 2015.

[99] S. Xia, Y. Shi, Y. Zhou, and X. Yuan, "Reconfigurable intelligent surface for massive connectivity: Joint activity detection and channel estimation," *IEEE Trans. Signal Process.*, vol. 69, pp. 5693–5707, Oct. 2021.

[100] P. Wang, J. Fang, X. Yuan, Z. Chen, and H. Li, "Intelligent reflecting surface-assisted millimeter wave communications: Joint active and passive precoding design," *IEEE Trans.s Veh. Technol.*, vol. 69, no. 12, pp. 14 960–14 973, Dec. 2020.

[101] Z. Wan, Z. Gao, F. Gao, M. D. Renzo, and M. S. Alouini, "Terahertz massive MIMO with holographic reconfigurable intelligent surfaces," *IEEE Trans. Commun.*, vol. 69, no. 7, pp. 4732–4750, Jul. 2021.

[102] B. Ning, Z. Chen, W. Chen, Y. Du, and J. Fang, "Terahertz multi-user massive MIMO with intelligent reflecting surface: Beam training and hybrid beamforming," *IEEE Trans. Veh. Technol.*, vol. 70, no. 2, pp. 1376–1393, Feb. 2021.

[103] C. Pan, H. Ren, K. Wang, M. Elkashlan, A. Nallanathan, J. Wang, and L. Hanzo, "Intelligent reflecting surface aided MIMO broadcasting for simultaneous wireless information and power transfer," *IEEE J. Sel. Areas Commun.*, vol. 38, no. 8, pp. 1719–1734, Aug. 2020.

[104] Q. Wu and R. Zhang, "Weighted sum power maximization for intelligent reflecting surface aided SWIPT," *IEEE Wireless Commun. Lett.*, vol. 9, no. 5, pp. 586–590, May 2020.

[105] R. Liu, Q. Wu, M. D. Renzo, and Y. Yuan, "A path to smart radio environments: An industrial viewpoint on reconfigurable intelligent surfaces," *IEEE Wireless Commun.*, vol. 29, no. 1, pp. 202–208, Feb. 2022.

[106] M. Jian, G. C. Alexandropoulos, E. Basar, C. Huang, R. Liu, Y. Liu, and C. Yuen, "Reconfigurable intelligent surfaces for wireless communications: Overview of hardware designs, channel models, and estimation techniques," *Intell. Converged Netw.*, vol. 3, no. 1, pp. 1–32, Mar. 2022.

[107] E. G. RIS-001, "Reconfigurable intelligent surfaces (RIS); Use cases, deployment scenarios and requirements." [Online]. Available: https://www.etsi.org/committee/1966-ris

[108] E. G. RIS-003, "Reconfigurable intelligent surfaces (RIS); Communication models, channel models, channel estimation and evaluation methodology." [Online]. Available: https://www.etsi.org/committee/1966-ris

[109] E. G. RIS-002, "Reconfigurable intelligent surfaces (RIS); Technological challenges, architecture and impact on standardization." [Online]. Available: https://www.etsi.org/committee/1966-ris

[110] ZTE Corporation, Sanechips, "Support of reconfigurable intelligent surface for 5G Advanced." [Online]. Available: https://www.3gpp.org/ftp/TSG_RAN/TSG_RAN/TSGR_91e/Docs/RP-210618.zip

[111] Q. Wu and R. Zhang, "Beamforming optimization for wireless network aided by intelligent reflecting surface with discrete phase shifts," *IEEE Trans. Commun.*, vol. 68, no. 3, pp. 1838–1851, Mar. 2020.

[112] Z. Zhou, N. Ge, Z. Wang, and L. Hanzo, "Joint transmit precoding and reconfigurable intelligent surface phase adjustment: A decomposition-aided channel estimation approach," *IEEE Trans. Commun.*, vol. 69, no. 2, pp. 1228–1243, Feb. 2021.

[113] B. Shamasundar and A. Nosratinia, "Canonical training is bad for reconfigurable intelligent surfaces," in *Proc. Int. Symp. Inf. Theory*, Espoo, Finland, Jun. 2022, pp. 2499–2504.

[114] D. Mishra and H. Johansson, "Channel estimation and low-complexity beamforming design for passive intelligent surface assisted MISO wireless energy transfer," in *Proc. IEEE 44th Int. Conf. Acoustics, Speech Signal Process.*, Brighton, U.K., May 2019, pp. 4659–4663.

[115] M. D. Renzo, K. Ntontin, J. Song, F. H. Danufane, X. Qian, F. Lazarakis, J. D. Rosny, D. T. P. Huy, O. Simeone, R. Zhang, M. Debbah, G. Lerosey, M. Fink, S. Tretyakov, and S. Shamai, "Reconfigurable intelligent surfaces vs. relaying: Differences, similarities, and performance comparison," *IEEE Open J. Commun. Soc.*, vol. 1, pp. 798–807, Jun. 2020.

[116] E. Björnson, Ö. Özdogan, and E. G. Larsson, "Intelligent reflecting surface versus decode-and-forward: How large surfaces are needed to beat relaying?" *IEEE Wireless Commun. Lett.*, vol. 9, no. 2, pp. 244–248, Feb. 2020.

[117] R. Long, Y. C. Liang, Y. Pei, and E. G. Larsson, "Active reconfigurable intelligent surface-aided wireless communications," *IEEE Trans. Wireless Commun.*, vol. 20, no. 8, pp. 4962–4975, Aug. 2021.

[118] K. Liu, Z. Zhang, L. Dai, S. Xu, and F. Yang, "Active reconfigurable intelligent surface: Fully-connected or sub-connected?" *IEEE Commun. Lett.*, vol. 26, no. 1, pp. 167–171, Jan. 2022.

[119] Z. Zhang, L. Dai, X. Chen, C. Liu, F. Yang, R. Schober, and H. V. Poor, "Active RIS vs. passive RIS: Which will prevail in 6G?" *IEEE Trans. Commun.*, vol. 71, no. 3, pp. 1707–1725, Mar. 2023.

[120] B. Zheng and R. Zhang, "IRS meets relaying: Joint resource allocation and passive beamforming optimization," *IEEE Wireless Commun. Lett.*, vol. 10, no. 9, pp. 2080–2084, Sep. 2021.

[121] Z. Kang, C. You, and R. Zhang, "IRS-aided wireless relaying: Deployment strategy and capacity scaling," *IEEE Wireless Commun. Lett.*, vol. 11, no. 2, pp. 215–219, Feb. 2022.

[122] Z. Abdullah, G. Chen, S. Lambotharan, and J. A. Chambers, "A hybrid relay and intelligent reflecting surface network and its ergodic performance analysis," *IEEE Wireless Commun. Lett.*, vol. 9, no. 10, pp. 1653–1657, Oct. 2020.

[123] I. Yildirim, F. Kilinc, E. Basar, and G. C. Alexandropoulos, "Hybrid RIS-empowered reflection and decode-and-forward relaying for coverage extension," *IEEE Commun. Lett.*, vol. 25, no. 5, pp. 1692–1696, May 2021.

[124] D. Tse and P. Viswanath, *Fundamentals of Wireless Communication*. Cambridge University Press, 2005.

[125] G. C. Alexandropoulos, A. Mokh, R. Khayatzadeh, J. Rosny, M. Kamoun, A. Ourir, A. Tourin, M. Fink, and M. Debbah, "Time reversal for 6G spatiotemporal focusing: Recent experiments, opportunities, and challenges," *IEEE Veh. Technol. Mag.*, vol. 17, no. 4, pp. 74–82, Dec. 2022.

[126] Y. Chen, F. Han, Y. H. Yang, H. Ma, Y. Han, C. Jiang, H. Q. Lai, D. Claffey, Z. Safar, and K. J. R. Liu, "Time-reversal wireless paradigm for green internet of things: An overview," *IEEE Internet Things J.*, vol. 1, no. 1, pp. 81–98, Feb. 2014.

[127] B. Wang, Y. Wu, F. Han, Y. H. Yang, and K. J. R. Liu, "Green wireless communications: A time-reversal paradigm," *IEEE J. Sel. Areas Commun.*, vol. 29, no. 8, pp. 1698–1710, Sep. 2011.

[128] M. Fink, "Time reversal of ultrasonic fields. i. basic principles," *IEEE Trans. Ultrason., Ferroelectr., Freq. Control*, vol. 39, no. 5, pp. 555–566, Sep. 1992.

[129] H. T. Nguyen, I. Z. Kovcs, and P. C. F. Eggers, "A time reversal transmission approach for multiuser UWB communications," *IEEE Trans. Antennas Propag.*, vol. 54, no. 11, pp. 3216–3224, Nov. 2006.

[130] Y. Han, Y. Chen, B. Wang, and K. J. R. Liu, "Time-reversal massive multipath effect: A single-antenna "massive MIMO" solution," *IEEE Trans. Commun.*, vol. 64, no. 8, pp. 3382–3394, Aug. 2016.

[131] I. S. Gradshteyn and I. M. Ryzhik, *Table of Integrals, Series, and Products*, 7th ed. Academic Press, 2007.

[132] F. Yilmaz and M. Alouini, "Product of shifted exponential variates and outage capacity of multicarrier systems," in *Proc. European Wireless Conf.*, Aalborg, Denmark, May 2009, pp. 282–286.

[133] L. Zheng and D. N. C. Tse, "Diversity and multiplexing: A fundamental tradeoff in multiple-antenna channels," *IEEE Trans. Inf. Theory*, vol. 49, no. 5, pp. 1073–1096, May 2003.

[134] J. Gil-Pelaez, "Note on the inversion theorem," *Biometrika*, vol. 38, no. 3-4, pp. 481–482, Dec. 1951.

[135] A. Papoulis and S. U. Pillai, *Probability, Random Variables, and Stochastic Processes*, 4th ed. McGraw Hill, 2002.

[136] X. Chen, D. W. K. Ng, W. Yu, E. G. Larsson, N. Al-Dhahir, and R. Schober, "Massive access for 5G and beyond," *IEEE J. Sel. Areas Commun.*, vol. 39, no. 3, pp. 615–637, Mar. 2021.

[137] M. N. Tehrani, M. Uysal, and H. Yanikomeroglu, "Device-to-device communication in 5G cellular networks: challenges, solutions, and future directions," *IEEE Commun. Mag.*, vol. 52, no. 5, pp. 86–92, May 2014.

[138] H. Wang, Y. Zhang, X. Zhang, and Z. Li, "Secrecy and covert communications against UAV surveillance via multi-hop networks," *IEEE Trans. Commun.*, vol. 68, no. 1, pp. 389–401, Jan. 2020.

[139] L. Ong and M. Motani, "Myopic coding in multiterminal networks," *IEEE Trans. Inf. Theory*, vol. 54, no. 7, pp. 3295–3314, Jul. 2008.

[140] D. Niyato, E. Hossain, and A. Fallahi, "Sleep and wakeup strategies in solar-powered wireless sensor/mesh networks: Performance analysis and optimization," *IEEE Trans. Mobile Comput.*, vol. 6, no. 2, pp. 221–236, Feb. 2007.

[141] B. Medepally and N. B. Mehta, "Voluntary energy harvesting relays and selection in cooperative wireless networks," *IEEE Trans. Wireless Commun.*, vol. 9, no. 11, pp. 3543–3553, Nov. 2010.

[142] Y. Luo, J. Zhang, and K. B. Letaief, "Relay selection for energy harvesting cooperative communication systems," in *Proc. IEEE Global Commun. Conf.*, Atlanta, GA, Dec. 2013, pp. 2514–2519.

[143] R. Morsi, D. S. Michalopoulos, and R. Schober, "Performance analysis of near-optimal energy buffer aided wireless powered communication," *IEEE Trans. Wireless Commun.*, vol. 17, no. 2, pp. 863–881, Feb. 2018.

[144] S. Wang, W. Guo, Z. Zhou, Y. Wu, and X. Chu, "Outage probability for multi-hop D2D communications with shortest path routing," *IEEE Commun. Lett.*, vol. 19, no. 11, pp. 1997–2000, Nov. 2015.

[145] L. Qu, J. He, and C. Assi, "Understanding the benefits of successive interference cancellation in multi-rate multi-hop wireless networks," *IEEE Trans. Commun.*, vol. 62, no. 7, pp. 2465–2477, Jul. 2014.

[146] T. Li, P. Fan, and K. B. Letaief, "Outage probability of energy harvesting relay-aided cooperative networks over Rayleigh fading channel," *IEEE Trans. Veh. Technol.*, vol. 65, no. 2, pp. 972–978, Feb. 2016.

[147] R. G. Gallager, *Stochastic Processes: Theory for Applications*. Cambridge University Press, 2013.

[148] I. Krikidis, T. Charalambous, and J. S. Thompson, "Buffer-aided relay selection for cooperative diversity systems without delay constraints," *IEEE Trans. Wireless Commun.*, vol. 11, no. 5, pp. 1957–1967, May 2012.

[149] J. Hu and N. C. Beaulieu, "Accurate simple closed-form approximations to Rayleigh sum distributions and densities," *IEEE Commun. Lett.*, vol. 9, no. 2, pp. 109–111, Feb. 2005.

[150] P. Hitczenko, "A note on a distribution of weighted sums of i.i.d. Rayleigh random variables," *Sankhyā: The Indian Journal of Statistics, Series A (1961-2002)*, vol. 60, no. 2, pp. 171–175, Jun. 1998.

[151] T. M. Cover and J. Thomas, *Elements of Information Theory*. Wiley, 1991.

[152] A. Goldsmith, *Wireless Communications*. Cambridge University Press, 2005.

[153] Wolfram Mathematica Documentation - NMinimize. [Online]. Available: https://reference.wolfram.com/language/ref/NMinimize.html

[154] D. Tyrovolas, P. V. Mekikis, S. A. Tegos, P. D. Diamantoulakis, C. K. Liaskos, and G. K. Karagiannidis, "Energy-aware design of UAV-mounted RIS networks for IoT data collection," 2022. [Online]. Available: https://arxiv.org/abs/2208.06016

[155] C. Huang, A. Zappone, G. C. Alexandropoulos, M. Debbah, and C. Yuen, "Reconfigurable intelligent surfaces for energy efficiency in wireless communication," *IEEE Trans. Wireless Commun.*, vol. 18, no. 8, pp. 4157–4170, Aug. 2019.

[156] Z. Shi, H. Wang, Y. Fu, G. Yang, S. Ma, and F. Gao, "Outage analysis of reconfigurable intelligent surface aided mimo communications with statistical CSI," *IEEE Trans. Wireless Commun.*, vol. 21, no. 2, pp. 823–839, Feb. 2022.

[157] M. Najafi, V. Jamali, R. Schober, and H. V. Poor, "Physics-based modeling and scalable optimization of large intelligent reflecting surfaces," *IEEE Trans. Commun.*, vol. 69, no. 4, pp. 2673–2691, Apr. 2021.

[158] K. L. Besser and E. A. Jorswieck, "Reconfigurable intelligent surface phase hopping for ultra-reliable communications," *IEEE Trans. Wireless Commun.*, vol. 21, no. 11, pp. 9082–9095, Nov. 2022.

[159] B. A. Nahhas, Q. U. A. Nadeem, and A. Chaaban, "Intelligent reflecting surface assisted MISO downlink: Channel estimation and asymptotic analysis," in *Proc. IEEE Global Commun. Conf.*, Taipei, Taiwan, Dec. 2020, pp. 1–6.

[160] S. Abeywickrama, R. Zhang, and C. Yuen, "Intelligent reflecting surface: Practical phase shift model and beamforming optimization," in *Proc. IEEE Int. Conf. Commun.*, Dublin, Ireland, Jun. 2020, pp. 1–6.

[161] V. Arun and H. Balakrishnan, "RFocus: Beamforming using thousands of passive antennas," in *Proc. USENIX Symp. Netw. Syst. Design Implement.*, Santa Clara, CA, Feb. 2020, pp. 1047–1061.

[162] G. Taricco and G. Alfano, "Outage information rate of spatially correlated multi-cluster scattering MIMO channels," in *Proc. Int. Symp. Inf. Theory*, Aachen, Germany, Jun. 2017, pp. 551–555.

[163] R. Pedarsani, O. Lévêque, and S. Yang, "On the DMT optimality of time-varying distributed rotation over slow fading relay channels," *IEEE Trans. Wireless Commun.*, vol. 14, no. 1, pp. 421–434, Jan. 2015.

[164] M. M. Amri, N. M. Tran, J. H. Park, D. I. Kim, and K. W. Choi, "A programmable binary metasurface for wireless power transfer application," in *Proc. IEEE Wireless Power Transfer Conf.*, Seoul, South Korea, Nov. 2020, pp. 334–337.

[165] N. C. Beaulieu and K. T. Hemachandra, "Novel simple representations for Gaussian class multivariate distributions with generalized correlation," *IEEE Trans. Inf. Theory*, vol. 57, no. 12, pp. 8072–8083, Dec. 2011.

[166] R. J. Muirhead, *Aspects of Multivariate Statistical Theory*. Wiley, 1982.

[167] S. Yang and J. Belfiore, "Diversity-multiplexing tradeoff of double scattering MIMO channels," *IEEE Trans. Inf. Theory*, vol. 57, no. 4, pp. 2027–2034, Apr. 2011.

[168] T. L. Jensen and E. D. Carvalho, "An optimal channel estimation scheme for intelligent reflecting surfaces based on a minimum variance unbiased estimator," in *Proc. Int. Conf. Acoustics, Speech Signal Process.*, Barcelona, Spain, May 2020, pp. 5000–5004.

[169] B. Zheng and R. Zhang, "Intelligent reflecting surface-enhanced OFDM: Channel estimation and reflection optimization," *IEEE Wireless Commun. Lett.*, vol. 9, no. 4, pp. 518–522, Apr. 2020.

[170] V. Jamali, G. C. Alexandropoulos, R. Schober, and H. V. Poor, "Low-to-zero-overhead IRS reconfiguration: Decoupling illumination and channel estimation," *IEEE Commun. Lett.*, vol. 26, no. 4, pp. 932–936, Apr. 2022.

[171] T. Yoo and A. Goldsmith, "Capacity and power allocation for fading MIMO channels with channel estimation error," *IEEE Trans. Inf. Theory*, vol. 52, no. 5, pp. 2203–2214, May 2006.

[172] E. Björnson and L. Sanguinetti, "Power scaling laws and near-field behaviors of massive MIMO and intelligent reflecting surfaces," *IEEE Open J. Commun. Soc.*, vol. 1, pp. 1306–1324, Sep. 2020.

[173] Y. Liu, Z. Wang, J. Xu, C. Ouyang, X. Mu, and R. Schober, "Near-field communications: A tutorial review," *IEEE Open J. Commun. Soc.*, vol. 4, pp. 1999–2049, Sep. 2023.

[174] U. K. Ganesan, E. Björnson, and E. G. Larsson, "Radioweaves for extreme spatial multiplexing in indoor environments," in *Proc. Asilomar Conf. Signals, Syst., Comput.*, Pacific Grove, CA, Nov. 2020, pp. 1007–1011.

[175] D. Dardari, N. Decarli, A. Guerra, and F. Guidi, "LOS/NLOS near-field localization with a large reconfigurable intelligent surface," *IEEE Trans. Wireless Commun.*, vol. 21, no. 6, pp. 4282–4294, Jun. 2022.

[176] E. Arslan, I. Yildirim, F. Kilinc, and E. Basar, "Over-the-air equalization with reconfigurable intelligent surfaces," *IET Commun.*, vol. 16, pp. 1486–1497, May 2021.

[177] J. An, C. Xu, D. W. K. Ng, C. Yuen, L. Gan, and L. Hanzo, "Reconfigurable intelligent surface-enhanced OFDM communications via delay adjustable metasurface," 2021. [Online]. Available: https://arxiv.org/abs/2110.09291

[178] H. Sun, S. Zhang, J. Ma, and O. A. Dobre, "Time-delay unit based beam squint mitigation for RIS-aided communications," *IEEE Commun. Lett.*, vol. 26, no. 9, pp. 2220–2224, Sep. 2022.

[179] T. Nakanishi and M. Kitano, "Storage and retrieval of electromagnetic waves using electromagnetically induced transparency in a nonlinear metamaterial," *Appl. Phys. Lett.*, vol. 112, no. 20, p. 201905, May 2018.

[180] A. Celik, I. Romdhane, G. Kaddoum, and A. M. Eltawil, "A top-down survey on optical wireless communications for the internet of things," *IEEE Commun. Surveys Tuts.*, vol. 25, no. 1, pp. 1–45, Nov. 2022.

[181] M. Najafi, B. Schmauss, and R. Schober, "Intelligent reflecting surfaces for free space optical communication systems," *IEEE Trans. Commun.*, vol. 69, no. 9, pp. 6134–6151, Sep. 2021.

[182] S. Aboagye, T. M. N. Ngatched, O. A. Dobre, and A. R. Ndjiongue, "Intelligent reflecting surface-aided indoor visible light communication systems," *IEEE Commun. Lett.*, vol. 25, no. 12, pp. 3913–3917, Dec. 2021.

[183] X. Yu, D. Xu, Y. Sun, D. W. K. Ng, and R. Schober, "Robust and secure wireless communications via intelligent reflecting surfaces," *IEEE J. Sel. Areas Commun.*, vol. 38, no. 11, pp. 2637–2652, Nov. 2020.

[184] Q. J. Lim, C. Ross, A. Ghosh, F. W. Vook, G. Gradoni, and Z. Peng, "Quantum-assisted combinatorial optimization for reconfigurable intelligent surfaces in smart electromagnetic environments," *IEEE Trans. Antennas Propag.*, vol. 72, no. 1, pp. 147–159, Jan. 2024.

[185] S. Kisseleff, S. Chatzinotas, and B. Ottersten, "Reconfigurable intelligent surfaces in challenging environments: Underwater, underground, industrial and disaster," *IEEE Access*, vol. 9, pp. 150 214–150 233, Nov. 2021.